4-27-2015

Wavelet analysis of non-stationary signals with applications

Maria Dorothea Van der Walt
University of Missouri-St. Louis, maryke.thom@gmail.com

Wavelet analysis of non-stationary signals with applications

Maria Dorothea van der Walt
M.Sc., Mathematics, Stellenbosch University, South Africa, 2012
B.Sc. Hons., Mathematics, Stellenbosch University, South Africa, 2010
B.Sc., Mathematical Sciences, Stellenbosch University, South Africa, 2009

A dissertation submitted to the Graduate School of the
University of Missouri-St. Louis
in partial fulfillment of the requirements for the degree
Doctor of Philosophy in Applied Mathematics

May 2015

Advisory Committee:

Charles Chui, Ph.D. (chair)

Haiyan Cai, Ph.D. (co-chair)

Qingtang Jiang, Ph.D.

Wenjie He, Ph.D.

Yuefeng Wu, Ph.D.

Abstract

The empirical mode decomposition (EMD) algorithm, introduced by N.E. Huang et al in 1998, is arguably the most popular mathematical scheme for non-stationary signal decomposition and analysis. The objective of EMD is to separate a given signal into a number of components, called intrinsic mode functions (IMF's), after which the instantaneous frequency (IF) and amplitude of each IMF are computed through Hilbert spectral analysis (HSA). On the other hand, the synchrosqueezed wavelet transform (SST), introduced by I. Daubechies and S. Maes in 1996 and further developed by I. Daubechies, J. Lu and H.-T. Wu in 2011, is first applied to estimate the IF's of all signal components of the given signal, based on one single frequency reassignment rule, under the assumption that the signal components satisfy certain strict properties of the so-called adaptive harmonic model, before the signal components of the model are recovered, based on the estimated IF's.

The objective of this dissertation is to develop a hybrid EMD-SST computational scheme by applying a modified SST to each IMF produced by a modified EMD, as an alternative approach to the original EMD-HSA method. While our modified SST assures non-negative instantaneous frequencies of the IMF's, application of the EMD scheme eliminates the dependence on a single frequency reassignment rule as well as the guessing work of the number of signal components in the original SST approach. Our modification of the SST consists of applying analytic vanishing moment wavelets (introduced in a recent paper by C.K. Chui, Y.-T. Lin and H.-T. Wu) with stacked knots to process signals on bounded or half-infinite time intervals, and spline curve fitting with optimal smoothing parameter selection through generalized cross-validation. In addition, we modify EMD by formulating a local spline interpolation scheme for bounded intervals, for real-time realization of the EMD sifting process. This scheme improves over the standard global cubic spline interpolation, both in quality and computational cost, particularly when applied to bounded and half-infinite time intervals.

Acknowledgments

I am deeply indebted to my advisor, Professor Charles Chui, for his guidance and vision throughout my studies at UMSL. His broad knowledge, sound instincts and ingenuity in the field of mathematics have been and will continue to be an inspiration for me.

A word of thanks to the other four members of my advisory committee, Professors Cai, Jiang, He and Wu, for their interest, time and effort.

My time at the math department at UMSL was made much easier and less stressful (and therefore more enjoyable) by the excellent direction and help, in all administrative matters, of Kimberly Stanger and Raina Traore-Gress; thank you very much.

I am also grateful for the financial support of the Graduate School at UMSL during the course of this study. My time at UMSL was truly enriched by having the opportunity to teach undergraduate mathematics courses – I will always remember fondly the hours I spent in Clark Hall 409 with my trigonometry students.

The code to execute the EMD algorithm in the numerical experiments of Chapter 9 of this dissertation was initially programmed by my fellow student, Joe Koester. I am grateful for his enthusiasm for EMD – and for just about any topic in mathematics, really. I would also like to thank Professor Hau-tieng Wu of the Department of Mathematics at the University of Toronto, for graciously providing me with his code to execute the SST.

I feel that these acknowledgments would not be complete without thanking Professor Johan de Villiers of the Department of Mathematical Sciences

at Stellenbosch University, for instilling in me a passion for conducting honest research and solving problems in mathematics. He is truly a remarkable person with an unquenchable zest for life.

A special thank you to the Kruger and Miller families from Harvester Christian Church and the Stulacs from Memorial Presbyterian Church, for being our family in a foreign country.

I want to thank my family for their love and encouragement. First, thank you to my loving parents, Jaco and Elmien Thom, who raised me to love learning new things, to work hard and to persevere, and who believed in me and supported me in all my pursuits. Second, I want to thank my lovely sisters, Matildie and Elmientjie, for their support, inspiration and camaraderie.

This last word of acknowledgment I have saved for my wonderful husband, Tjaart. Thank you for leaving everything we had in South Africa so we could embrace this adventure together; for encouraging me and helping me keep a clear perspective; for your common sense and steadfastness; for believing in me and supporting me throughout this study. I could not have done it without you.

Soli Deo Gloria.

Contents

List of Figures

List of Tables

Abbreviations

AHM: adaptive harmonic model
AM: amplitude-modulated
CWT: continuous wavelet transform
EEMD: ensemble empirical mode decomposition
EMD: empirical mode decomposition
FM: frequency-modulated
FRA: frequency reassignment
GCV: generalized cross-validation
HSA: Hilbert spectral analysis
IA: instantaneous amplitude
IF: instantaneous frequency
IMF: intrinsic mode function
NHT: normalized Hilbert transform
SST: synchrosqueezed wavelet transform
VM: vanishing moment

Chapter 1

Introduction

Time-frequency analysis is one of the most important and powerful tools in signal processing for understanding the oscillatory features of signals.

Let us consider the signal (or function)

$$f(t) = a_0 + \sum_{j=1}^{N} a_j \cos(2\pi\omega_j t), \tag{1.0.1}$$

for arbitrary real values $\omega_j > 0$ and $a_j \in \mathbb{R}$. It is clear from (1.0.1) that f is a superposition of the signal components $f_j(t) = a_j \cos(2\pi\omega_j t),\ j = 1, \ldots, N$, each with a frequency of ω_jHz. Since each ω_j is a constant, independent of the time variable t, such a signal is classified as *stationary*.

However, most real-world signals (for example, biological signals, speech signals and music signals) are *non-stationary*, meaning that their frequencies may change with time. In the literature, these types of signals are represented by a generalization of the model in (1.0.1), namely

$$f(t) = A_0(t) + \sum_{j=1}^{N} A_j(t) \cos 2\pi\phi_j(t), \tag{1.0.2}$$

where $A_j(t) \geq 0$ and each $\phi_j(t)$ is a general C^1 function such that $\phi_j'(t) > 0$ (where C^1 denotes the space of all functions with continuous first derivatives). The derivative $\phi_j'(t)$ is a natural extension of the frequency ω_j in (1.0.1), and is called the *instantaneous frequency* (IF) of the component

$f_j(t) = A_j(t)\cos 2\pi\phi_j(t),\ j = 1, \ldots, N$. While the mathematical theory to analyze stationary signals is well developed in the literature (and is mainly founded on Fourier analysis), the study of non-stationary signals is still a relatively new field, only developing over the last thirty years [31, 17, 23, 2].

The contributions of this dissertation can be grouped into two parts: first, the development of a spline interpolation scheme, which is then applied in the second part, which concerns the non-stationary signal analysis problem described above.

In the first part, we formulate a new spline interpolation scheme for a bounded interval $[a, b]$, in terms of the m^{th} order B-splines. We start by developing a quasi-interpolation operator $\mathcal{Q}_m$ with a local formulation (in the sense that the value of $\mathcal{Q}_m$ applied to a given function f at any $x^* \in [a, b]$ only depends on the values of f in a small neighborhood of x^*), which preserves polynomials of degree $\leq m - 1$. This quasi-interpolation operator is based on a scheme introduced in [9]; however, the method in [9] is formulated for an unbounded interval, and is adapted here (in a non-trivial way) for a bounded interval.

The next step is to develop a local spline interpolation operator $\mathcal{R}_m$, such that $\mathcal{R}_m f$ interpolates the function f at a given sequence of discrete data points in $[a, b]$ and satisfies certain Hermite interpolation conditions at the endpoints of the interval $x = a$ and $x = b$. We base our local spline interpolation operator on an idea described in [15]; it is adapted here to include the Hermite interpolation conditions at the endpoints.

The quasi-interpolation operator $\mathcal{Q}_m$ and interpolation operator $\mathcal{R}_m$ are then combined in a smart way to form a so-called *blending operator* $\mathcal{P}_m$ (first considered in [13]), such that $\mathcal{P}_m$ meets all the requirements met by $\mathcal{Q}_m$ and $\mathcal{R}_m$. Corresponding error bounds for both $\mathcal{Q}_m$ and $\mathcal{P}_m$ are also derived rigorously.

The local formulation and boundary considerations make this spline interpolation method particularly useful. A specific application for this scheme is presented in our approach to instantaneous frequency estimation of non-stationary signal components, considered in the second part of this dissertation.

The *empirical mode decomposition* (EMD) algorithm, introduced by N.E. Huang and others in 1998 [36], is currently one of the most popular mathematical schemes for non-stationary signal decomposition and time-frequency analysis. The objective of EMD is to decompose a given (non-stationary) signal into a number of oscillating components, called *intrinsic mode functions* (IMF's), and a monotone or slowly oscillating remainder. This is done through an algorithm that is based on standard cubic spline interpolation. Each IMF is then extended to an amplitude-frequency modulated (AM-FM) signal through *Hilbert spectral analysis* (HSA), based on the Hilbert transform, in order to compute its instantaneous frequency and amplitude.

However, the EMD scheme, and the current modifications and improvements of it [53, 55], have several limitations. Firstly, there is no guarantee that the AM-FM extension of an IMF will yield a non-negative IF. This is a serious defect, since negative frequency is meaningless for signals and limits the application of EMD. Moreover, since the Hilbert transform is defined for functions on an unbounded interval, while real-life signals are typically defined on bounded or half-infinite intervals, artificial extension of an IMF to the real line is necessary in order to apply the Hilbert transform, often yielding unreliable results.

Instead of computing the IF's after the signal is decomposed as is done when applying EMD, the approach that I. Daubechies and others [20, 21] proposed is to first estimate the IF's of the signal components, under the assumption that the signal satisfies certain strict properties of the model in (1.0.2), before recovering the signal components of the model. For this purpose, the notion of the *synchrosqueezed wavelet transform* (SST), based on the continuous wavelet transform, was introduced to compute a single reassignment rule, or IF reference function, through which the IF's of all the signal components are "squeezed out" from the input signal in the form of a digital image displaying a set of IF curves, allowing the estimation of the individual IF functions and the signal components themselves.

Again, there are a few limitations to the SST. First, to estimate the instantaneous frequencies of signal components, the IF curves represented in the digital image output of the SST must be extracted, one by one, through

a suitable curve fitting scheme. In general, this can be quite complicated, particularly for over four of five IF curves, and therefore, the process must be supervised. Moreover, the SST's original formulation is not suited to real-time implementation.

Our approach to instantaneous frequency estimation of non-stationary signal components consists of combining the "best" parts of EMD and SST to form a hybrid EMD-SST scheme. In a nutshell, we apply a modified SST to each IMF produced by a modified EMD. With this approach, we are assured of non-negative instantaneous frequencies of the IMF's through the SST, while the EMD eliminates the need to extract multiple IF curves from the digital image output of the original SST approach. In addition, since the Hilbert transform of the original EMD approach is replaced by our modified SST, artificial extension of the IMF's to the real line is avoided, solving many computational issues. The modification of the SST consists in applying so-called *analytic vanishing moment wavelets* with stacked knots (first considered in [15]) to allow processing of signals on bounded or half-infinite time intervals, as well as applying spline curve fitting with optimal smoothing parameter selection through generalized cross-validation to identify the IF curve displayed in the digital image output of the SST. The modification of EMD consists in replacing the standard cubic spline interpolation in the original algorithm with our real-time spline interpolation scheme for bounded intervals.

According to our results, the instantaneous frequency estimation of signal components is remarkably more accurate when using our approach, compared to the original EMD-HSA approach. The construction of IMF's through EMD is also improved by our real-time spline interpolation scheme.

The next chapter is devoted to the study of the preliminary results that we will rely on in this dissertation. Specifically, we will study the theory of Fourier series and the Fourier transform, B-splines and spline interpolation, the continuous wavelet transform, and the Hilbert transform.

In Chapter 3, we introduce our quasi-interpolation scheme for a bounded interval in terms of the m^{th} order B-splines. We consider two variants of this scheme, developed for different types of knot sequences and sampling points. A corresponding approximation order analysis is also derived. We

formulate our local spline interpolation operator in Chapter 4, again considering two variants for different knot sequences and sampling points. The blending operator and corresponding error bounds are also derived in Chapter 4.

Next, we move on to the second part of the dissertation, namely the study of instantaneous frequency estimation of non-stationary signal components. To this end, we start, in Chapter 5, by considering the notions of stationary and non-stationary signals in greater detail, as well as different time-frequency methods in the literature. The EMD algorithm, some modifications and improvements of it and its limitations are studied in detail in Chapter 6, while the SST and its limitations are discussed in Chapter 7. The essential properties and computational algorithms of the analytic vanishing moment wavelets are described in Chapter 8. In Chapter 9, we describe our hybrid EMD-SST scheme in greater detail and provide graphical results, numerical experiments and comparisons, based on a number of representative test signals.

Final remarks and conclusions follow in Chapter 10.

Chapter 2

Preliminaries

This chapter is devoted to the development of preliminary results that will be needed later in this dissertation.

In Section 2.1, we discuss Fourier series, with specific reference to the Fourier cosine series (which occur often in signal processing applications). The Fourier transform and its properties are studied in Section 2.2. Section 2.3 is devoted to B-splines and its properties, and in Section 2.4, we consider the basic theory of spline interpolation, including quasi-interpolation and Hermite interpolation. Next, in Section 2.5, we define the notions of wavelets and the continuous wavelet transform. Lastly, in Section 2.6, we consider the Hilbert spectral analysis technique, a method in the signal analysis literature to estimate a signal's instantaneous frequency, which is based on the Hilbert transform.

2.1 Fourier series

Traditionally, signal analysis has been based on finding a Fourier representation of a signal. In this section, we examine the notions of *Fourier series* and *Fourier cosine series*.

To this end, let $L^2[-\frac{L}{2}, \frac{L}{2}]$ denote the set of square-integrable functions on $[-\frac{L}{2}, \frac{L}{2}]$ (for some $L > 0$). Any function $f \in L^2[-\frac{L}{2}, \frac{L}{2}]$ can be extended

to an L-periodic function $F(x)$ on $\mathbb{R}$ through the definition

$$\begin{cases} F(x) = f(x), \quad x \in (-\frac{L}{2}, \frac{L}{2}); \\ F(-\frac{L}{2}) = F(\frac{L}{2}) = \frac{1}{2}\left(f(\frac{L}{2}) + f(-\frac{L}{2})\right); \\ F(x + kL) = F(x), \quad k \in \mathbb{Z}. \end{cases}$$

For convenience, we will rename $F(x)$ as $f(x)$ also. With this definition, we denote the inner product space of all L-periodic square-integrable functions by $L^{2\star}[-\frac{L}{2}, \frac{L}{2}]$, with inner product

$$\langle f, g\rangle = \int_{-\frac{L}{2}}^{\frac{L}{2}} f(x)\overline{g(x)}\mathrm{d}x.$$

Definition 2.1.1 (Fourier series) *If $f \in L^{2\star}$, its Fourier series $\mathcal{S}f$ is defined by*

$$(\mathcal{S}f)(x) = \frac{a_0}{2} + \sum_{j=1}^{\infty}\left(a_j \cos\left(\frac{2\pi jx}{L}\right) + b_j \sin\left(\frac{2\pi jx}{L}\right)\right), \tag{2.1.1}$$

where

$$\begin{cases} a_j = \dfrac{2}{L}\displaystyle\int_{-\infty}^{\infty} f(x)\cos\left(\frac{2\pi jx}{L}\right)\mathrm{d}x, \quad j = 0, 1, 2, \ldots; \\ b_j = \dfrac{2}{L}\displaystyle\int_{-\infty}^{\infty} f(x)\sin\left(\frac{2\pi jx}{L}\right)\mathrm{d}x, \quad j = 1, 2, \ldots. \end{cases} \tag{2.1.2}$$

The significance of the Fourier series in Definition 2.1.1 is the following (see [14, Theorem 2, p.282]):

Theorem 2.1.1 (Fourier series) *For $L > 0$, the family*

$$\left\{\frac{1}{\sqrt{L}}, \sqrt{\frac{2}{L}}\cos\left(\frac{2\pi jx}{L}\right), \sqrt{\frac{2}{L}}\sin\left(\frac{2\pi jx}{L}\right) : \ j = 1, 2, \ldots\right\}$$

is an orthonormal basis of $L^2[-\frac{L}{2}, \frac{L}{2}]$. Therefore, any $f \in L^2[-\frac{L}{2}, \frac{L}{2}]$ can be represented by its Fourier series, namely

$$f(x) = (\mathcal{S}f)(x) = \frac{a_0}{2} + \sum_{j=1}^{\infty}\left(a_j \cos\left(\frac{2\pi jx}{L}\right) + b_j \sin\left(\frac{2\pi jx}{L}\right)\right),$$

which converges to f in $L^2[-\frac{L}{2}, \frac{L}{2}]$, where a_j, $j = 0, 1, 2, \ldots$ and b_j, $j = 1, 2, \ldots$ are defined in (2.1.2).

The convergence of the Fourier series in Theorem 2.1.1 rests upon the fact that the partial sums of the Fourier series of f are best L^2-approximations of f from the space of all trigonometric polynomials, and is proved in [14, Chapter 6].

For signal analysis, to reduce computational complexity, it is customary in the literature to find a Fourier cosine series representation of a signal instead of the Fourier series representation in terms of both cosines and sines. To this end, we consider a function $f \in L^2[0, \frac{L}{2}]$, and extend f to an even function f_e on $[-\frac{L}{2}, \frac{L}{2}]$ through the definition

$$f_e(x) := \begin{cases} f(x), & 0 \leq x \leq \frac{L}{2}, \\ f(-x), & -\frac{L}{2} \leq x < 0. \end{cases}$$

This implies that the coefficient b_j of the Fourier series of f_e (defined in (2.1.2)) is 0, since $\sin\left(\frac{2\pi jx}{L}\right)$ in (2.1.2) is an odd function. Therefore, the Fourier series in (2.1.1) of f_e reduces to the Fourier cosine series

$$(\mathcal{S}f_e)(x) = \frac{a_0}{2} + \sum_{j=1}^{\infty} a_j \cos\left(\frac{2\pi jx}{L}\right),$$

with

$$a_j = \frac{2}{L}\int_{-\frac{L}{2}}^{\frac{L}{2}} f_e(x)\cos\left(\frac{2\pi jx}{L}\right)\mathrm{d}x = \frac{4}{L}\int_0^{\frac{L}{2}} f(x)\cos\left(\frac{2\pi jx}{L}\right)\mathrm{d}x,$$

for $j = 0, 1, 2, \ldots$. From Theorem 2.1.1, we have that

$$(\mathcal{S}_n f_e)(x) = \frac{a_0}{2} + \sum_{j=1}^{n} a_j \cos\left(\frac{2\pi jx}{L}\right)$$

converges to f_e in $L^2[-\frac{L}{2}, \frac{L}{2}]$ as $n \to \infty$, so that $\mathcal{S}_n f_e$ restricted to $[0, \frac{L}{2}]$ converges to f in $L^2[0, \frac{L}{2}]$.

We therefore have the following (see [14, Theorem 3, p.284]):

Theorem 2.1.2 (Fourier cosine series) *For $L > 0$, the family*

$$\left\{ \frac{1}{\sqrt{L}}, \sqrt{\frac{2}{L}} \cos\left(\frac{2\pi jx}{L}\right) : \ j = 1, 2, \ldots \right\}$$

is an orthonormal basis of $L^2[0, \frac{L}{2}]$. Therefore, any $f \in L^2[0, \frac{L}{2}]$ can be represented by its Fourier cosine series, namely

$$f(x) = (\mathcal{S}^e f)(x) = \frac{a_0}{2} + \sum_{j=1}^{\infty} a_j \cos\left(\frac{2\pi jx}{L}\right),$$

which converges to f in $L^2[0, \frac{L}{2}]$, where a_j, $j = 0, 1, 2, \ldots$ is given by

$$a_j = \frac{4}{L} \int_0^{\frac{L}{2}} f(x) \cos\left(\frac{2\pi jx}{L}\right) \mathrm{d}x, \quad j = 0, 1, 2, \ldots.$$

We note that a Fourier sine representation may be found in a similar way (by extending the function $f \in L^2[0, \frac{L}{2}]$ to an odd function instead of an even one), but this is not conventional for signal analysis in the literature.

2.2 Fourier transform

The Fourier series, considered in Section 2.1, provides us with a method to study the frequency contents of periodic functions (as we shall see in Chapter 5). In this section, we consider the *Fourier transform*, which may be used instead to study the frequency contents of stationary signals.

Definition 2.2.1 (Fourier transform) *Let f be a function in $L^1(\mathbb{R})$, where L^1 denotes the space of all integrable functions. Then the Fourier transform of f, which we denote by $\hat{f}$ or $\mathcal{F}f$, is defined by*

$$\hat{f}(\omega) = (\mathcal{F}f)(\omega) = \int_{-\infty}^{\infty} f(x) e^{-i2\pi\omega x} \mathrm{d}x, \quad \omega \in \mathbb{R}. \tag{2.2.1}$$

In Theorem 2.2.1, we list some important properties of the Fourier transform of a function f in $L^1(\mathbb{R})$ or $L^1[0, \infty)$. We will make use of the following function operations:

- Even extension:
  For $f \in L^1[0,\infty)$, the even extension f_e of f is defined by

$$f_e(x) := \begin{cases} f(x), & x \geq 0; \\ f(-x), & x < 0. \end{cases} \tag{2.2.2}$$

- Translation:
  For $f \in L^1(\mathbb{R})$ and $b \in \mathbb{R}$, the translation operator T_b is given by

$$(T_b f)(x) := f(x-b). \tag{2.2.3}$$

- Dilation:
  For $f \in L^1(\mathbb{R})$ and $a > 0$, the dilation operator D_a is defined by

$$(D_a f)(x) := f(ax). \tag{2.2.4}$$

- Frequency modulation:
  For $f \in L^1(\mathbb{R})$ and $c \in \mathbb{R},\ c \neq 0$, the (frequency) modulation operator M_c is defined by

$$(M_c f)(x) := f(x)e^{i2\pi cx}. \tag{2.2.5}$$

- Convolution:
  Let $f,\ h$ be functions on $\mathbb{R}$. Then the convolution of f with h is defined by

$$(f \star h)(x) := \int_{-\infty}^{\infty} f(t)h(x-t)\mathrm{d}t. \tag{2.2.6}$$

We note that each of the function operations in (2.2.2)-(2.2.5) are in $L^1(\mathbb{R})$. If $f, h \in L^1(\mathbb{R})$, then the convolution $f \star h$ in (2.2.6) is also in $L^1(\mathbb{R})$; that is,

$$\int_{-\infty}^{\infty} |(f \star h)(x)|\mathrm{d}x \leq \int_{-\infty}^{\infty}\int_{-\infty}^{\infty} |f(t)h(x-t)|\mathrm{d}t\mathrm{d}x < \infty. \tag{2.2.7}$$

This follows from Fubini's Theorem (see, for example, [14, Theorem 1, p.376]), by which we may interchange the order of integration in (2.2.7).

Theorem 2.2.1 (Properties of Fourier transform) *The Fourier transform satisfies the following properties:*

(i) Let f_e be the even extension of $f \in L^1[0,\infty)$. Then

$$\hat{f}_e(\omega) = 2\int_0^\infty f(x)\cos 2\pi\omega x \mathrm{d}x;$$

(ii) For $f \in L^1(\mathbb{R})$ and $b \in \mathbb{R}$,

$$\widehat{(T_b f)}(\omega) = e^{-i2\pi\omega b}\hat{f}(\omega); \tag{2.2.8}$$

(iii) For $f \in L^1(\mathbb{R})$ and $a > 0$,

$$\widehat{(D_a f)}(\omega) = \frac{1}{a}\hat{f}\left(\frac{\omega}{a}\right); \tag{2.2.9}$$

(iv) For $f \in L^1(\mathbb{R})$ and $c \in \mathbb{R},\ c \neq 0$,

$$\widehat{(M_c f)}(\omega) = \hat{f}\left(\omega - c\right); \tag{2.2.10}$$

(v) Let $f, h \in L^1(\mathbb{R})$. Then

$$\widehat{(f \star h)}(\omega) = \hat{f}(\omega)\hat{h}(\omega).$$

Proof:

(i) From (2.2.1) and (2.2.2), we have

$$\begin{aligned}
\hat{f}_e(\omega) &= \int_{-\infty}^{\infty} f_e(x)e^{-i2\pi\omega x}\mathrm{d}x \\
&= \int_{-\infty}^{0} f(-x)e^{-i2\pi\omega x}\mathrm{d}x + \int_0^\infty f(x)e^{-i2\pi\omega x}\mathrm{d}x \\
&= -\int_{\infty}^{0} f(x)e^{i2\pi\omega x}\mathrm{d}x + \int_0^\infty f(x)e^{-i2\pi\omega x}\mathrm{d}x \\
&= \int_0^\infty f(x)\left[e^{i2\pi\omega x} + e^{-i2\pi\omega x}\right]\mathrm{d}x = 2\int_0^\infty f(x)\cos 2\pi\omega x \mathrm{d}x,
\end{aligned}$$

from Euler's formula $e^{i\theta} = \cos\theta + i\sin\theta$ for $\theta \in \mathbb{R}$.

(ii) From (2.2.1) and (2.2.3), it follows that

$$\begin{aligned}\widehat{(T_b f)}(\omega) &= \int_{-\infty}^{\infty} f(x-b)e^{-i2\pi\omega x}\mathrm{d}x \\ &= \int_{-\infty}^{\infty} f(x)e^{-i2\pi\omega(x+b)}\mathrm{d}x \\ &= e^{-i2\pi\omega b}\int_{-\infty}^{\infty} f(x)e^{-i2\pi\omega x}\mathrm{d}x = e^{-i2\pi\omega b}\hat{f}(\omega).\end{aligned}$$

(iii) From (2.2.1) and (2.2.4), it follows that

$$\begin{aligned}\widehat{(D_a f)}(\omega) &= \int_{-\infty}^{\infty} f(ax)e^{-i2\pi\omega x}\mathrm{d}x \\ &= \frac{1}{a}\int_{-\infty}^{\infty} f(x)e^{-i2\pi\omega(x/a)}\mathrm{d}x \\ &= \frac{1}{a}\int_{-\infty}^{\infty} f(x)e^{-i2\pi(\omega/a)x}\mathrm{d}x = \frac{1}{a}\hat{f}\left(\frac{\omega}{a}\right).\end{aligned}$$

(iv) From (2.2.1) and (2.2.5), it follows that

$$\begin{aligned}\widehat{(M_c f)}(\omega) &= \int_{-\infty}^{\infty} f(x)e^{i2\pi cx}e^{-i2\pi\omega x}\mathrm{d}x \\ &= \int_{-\infty}^{\infty} f(x)e^{-i2\pi(\omega-c)x}\mathrm{d}x = \hat{f}(\omega-c).\end{aligned}$$

(v) From (2.2.1), (2.2.6) and Fubini's theorem, we have

$$\begin{aligned}\widehat{(f\star h)}(\omega) &= \int_{-\infty}^{\infty}(f\star h)(x)e^{-i2\pi\omega x}\mathrm{d}x \\ &= \int_{-\infty}^{\infty}\left[\int_{-\infty}^{\infty} f(t)h(x-t)\mathrm{d}t\right]e^{-i2\pi\omega x}\mathrm{d}x \\ &= \int_{-\infty}^{\infty} f(t)\left[\int_{-\infty}^{\infty} h(x-t)e^{-i2\pi\omega x}\mathrm{d}x\right]\mathrm{d}t \\ &= \int_{-\infty}^{\infty} f(t)\left[\int_{-\infty}^{\infty} h(x)e^{-i2\pi\omega(x+t)}\mathrm{d}x\right]\mathrm{d}t \\ &= \int_{-\infty}^{\infty} f(t)\hat{h}(\omega)e^{-i2\pi\omega t}\mathrm{d}t = \hat{f}(\omega)\hat{h}(\omega).\end{aligned}$$

■

Example 2.2.1

(a) For $f(x) = \cos 2\pi cx$ *with* $c > 0$,

$$\hat{f}(\omega) = \frac{1}{2}\left(\delta(\omega - c) + \delta(\omega + c)\right). \tag{2.2.11}$$

(b) For $f(x) = \sin 2\pi cx$ *with* $c > 0$,

$$\hat{f}(\omega) = \frac{1}{2i}\left(\delta(\omega - c) - \delta(\omega + c)\right). \tag{2.2.12}$$

Solution:

(a) From the definition of the Fourier transform in (2.2.1), we have

$$\begin{aligned}
\hat{f}(\omega) &= \int_{-\infty}^{\infty} \cos(2\pi cx) e^{-i2\pi\omega x} \mathrm{d}x \\
&= \frac{1}{2}\int_{-\infty}^{\infty} \left(e^{i2\pi cx} + e^{-i2\pi cx}\right) e^{-i2\pi\omega x} \mathrm{d}x \\
&= \frac{1}{2}\int_{-\infty}^{\infty} \left(e^{-i2\pi(\omega - c)x} + e^{-i2\pi(\omega + c)x}\right) \mathrm{d}x \\
&= \frac{1}{2}\left(\delta\left(\omega - c\right) + \delta\left(\omega + c\right)\right),
\end{aligned}$$

where δ denotes the Dirac delta distribution.

(b) The solution is obtained in a similar way to the solution of (2.2.11) above. ■

If $f \in L^2(\mathbb{R})$ such that its Fourier transform $\hat{f}$ is in $L^1(\mathbb{R})$, f may be recovered from its Fourier transform (as shown in [14, Theorem 4, p.335]):

Theorem 2.2.2 (Inverse Fourier transform) *For a function* $f \in L^2(\mathbb{R})$, *let* $g(\omega) = \hat{f}(\omega) \in L^1(\mathbb{R})$. *Then*

$$f(x) = \check{g}(x) := \int_{-\infty}^{\infty} g(\omega) e^{i2\pi\omega x} \mathrm{d}\omega.$$

The function $\check{g}$ *is called the inverse Fourier transform of* f.

In Section 5.1 in Chapter 5, we will see how the Fourier transform may be applied to reveal the frequency content of stationary signals.

2.3 B-splines

We start this section by defining the m^{th} order spline space $S_{\mathbf{x},m}[a,b]$ with knot sequence $\mathbf{x}$, for $m \geq 1$.

Definition 2.3.1 (Spline space) *For positive integers m and N and $a, b \in \mathbb{R}$, let*

$$\mathbf{x}: \quad x_{-m+1} = \cdots = a = x_0 < x_1 < \cdots < x_{N+1} = b = \cdots = x_{N+m}. \tag{2.3.1}$$

We denote by $S_{\mathbf{x},m}[a,b]$ the linear space of m^{th} order polynomial splines on $[a,b]$ with knots in $\mathbf{x}$, namely

$$S_{\mathbf{x},m}[a,b] = \left\{ f(x) \in C^{m-2}[a,b] : \ f|_{[x_i,x_{i+1}]} \in \pi_{m-1}, \ i = 0,\ldots,N \right\}, \tag{2.3.2}$$

where $C^{m-2}[a,b]$ denotes the space of all functions on $[a,b]$ with $m-2$ continuous derivatives, and π_{m-1} denotes the space of all polynomials of degree $\leq m-1$.

As shown in [19],[6, Theorem IX.1], a locally supported basis for $S_{\mathbf{x},m}[a,b]$ is given by the set of normalized m^{th} order *B-splines*

$$\{N_{\mathbf{x},m,j} : \ j = -m+1,\ldots,N\},$$

where each $N_{\mathbf{x},m,j}$ is defined in terms of divided differences of truncated powers (to be made precise in Definition 2.3.2 below). Divided differences are defined by

$$[u,\ldots,u]g := \frac{g^{\ell}(u)}{\ell!} \tag{2.3.3}$$

if there are $\ell+1$ entries in $[u\ldots,u]$, and

$$[u_0,\ldots,u_n]g := \frac{[u_1,\ldots,u_n]g - [u_0,\ldots,u_{n-1}]g}{u_n - u_0} \tag{2.3.4}$$

if $u_0 \leq u_1 \leq \cdots \leq u_n$ with $u_n > u_0$, where $[u_i]g := g(u_i)$. The truncated powers are given by

$$x_+^n := (\max\{0,x\})^n. \tag{2.3.5}$$

Definition 2.3.2 (B-splines) *For the sequence* $\mathbf{x}$ *in (2.3.1), the normalized* m^{th} *order B-splines* $N_{\mathbf{x},m,j},\ j = -m+1,\ldots,N$, *are defined by*

$$N_{\mathbf{x},m,j}(x) := (x_{j+m} - x_j)[x_j,\ldots,x_{j+m}](\cdot - x)_+^{m-1}, \quad j = -m+1,\ldots,N. \tag{2.3.6}$$

For the knot sequence $\mathbf{x}$ in (2.3.1), the B-splines $N_{\mathbf{x},m,j},\ j = 0,\ldots,N-m+1$, are called *interior B-splines*, while $N_{\mathbf{x},m,j},\ j = -m+1,\ldots,-1; N-m+2,\ldots,N$, are called *left hand side* and *right hand side boundary B-splines*, respectively.

We note that

$$N_{\mathbf{x},m,j} \equiv 0,\ j \notin \{-m+1,\ldots,N\}\,. \tag{2.3.7}$$

By expanding the divided differences in the definition of B-splines (2.3.6), we obtain the following special formulations for the boundary B-splines $N_{\mathbf{x},m,-m+1}$ and $N_{\mathbf{x},m,N}$.

Theorem 2.3.1 (Boundary B-splines) *For the knot sequence* $\mathbf{x}$ *in (2.3.1), the boundary B-splines* $N_{\mathbf{x},m,-m+1}$ *and* $N_{\mathbf{x},m,N}$ *satisfy the formulations*

$$N_{\mathbf{x},m,-m+1}(x) = \begin{cases} \left(\frac{x_1-x}{x_1-a}\right)^{m-1}, & a \le x \le x_1; \\ 0, & \text{otherwise}, \end{cases} \tag{2.3.8}$$

and

$$N_{\mathbf{x},m,N}(x) = \begin{cases} \left(\frac{x-x_N}{b-x_N}\right)^{m-1}, & x_N \le x \le b; \\ 0, & \text{otherwise}. \end{cases} \tag{2.3.9}$$

Proof:

We proceed to prove (2.3.9); the proof of (2.3.8) is similar.

From (2.3.6) and the definition of divided differences in (2.3.3)-(2.3.4), we have

$N_{\mathbf{x},m,N}(x)$

$$
\begin{aligned}
&= (x_{N+m} - x_N)\,[x_N, \ldots, x_{N+m}]\,(\cdot - x)_+^{m-1} \\
&= (x_{N+m} - x_N)\,\frac{[x_{N+1}, \ldots, x_{N+m}]\,(\cdot - x)_+^{m-1} - [x_N, \ldots, x_{N+m-1}]\,(\cdot - x)_+^{m-1}}{x_{N+m} - x_N} \\
&= \frac{(m-1)!\,(b-x)_+^0}{(m-1)!} \\
&\qquad - \frac{[x_{N+1}, \ldots, x_{N+m-1}]\,(\cdot - x)_+^{m-1} - [x_N, \ldots, x_{N+m-2}]\,(\cdot - x)_+^{m-1}}{x_{N+m-1} - x_N} \\
&= \frac{(m-1)!\,(b-x)_+^0}{(m-1)!} - \frac{(m-1)!\,(b-x)_+^1}{(m-2)!1!(b-x_N)} \\
&\qquad + \frac{[x_{N+1}, \ldots, x_{N+m-2}]\,(\cdot - x)_+^{m-1} - [x_N, \ldots, x_{N+m-3}]\,(\cdot - x)_+^{m-1}}{(b-x)(x_{N+m-2} - x_N)} \\
&= \frac{(m-1)!\,(b-x)_+^0}{(m-1)!} - \frac{(m-1)!\,(b-x)_+^1}{(m-2)!1!(b-x_N)} + \frac{(m-1)!\,(b-x)_+^2}{(m-3)!2!(b-x_N)^2} \\
&\qquad - \frac{[x_{N+1}, \ldots, x_{N+m-3}]\,(\cdot - x)_+^{m-1} - [x_N, \ldots, x_{N+m-4}]\,(\cdot - x)_+^{m-1}}{(b-x_N)^2(x_{N+m-3} - x_N)} \\
&= \cdots \\
&= \sum_{i=0}^{m-1} (-1)^i \binom{m-1}{i} \frac{(b-x)_+^i}{(b-x_N)^i} + \frac{(-1)^m (x_N - x)_+^{m-1}}{(b-x_N)^{m-1}}.
\end{aligned}
$$

From the definition of truncated powers (2.3.5), we have

$$N_{\mathbf{x},m,N}(x) = 0, \quad x > b.$$

Therefore, let $x \leq b$, so that

$$
\begin{aligned}
&N_{\mathbf{x},m,N}(x) \\
&= \sum_{i=0}^{m-1} (-1)^i \binom{m-1}{i} \left(\frac{b-x}{b-x_N}\right)^i + \frac{(-1)^m (x_N - x)_+^{m-1}}{(b-x_N)^{m-1}} \\
&= \sum_{i=0}^{m-1} \binom{m-1}{i} \left(\frac{x-b}{b-x_N}\right)^i + \frac{(-1)^m (x_N - x)_+^{m-1}}{(b-x_N)^{m-1}} \\
&= \left(\frac{x-b}{b-x_N} + 1\right)^{m-1} + \frac{(-1)^m (x_N - x)_+^{m-1}}{(b-x_N)^{m-1}} \\
&= \left(\frac{x-x_N}{b-x_N}\right)^{m-1} + \frac{(-1)^m (x_N - x)_+^{m-1}}{(b-x_N)^{m-1}},
\end{aligned}
$$

from the binomial theorem. If $x < x_N$, it follows from the definition of truncated powers (2.3.5) that

$$N_{\mathbf{x},m,N}(x) = \left(\frac{x - x_N}{b - x_N}\right)^{m-1} + \frac{(-1)^m (x_N - x)^{m-1}}{(b - x_N)^{m-1}}$$
$$= \left(\frac{x - x_N}{b - x_N}\right)^{m-1} - \left(\frac{x - x_N}{b - x_N}\right)^{m-1} = 0,$$

while, if $x_N \leq x \leq b$, we have

$$N_{\mathbf{x},m,N}(x) = \left(\frac{x - x_N}{b - x_N}\right)^{m-1},$$

again from (2.3.5), completing our proof of (2.3.9). ■

The normalized m^{th} order B-splines $N_{\mathbf{x},m,j},\ j = -m+1, \ldots, N$, in (2.3.6) satisfy the following properties (see, for example, [12, Theorem 6.4] and [22, Theorems 10.2.2, 10.2.5, 10.2.6] and [5]).

Theorem 2.3.2 (Properties of B-splines) *The B-splines* $\{N_{\mathbf{x},m,j} : \ j = -m+1, \ldots, N\}$ *with knot sequence* $\mathbf{x}$*, as defined in (2.3.6) and (2.3.1), respectively, satisfy the following properties:*

(i)

$$\text{supp} N_{\mathbf{x}m,j} = [a, b] \cap [x_j, x_{j+m}], \quad j = -m+1, \ldots, N; \tag{2.3.10}$$

(ii) $N_{\mathbf{x},m,j},\ j = -m+1, \ldots, N$, *may be computed recursively through*

$$N_{\mathbf{x},m,j}(x) = \frac{x - x_j}{x_{j+m-1} - x_j} N_{\mathbf{x},m-1,j}(x) + \frac{x_{j+m} - x}{x_{j+m} - x_{j+1}} N_{\mathbf{x},m-1,j+1}(x), \tag{2.3.11}$$

where

$$N_{\mathbf{x},1,j}(x) = \chi_{[x_j, x_{j+1})(x)}, \quad j = 0, \ldots, N, \tag{2.3.12}$$

the characteristic function on the interval $[x_j, x_{j+1})$*;*

(iii)

$$N_{\mathbf{x},m,j}(x) > 0, \quad x \in (x_j, x_{j+m}); \tag{2.3.13}$$

(iv) The B-splines $\{N_{\mathbf{x},m,j} : j = -m+1, \ldots, N\}$ *form a partition of unity; that is,*

$$\sum_{j=-m+1}^{N} N_{\mathbf{x},m,j}(x) = 1, \quad x \in [a,b]; \tag{2.3.14}$$

(v) The derivative of $N_{\mathbf{x},m,j}$, $j = -m+1, \ldots, N$, *may be computed recursively through*

$$N'_{\mathbf{x},m,j}(x) = \frac{m-1}{x_{j+m-1} - x_j} N_{\mathbf{x},m-1,j}(x) - \frac{m-1}{x_{j+m} - x_{j+1}} N_{\mathbf{x},m-1,j+1}(x), \tag{2.3.15}$$

for $m \geq 2$.

Proof:

(i) First, let $x > x_{j+m}$ for some fixed j. Then

$$N_{\mathbf{x},m,j}(x) = (x_{j+m} - x_j)[x_j, \ldots, x_{j+m}](\cdot - x)_+^{m-1} = 0,$$

from the definition of truncated powers. On the other hand, if we let $x < x_j$, we have

$$\begin{aligned} N_{\mathbf{x},m,j}(x) &= (x_{j+m} - x_j)[x_j, \ldots, x_{j+m}](\cdot - x)_+^{m-1} \\ &= (x_{j+m} - x_j)[x_j, \ldots, x_{j+m}](\cdot - x)^{m-1}. \end{aligned} \tag{2.3.16}$$

We now use the fact that, if g is a function with n continuous derivatives in the smallest interval containing the points $\{u_0, \ldots, u_n\}$, then

$$[u_0, \ldots, u_n]g = \frac{g^{(n)}(\xi)}{n!}$$

for some point ξ in the smallest interval containing the points $\{u_0, \ldots, u_n\}$ (see [22, Theorem 2.1.2]). With $g := (\cdot - x)^{m-1}$, (2.3.16) therefore becomes

$$N_{\mathbf{x},m,j}(x) = (x_{j+m} - x_j)[x_j, \ldots, x_{j+m}]g = (x_{j+m} - x_j)\frac{g^{(m)}(\xi)}{m!} = 0,$$

where ξ is some point in the smallest interval containing $\{x_j, \ldots, x_{j+m}\}$, since $g \in \pi_{m-1}$.

(ii) The formulation (2.3.12) for $N_{\mathbf{x},1,j},\ j = 0, \ldots, N$, follows directly from the definition (2.3.6) with $m = 1$ and the definition of divided differences (2.3.4).

For $j = -m + 1$ and $j = N$, the formulation (2.3.11) follows from Theorem 2.3.1. Indeed, if $j = N$ and $x \in \mathbb{R}$ is fixed, we have

$$\begin{aligned}
&\frac{x - x_N}{x_{N+m-1} - x_N} N_{\mathbf{x},m-1,N}(x) + \frac{x_{N+m} - x}{x_{N+m} - x_{N+1}} N_{\mathbf{x},m-1,N+1}(x) \\
&= \frac{x - x_N}{b - x_N} \left(\frac{x - x_N}{b - x_N} \right)^{m-2} + 0 \\
&= \left(\frac{x - x_N}{b - x_N} \right)^{m-1} = N_{\mathbf{x},m,N}(x),
\end{aligned}$$

using also (2.3.7). The result follows similarly if $j = -m + 1$.

Hence, let $j \in \{-m + 2, \ldots, N - 1\}$, so that $x_{j+m-1} > x_j$ and $x_j > x_{j+1}$ both hold, and let $x \in \mathbb{R}$ be fixed. To prove (2.3.11), we recall the Leibniz rule for the divided difference of a product, namely, for two functions f and g and any sequence of points $\{u_0, \ldots, u_n\}$,

$$[u_0, \ldots, u_n](fg) = \sum_{j=0}^{n} [u_0, \ldots, u_j] f [u_j, \ldots, u_n] g.$$

(see [45, Theorem 2.52]). Using also (2.3.6) and (2.3.4), we have

$$\begin{aligned}
&N_{\mathbf{x},m,j}(x) \\
&= (x_{j+m} - x_j)[x_j, \ldots, x_{j+m}](\cdot - x)_+^{m-1} \\
&= (x_{j+m} - x_j)[x_j, \ldots, x_{j+m}](\cdot - x)(\cdot - x)_+^{m-2} \\
&= (x_{j+m} - x_j) \sum_{k=j}^{j+m} [x_j, \ldots, x_k](\cdot - x)[x_k, \ldots, x_{j+m}](\cdot - x)_+^{m-2} \\
&= (x_{j+m} - x_j) \left[(x_j - x)[x_j, \ldots, x_{j+m}](\cdot - x)_+^{m-2} \right. \\
&\qquad \left. + [x_{j+1}, \ldots, x_{j+m}](\cdot - x)_+^{m-2} \right] \\
&= (x_{j+m} - x_j) \times \\
&\left[(x_j - x) \frac{[x_{j+1}, \ldots, x_{j+m}](\cdot - x)_+^{m-2} - [x_j - x_{j+m-1}](\cdot - x)_+^{m-2}}{x_{j+m} - x_j} \right.
\end{aligned}$$

$$
\begin{aligned}
&\qquad\qquad\qquad\qquad + [x_{j+1},\ldots,x_{j+m}](\cdot - x)_+^{m-2}\Big] \\
&= (x_j - x)[x_{j+1},\ldots,x_{j+m}](\cdot - x)_+^{m-2} \\
&\qquad -(x_j - x)[x_j,\ldots,x_{j+m-1}](\cdot - x)_+^{m-2} \\
&\qquad\qquad +(x_{j+m} - x_j)[x_{j+1},\ldots,x_{j+m}](\cdot - x)_+^{m-2} \\
&= [x_{j+1},\ldots,x_{j+m}](\cdot - x)_+^{m-2}\,(x_j - x + x_{j+m} - x_j) \\
&\qquad\qquad +(x - x_j)[x_j,\ldots,x_{j+m-1}](\cdot - x)_+^{m-2} \\
&= \frac{x_{j+m} - x}{x_{j+m} - x_{j+1}}\,(x_{j+m} - x_{j+1})\,[x_{j+1},\ldots,x_{j+m}](\cdot - x)_+^{m-2} \\
&\qquad + \frac{x - x_j}{x_{j+m-1} - x_j}\,(x_{j+m-1} - x_j)\,[x_j,\ldots,x_{j+m-1}](\cdot - x)_+^{m-2} \\
&= \frac{x_{j+m} - x}{x_{j+m} - x_{j+1}} N_{\mathbf{x},m-1,j+1}(x) + \frac{x - x_j}{x_{j+m-1} - x_j} N_{\mathbf{x},m-1,j}(x).
\end{aligned}
$$

(iii) We know that $\text{supp}N_{\mathbf{x},m,j} = [x_j, x_{j+m}]$, $j = -m+1,\ldots,N$, so that $N_{\mathbf{x},m,j}(x) = 0$, $x \in \mathbb{R} \setminus [x_j, x_{j+m}]$. We now proceed to show by induction that (2.3.13) holds. Since $N_{\mathbf{x},1,j}(x) = \chi_{[x_j,x_{j+1})}(x)$ (as follows from (ii)), it is clear that the result holds for $m = 1$. Next, we assume that (2.3.13) holds for a fixed non-negative integer $m-1$, and let $x \in (x_j, x_{j+m})$. From the recursion formula (2.3.11), we have

$$
N_{\mathbf{x},m,j}(x) = \frac{x - x_j}{x_{j+m-1} - x_j} N_{\mathbf{x},m-1,j}(x) + \frac{x_{j+m} - x}{x_{j+m} - x_{j+1}} N_{\mathbf{x},m-1,j+1}(x).
$$

Next, we note that, from the support property (2.3.10),

$$
\begin{cases} N_{\mathbf{x},m-1,j}(x) = 0, & x \in [x_{j+m-1}, x_{j+m}); \\ N_{\mathbf{x},m-1,j+1}(x) = 0, & x \in (x_j, x_{j+1}], \end{cases}
$$

for all $j = -m+1,\ldots,N$. Therefore, using also the induction hypothesis, we deduce that

$$
N_{\mathbf{x},m,j}(x) > 0, \quad x \in (x_j, x_{j+m}),
$$

for all $j = -m+1,\ldots,N$, which completes our inductive proof of (2.3.13).

(iv) Our proof is once again by induction on m. Since $N_{\mathbf{x},1,j}(x) = \chi_{[x_j,x_{j+1})}(x)$, it is clear that (2.3.14) holds for $m = 1$. Next, we assume the result

holds for a fixed non-negative integer $m-1$ and let $x \in [a,b]$. From the recursive formulation in (2.3.11), it follows that

$$\begin{aligned}
&\sum_{j=-m+1}^{N} N_{\mathbf{x},m,j}(x) \\
&= \sum_{j=-m+1}^{N} \frac{x-x_j}{x_{j+m-1}-x_j} N_{\mathbf{x},m-1,j}(x) + \sum_{j=-m+1}^{N} \frac{x_{j+m}-x}{x_{j+m}-x_{j+1}} N_{\mathbf{x},m-1,j+1}(x) \\
&= \sum_{j=-m+1}^{N} \frac{x-x_j}{x_{j+m-1}-x_j} N_{\mathbf{x},m-1,j}(x) + \sum_{j=-m+2}^{N+1} \frac{x_{j+m-1}-x}{x_{j+m-1}-x_j} N_{\mathbf{x},m-1,j}(x) \\
&= \sum_{j=-m+2}^{N} \frac{x-x_j}{x_{j+m-1}-x_j} N_{\mathbf{x},m-1,j}(x) + \sum_{j=-m+2}^{N} \frac{x_{j+m-1}-x}{x_{j+m-1}-x_j} N_{\mathbf{x},m-1,j}(x),
\end{aligned}$$

from the support property (2.3.10). It therefore follows that

$$\begin{aligned}
\sum_{j=-m+1}^{N} N_{\mathbf{x},m,j}(x) &= \sum_{j=-m+2}^{N} \frac{x-x_j+x_{j+m-1}-x}{x_{j+m-1}-x_j} N_{\mathbf{x},m-1,j}(x) \\
&= \sum_{j=-m+2}^{N} \frac{x_{j+m-1}-x_j}{x_{j+m-1}-x_j} N_{\mathbf{x},m-1,j}(x) \\
&= \sum_{j=-m+2}^{N} N_{\mathbf{x},m-1,j}(x) = 1,
\end{aligned}$$

from the induction hypothesis, completing our proof of (2.3.14).

(v) Lastly, to verify (2.3.15), we differentiate (2.3.6) and use (2.3.4) to obtain

$$\begin{aligned}
N'_{\mathbf{x},m,j}(x) &= -(m-1)\,(x_{j+m}-x_j)\,[x_j,\ldots,x_{j+m}]\,(\cdot-x)_+^{m-2} \\
&= -(m-1)\,(x_{j+m}-x_j)\times \\
&\qquad \frac{[x_{j+1},\ldots,x_{j+m}]\,(\cdot-x)_+^{m-2} - [x_j,\ldots,x_{j+m-1}]\,(\cdot-x)_+^{m-2}}{x_{j+m}-x_j} \\
&= -(m-1)\,[x_{j+1},\ldots,x_{j+m}]\,(\cdot-x)_+^{m-2} \\
&\qquad\qquad +(m-1)\,[x_j,\ldots,x_{j+m-1}]\,(\cdot-x)_+^{m-2}
\end{aligned}$$

$$
\begin{aligned}
&= -\frac{m-1}{x_{j+m}-x_{j+1}}\left(x_{j+m}-x_{j+1}\right)\left[x_{j+1},\ldots,x_{j+m}\right]\left(\cdot-x\right)_+^{m-2} \\
&\quad +\frac{m-1}{x_{j+m-1}-x_j}\left(x_{j+m-1}-x_j\right)\left[x_j,\ldots,x_{j+m-1}\right]\left(\cdot-x\right)_+^{m-2} \\
&= \frac{m-1}{x_{j+m-1}-x_j}N_{\mathbf{x},m-1,j}(x)-\frac{m-1}{x_{j+m}-x_{j+1}}N_{\mathbf{x},m-1,j+1}(x),
\end{aligned}
$$

from (2.3.6). ■

2.4 Spline interpolation

B-splines are useful in many applications, including spline interpolation and approximations problems (the applications that we will be studying in this dissertation).

Before defining a spline interpolation operator in terms of B-splines of any arbitrary order, we start this section by reviewing the *standard cubic spline interpolation scheme* in [6, Chapter IV], since it is one of the most popular interpolation methods in current applications (due to the simplicity to implement it).

For a function $f : [a, b] \to \mathbb{R}$ and a sequence

$$\mathbf{y}: \quad a = y_1 < y_2 < \cdots < y_n = b,$$

we proceed to investigate the construction of a cubic spline interpolant S, with knot sequence $\mathbf{y}$, that satisfies the interpolation conditions

$$S(y_i) = f(y_i), \quad i = 1, \ldots, n.$$

Since S is a cubic polynomial spline, we know that

$$S \in C^2 \quad \text{and} \quad S|_{[y_i,y_{i+1}]} \in \pi_3$$

(as in (2.3.2)). Therefore, we have

$$S(x) = p_i(x), \quad x \in [y_i, y_{i+1}],$$

for all $i = 1, \ldots, n-1$, for some cubic polynomials

$$p_i(x) = a_i + b_i\left(x-y_i\right) + c_i\left(x-y_i\right)^2 + d_i\left(x-y_i\right)^3, \quad i = 1, \ldots, n-1, \tag{2.4.1}$$

such that

$$\begin{cases} p_i(y_i) = f(y_i); & p_i(y_{i+1}) = f(y_{i+1}); \\ p_i'(y_i) = s_i; & p_i'(y_{i+1}) = s_{i+1}, \end{cases} \tag{2.4.2}$$

for $i = 1, \ldots, n-1$, where $s_1, \ldots, s_n$ are free parameters determining the slope of each polynomial p_i, and such that

$$p_{i-1}''(y_i) = p_i''(y_i), \quad i = 2, \ldots, n-1. \tag{2.4.3}$$

By substituting the conditions (2.4.2) in the polynomial formulations (2.4.1), we may solve for $a_i,\ b_i,\ c_i,\ d_i,\ i = 1, \ldots, n-1$, in terms of the parameters $s_1, \ldots, s_n$. Assuming that the parameters s_1 and s_n are chosen by the user in some way, the remaining $n-2$ free parameters $s_2, \ldots, s_{n-1}$ are then determined uniquely by the $n-2$ conditions in (2.4.3).

There exist different approaches in the literature to choosing the boundary slopes s_1 and s_n. The most popular techniques include the so-called *natural* spline interpolation, where s_1 and s_n are chosen to satisfy the *free-end* condition $S''(y_1) = S''(y_n) = 0$, and the spline resulting from the *not-a-knot* condition $p_1 = p_2$ and $p_{n-2} = p_{n-1}$ (so that the knots y_2 and y_{n-1} are not active).

We now turn our attention to spline interpolation schemes in terms of B-splines with arbitrary order m (the type of spline interpolation methods that we will be considering in this dissertation), and where the spline knot sequence $\mathbf{x}$ need not coincide with the interpolation points $\mathbf{y}$.

For a function $f : [a, b] \to \mathbb{R}$, we will be interested in finding a spline interpolation operator $\mathcal{S}_m : C[a, b] \to S_{\mathbf{x},m}$, where $C[a, b]$ denotes the space of continuous functions on the interval $[a, b]$ and with the spline space $S_{\mathbf{x},m}$ defined in (2.3.2) for the knot sequence $\mathbf{x}$ in (2.3.1), such that the spline $\mathcal{S}_m f$ interpolates the function f at a given sequence of discrete data points on the interval $[a, b]$.

Since the set of normalized B-splines $\{N_{\mathbf{x},m,j} :\ j = -m+1, \ldots, N\}$ forms a basis for the spline space $S_{\mathbf{x},m}$, the dimension of $S_{\mathbf{x},m}$ is $m+N$. This means that we can accommodate $m + N$ interpolation conditions on the interval $[a, b]$.

Definition 2.4.1 (Spline interpolation operator) *Given a function* $f : [a,b] \to \mathbb{R}$*, let* $\mathbf{y} = \{y_1, \ldots, y_{m+N}\}$ *denote a sequence of* $m+N$ *distinct points in the interval* $[a,b]$*, with*

$$\mathbf{y}: \quad a \leq y_1 < y_2 < \cdots y_{m+N} \leq b. \tag{2.4.4}$$

Then the spline interpolation operator $\mathcal{S}_m : C[a,b] \to S_{\mathbf{x},m}$*, with knot sequence* $\mathbf{x}$ *given in (2.3.1), satisfies the* $m+N$ *interpolation conditions*

$$(\mathcal{S}_m f)(y_i) = f(y_i), \quad i = 1, \ldots, m+N. \tag{2.4.5}$$

Spline interpolation has the advantage over traditional polynomial interpolation (for example, the Lagrange and Newton interpolation formulas [22, Sections 1.2, 1.3]) that the approximation accuracy may be improved by decreasing the distance between consecutive knots in $\mathbf{x}$ while keeping the polynomial degree $m-1$ relatively low.

Now, since $\{N_{\mathbf{x},m,j} : \ j = -m+1, \ldots, N\}$ forms a basis for the spline space $S_{\mathbf{x},m}$, we know that there exists a spline $\mathcal{S}_m f$ satisfying (2.4.5) if and only if

$$(\mathcal{S}_m f)(x) = \sum_{j=-m+1}^{N} c_j^f N_{\mathbf{x},m,j}(x), \quad x \in [a,b]$$

for certain coefficients $\left\{c_{-m+1}^f, \ldots, c_N^f\right\} \subseteq \mathbb{R}$, such that

$$\sum_{j=-m+1}^{N} c_j^f N_{\mathbf{x},m,j}(y_i) = f(y_i), \quad i = 1, \ldots, m+N. \tag{2.4.6}$$

In other words, the vector $\mathbf{c}_f := \left(c_{-m+1}^f, \ldots, c_N^f\right)^T \in \mathbb{R}^{m+N}$, where $\mathbb{R}^{m+N}$ denotes the $(m+N)$-dimensional real space, is a solution to the matrix equation

$$A_{m,N}\mathbf{c}_f = \mathbf{f}_{m+N},$$

with $\mathbf{f}_{m+N} := (f(y_1), \ldots, f(y_{m+N}))^T \in \mathbb{R}^{m+N}$, and where $A_{m,N}$ is the $(m+N) \times (m+N)$ coefficient matrix

$$A_{m,N} = \begin{bmatrix} N_{\mathbf{x},m,-m+1}(y_1) & N_{\mathbf{x},m,-m+2}(y_1) & \cdots & N_{\mathbf{x},m,N}(y_1) \\ N_{\mathbf{x},m,-m+1}(y_2) & N_{\mathbf{x},m,-m+2}(y_2) & \cdots & N_{\mathbf{x},m,N}(y_2) \\ \vdots & \vdots & & \vdots \\ N_{\mathbf{x},m,-m+1}(y_{m+N}) & N_{\mathbf{x},m,-m+2}(y_{m+N}) & \cdots & N_{\mathbf{x},m,N}(y_{m+N}) \end{bmatrix}. \tag{2.4.7}$$

A necessary and sufficient condition for the matrix $A_{m,N}$ to be invertible is given by the Schoenberg-Whitney theorem [44]:

Theorem 2.4.1 (Schoenberg-Whitney) *The matrix $A_{m,N}$ in (2.4.7) of the linear system (2.4.6) is invertible if and only if*

$$N_{\mathbf{x},m,-m+i}(y_i) \neq 0, \quad i = 1, \ldots, m+N.$$

In other words, from the B-spline support property (2.3.10), the linear system (2.4.6) has a unique solution if and only if

$$x_{-m+i} \leq y_i \leq x_i, \quad i = 1, \ldots, m+N,$$

in which case the spline interpolant is given by

$$(\mathcal{S}_m f)(x) = \sum_{j=-m+1}^{N} \left(A_{m,N}^{-1} \mathbf{f}_{m+N}\right)_j N_{\mathbf{x},m,j}(x), \quad x \in [a,b]. \tag{2.4.8}$$

This gives an existence and uniqueness result for spline interpolation in terms of the normalized m^{th} order B-splines, for any arbitrary order m.

In general, the inverse matrix $A_{m,N}^{-1}$ is not banded, but a full matrix. This means that the value of $(\mathcal{S}_m f)(x)$ in (2.4.8) at any $x \in [a,b]$ depends on most, if not all, of the function values $\{f(y_1), \ldots, f(y_{m+N})\}$. The spline interpolant in (2.4.8) is therefore not a local interpolant. In Chapter 4, we will investigate the construction of local interpolation schemes in terms of B-splines.

In some applications, it might be advantageous to not only interpolate function values $f(y_i)$, $i = 1, \ldots, m+N$, as in (2.4.5) in Definition 2.4.1,

but derivative values of f as well. If $\{r_1, \ldots, r_{m+N}\}$ is a sequence of $m+N$ non-negative integers such that

$$r_1 + \cdots + r_{m+N} = m + N,$$

the $m+N$ interpolation conditions in (2.4.5) in Definition 2.4.1 become

$$(\mathcal{S}_m f)^{(\ell)}(y_i) = f^{(\ell)}(y_i), \quad \ell = 1, \ldots, r_i;\ i = 1, \ldots, m+N,$$

called *Hermite interpolation conditions*. We will investigate spline interpolation operators with this type of interpolation conditions in Chapter 4.

We note that, in practice, the ℓ^{th} order derivative values of the function f may also be approximated with the ℓ^{th} order divided differences of f, with the divided differences defined in (2.3.3)-(2.3.4).

In this dissertation, we will also be interested in certain spline approximation operators, called *quasi-interpolation operators*, first introduced by De Boor and Fix in [7].

Definition 2.4.2 (Spline quasi-interpolation operator) *The spline approximation operator $\mathcal{Q}_m : C[a,b] \to S_{\mathbf{x},m}$ with knot sequence $\mathbf{x}$ in (2.3.1) is called a quasi-interpolation operator if it reproduces polynomials of degree $\leq n$ for any non-negative integer n; that is,*

$$(\mathcal{Q}_m p)(x) = p(x), \quad x \in [a,b], \tag{2.4.9}$$

for polynomials $p \in \pi_n$.

Again, since $\{N_{\mathbf{x},m,j} :\ j = -m+1, \ldots, N\}$ forms a basis for the spline space $S_{\mathbf{x},m}$, we know that there exists a spline $\mathcal{Q}_m f$ satisfying (2.4.9) if

$$(\mathcal{Q}_m f)(x) = \sum_{j=-m+1}^{N} c_j^f N_{\mathbf{x},m,j}(x), \quad x \in [a,b]$$

for certain coefficients $\left\{c_{-m+1}^f, \ldots, c_N^f\right\} \subseteq \mathbb{R}$, such that

$$\sum_{j=-m+1}^{N} c_j^p N_{\mathbf{x},m,j}(x) = p(x), \quad p \in \pi_n.$$

We will investigate the construction of quasi-interpolation operators, with a local formulation in terms of the normalized m^{th} order B-splines, in Chapter 3.

2.5 Continuous wavelet transform

Let us consider a function $\psi \in L^2(\mathbb{R})$. If ψ satisfies the conditions

$$\psi(x) \to 0, \quad x \to \pm\infty, \tag{2.5.1}$$

and

$$\text{p.v.} \int_{-\infty}^{\infty} \psi(x)\mathrm{d}x = \lim_{A\to\infty} \int_{-A}^{A} \psi(x)\mathrm{d}x = 0, \tag{2.5.2}$$

where "p.v." denotes the Cauchy principal value, then ψ is called a *wavelet*. From (2.5.2), we see that ψ oscillates (ψ has a "wavy" shape), while the condition (2.5.1) ensures that the function ψ dies down as $x \to \pm\infty$, so that the graph of ψ looks like a "short wave" or wavelet.

Given a wavelet ψ, we can generate a whole family of wavelets through

$$\psi_{b,a}(x) := \frac{1}{a}\psi\left(\frac{x-b}{a}\right), \tag{2.5.3}$$

where $b \in \mathbb{R}$ and $a > 0$. The factor a is used to adjust the scale and length of the wavelet, while the support interval of $\psi_{b,a}$ can be shifted over the entire real axis by changing the value of b.

There are many applications of wavelets in the literature. In this dissertation, we will mainly be interested in the *continuous wavelet transform* (CWT), where the wavelets $\psi_{b,a}$ (2.5.3) generated by ψ are used as integration kernel.

Definition 2.5.1 (Continuous wavelet transform) *For a function $f \in L^2(\mathbb{R})$, the CWT $\mathcal{W}_\psi f$ of f at the time-scale point (b, a) is defined as the inner product of f with the wavelet $\psi_{b,a}$; that is,*

$$(\mathcal{W}_\psi f)(b, a) = \langle f, \psi_{b,a}\rangle = \frac{1}{a}\int_{-\infty}^{\infty} f(x)\overline{\psi\left(\frac{x-b}{a}\right)}\mathrm{d}x. \tag{2.5.4}$$

The CWT is a time-frequency method used to analyze the time and frequency contents of a function f. In this regard, the wavelet $\psi_{b,a}$ is called a *window function*, and it is used to localize f in order to examine its time and frequency contents. This localization depends on the width of the window function. In general, the window width of a time-frequency window function is calculated as follows.

Definition 2.5.2 (Time-frequency window width) *Let $u \in (L^1 \cap L^2)(\mathbb{R})$ be a non-trivial window function such that $xu(x) \in L^2(\mathbb{R})$. The center of the localization window function $u(x)$ is defined by*

$$x_u^\star := \frac{\int_{-\infty}^{\infty} x|u(x)|^2 \mathrm{d}x}{\int_{-\infty}^{\infty} |u(x)|^2 \mathrm{d}x}, \tag{2.5.5}$$

and the radius of the window function $u(x)$ is defined by

$$\Delta_u := \left[\frac{\int_{-\infty}^{\infty} (x - x_u^\star)^2 |u(x)|^2 \mathrm{d}x}{\int_{-\infty}^{\infty} |u(x)|^2 \mathrm{d}x} \right]^{\frac{1}{2}}. \tag{2.5.6}$$

The window width of $u(x)$ is defined by $2\Delta_u$.

With this definition, and using also (2.5.3), we may calculate the center of the window function $\psi_{b,a}$ to be

$$x_{\psi_{b,a}}^\star = \frac{\int_{-\infty}^{\infty} x|\psi\left(\frac{x-b}{a}\right)|^2 \mathrm{d}x}{\int_{-\infty}^{\infty} |\psi\left(\frac{x-b}{a}\right)|^2 \mathrm{d}x} = \frac{\int_{-\infty}^{\infty} (ax+b)|\psi(x)|^2 \mathrm{d}x}{\int_{-\infty}^{\infty} |\psi(x)|^2 \mathrm{d}x} = ax_\psi^\star + b,$$

while

$$\begin{aligned} \Delta_{\psi_{b,a}} &= \left[\frac{\int_{-\infty}^{\infty} (x - x_{\psi_{b,a}}^\star)^2 |\psi\left(\frac{x-b}{a}\right)|^2 \mathrm{d}x}{\int_{-\infty}^{\infty} |\psi\left(\frac{x-b}{a}\right)|^2 \mathrm{d}x} \right]^{\frac{1}{2}} \\ &= \left[\frac{\int_{-\infty}^{\infty} (ax + b - (ax_\psi^\star + b))^2 |\psi(x)|^2 \mathrm{d}x}{\int_{-\infty}^{\infty} |\psi(x)|^2 \mathrm{d}x} \right]^{\frac{1}{2}} = a\Delta_\psi. \end{aligned} \tag{2.5.7}$$

With the Fourier transform of a function $f \in L^1(\mathbb{R})$ defined by (2.2.1), we may also consider $\omega_{\hat{\psi}_{b,a}}^\star$ and $\Delta_{\hat{\psi}_{b,a}}$, which describe the center and radius of the window function $\hat{\psi}_{b,a}$ in the frequency domain. Since

$$\hat{\psi}_{b,a}(\omega) = e^{-i2\pi\omega b} \hat{\psi}(a\omega),$$

from the definition (2.5.3) of $\psi_{b,a}$ and the Fourier transform properties (2.2.8) and (2.2.9) in Theorem 2.2.1, we have

$$\omega_{\hat{\psi}_{b,a}}^\star = \frac{\int_{-\infty}^{\infty} \omega|\hat{\psi}(a\omega)|^2 \mathrm{d}\omega}{\int_{-\infty}^{\infty} |\hat{\psi}(a\omega)|^2 \mathrm{d}\omega} = \frac{\int_{-\infty}^{\infty} \frac{\omega}{a}|\hat{\psi}(\omega)|^2 \mathrm{d}\omega}{\int_{-\infty}^{\infty} |\hat{\psi}(\omega)|^2 \mathrm{d}\omega} = \frac{1}{a}\omega_{\hat{\psi}}^\star$$

and

$$\Delta_{\hat{\psi}_{b,a}} = \left[\frac{\int_{-\infty}^{\infty}(\omega-\omega^{\star}_{\hat{\psi}_{b,a}})^2|\hat{\psi}(a\omega)|^2\mathrm{d}\omega}{\int_{-\infty}^{\infty}|\hat{\psi}(a\omega)|^2\mathrm{d}\omega}\right]^{\frac{1}{2}}$$
$$= \left[\frac{\int_{-\infty}^{\infty}(\frac{\omega}{a}-\frac{\omega^{\star}_{\hat{\psi}}}{a})^2|\hat{\psi}(\omega)|^2\mathrm{d}\omega}{\int_{-\infty}^{\infty}|\hat{\psi}(\omega)|^2\mathrm{d}\omega}\right]^{\frac{1}{2}} = \frac{1}{a}\Delta_{\hat{\psi}}, \tag{2.5.8}$$

from (2.5.5) and (2.5.6).

From (2.5.7) and (2.5.8), it is clear that the localization window $\psi_{b,a}$ in the CWT has the advantage that the window width is not fixed (in contrast to the short-time Fourier transform, for example [14, (7.4.1), p.354]); it varies with a. When the value of a is larger, the window width $2\Delta_{\psi_{b,a}} = 2a\Delta_{\psi}$ widens (in other words, the CWT "zooms out"), while the frequency window width $2\Delta_{\hat{\psi}_{b,a}} = \frac{2}{a}\Delta_{\hat{\psi}}$ narrows, facilitating analysis of high-frequency contents. On the other hand, when the value of a is smaller, the window width $2a\Delta_{\psi}$ narrows (the CWT "zooms in"), providing higher resolution in the time domain, while the frequency window width $\frac{2}{a}\Delta_{\hat{\psi}}$ widens.

At the same time, the window function $\psi_{b,a}$ "slides" across the entire real axis as the value of $b \in \mathbb{R}$ changes. In this way, the window $\psi_{b,a}$ facilitates the analysis of f for different time and frequency detail over the whole real line or "time axis".

The CWT is equipped with an "inversion" or "recovery" formula, called the *inverse CWT*. This allows us to recover a function f from its CWT $\mathcal{W}_{\psi}f$ (see [14, Theorem 3, p.391]).

Theorem 2.5.1 (Inverse continuous wavelet transform) *Let $\psi \in L^2(\mathbb{R})$ be an admissible wavelet, in the sense that*

$$C_{\psi} := \int_0^{\infty}\frac{|\hat{\psi}(\omega)|^2}{\omega}\mathrm{d}\omega < \infty.$$

Then

$$f(x) = \frac{1}{C_{\psi}}\int_0^{\infty}\left[\int_{-\infty}^{\infty}(\mathcal{W}_{\psi}f)(b,a)\psi\left(\frac{x-b}{a}\right)\mathrm{d}b\right]\frac{\mathrm{d}a}{a^2},$$

for all $f \in (L^2 \cap L^\infty)(\mathbb{R})$, where L^∞ denotes the space of all bounded functions.

2.6 Hilbert spectral analysis

We end this chapter by considering the notion of Hilbert spectral analysis, which is based on the Hilbert transform, defined as follows.

Definition 2.6.1 (Hilbert transform) *Let f be a measurable real-valued function and let*

$$h(x) := \frac{1}{\pi x}$$

denote the Hilbert kernel. Then the Hilbert transform of f is defined as the convolution of f with the Hilbert kernel h; that is,

$$(\mathcal{H}f)(x) = (h \star f)(x) = \frac{1}{\pi}\text{p.v.} \int_{-\infty}^{\infty} \frac{f(s)}{x-s}\mathrm{d}s, \tag{2.6.1}$$

or, equivalently,

$$(\mathcal{H}f)(x) = \frac{1}{\pi}\text{p.v.} \int_{-\infty}^{\infty} \frac{f(x-s)}{s}\mathrm{d}s,$$

provided that the integral in (2.6.1) exists and is finite.

The Hilbert transform in (2.6.1) satisfies the following properties (see [40, Chapter 4]):

Theorem 2.6.1 (Properties of Hilbert transform) *The Hilbert transform operator in (2.6.1) satisfies the following properties:*

(i) The Hilbert transform operator is linear; that is, for real-valued functions f and g and $a, b, \in \mathbb{R}$,

$$\mathcal{H}(af + bg) = a\mathcal{H}f + b\mathcal{H}g;$$

(ii) For a real-valued function f and $a, b \in \mathbb{R}$,

$$\mathcal{H}\left(f(ax+b)\right) = \text{sgn}(a)(\mathcal{H}f)(ax+b),$$

where sgn *denotes the sign of* a*, namely*

$$\operatorname{sgn}(a) := \begin{cases} -1, & \text{if } a < 0; \\ 0, & \text{if } a = 0; \\ 1, & \text{if } a > 0; \end{cases}$$

(iii) For a real-valued function f*,*

$$\mathcal{H}\left(\frac{df(x)}{dx}\right) = \frac{d}{dx}(\mathcal{H}f)(x).$$

Proof:

(i) From the definition of the Hilbert transform in (2.6.1), it is clear that

$$\begin{aligned} \mathcal{H}(af+bg)(x) &= \frac{1}{\pi}\text{p.v.}\int_{-\infty}^{\infty}\frac{(af+bg)(s)}{x-s}\mathrm{d}s \\ &= \frac{a}{\pi}\text{p.v.}\int_{-\infty}^{\infty}\frac{f(s)}{x-s}\mathrm{d}s + \frac{b}{\pi}\text{p.v.}\int_{-\infty}^{\infty}\frac{g(s)}{x-s}\mathrm{d}s \\ &= a(\mathcal{H}f)(x) + b(\mathcal{H}g)(x). \end{aligned}$$

(ii) From (2.6.1), we have

$$\begin{aligned} \mathcal{H}\left(f(ax+b)\right) &= \frac{1}{\pi}\text{p.v.}\int_{-\infty}^{\infty}\frac{f(as+b)}{x-s}\mathrm{d}s \\ &= \begin{cases} \frac{1}{\pi}\text{p.v.}\int_{-\infty}^{\infty}\frac{f(s)}{ax+b-s}\mathrm{d}s, & a>0; \\ -\frac{1}{\pi}\text{p.v.}\int_{-\infty}^{\infty}\frac{f(s)}{ax+b-s}\mathrm{d}s, & a<0; \end{cases} \\ &= \operatorname{sgn}(a)\left(\mathcal{H}f\right)(ax+b). \end{aligned}$$

(iii) We start by recalling the Leibniz integral rule

$$\begin{aligned} &\frac{d}{dz}\int_{\alpha(z)}^{\beta(z)} f(x,z)dx \\ &\qquad = \int_{\alpha(z)}^{\beta(z)}\frac{\partial}{\partial z}f(x,z)dx + f(\beta(z),z)\frac{d\beta(z)}{dz} - f(\alpha(z),z)\frac{d\alpha(z)}{dz}, \end{aligned}$$

so that, if α and β are independent of z,

$$\frac{d}{dz}\int_{\alpha}^{\beta} f(x,z)dx = \int_{\alpha}^{\beta} \frac{\partial}{\partial z} f(x,z)dx.$$

We therefore have

$$\begin{aligned}
\frac{d}{dx}(\mathcal{H}f)(x) &= \frac{1}{\pi}\frac{d}{dx}\text{p.v.}\int_{-\infty}^{\infty}\frac{f(s)}{x-s}\text{d}s \\
&= \frac{1}{\pi}\frac{d}{dx}\text{p.v.}\int_{-\infty}^{\infty}\frac{f(x-s)}{s}\text{d}s \\
&= \frac{1}{\pi}\text{p.v.}\int_{-\infty}^{\infty}\frac{sf'(x-s)}{s^2}\text{d}s \\
&= \frac{1}{\pi}\text{p.v.}\int_{-\infty}^{\infty}\frac{f'(x-s)}{s}\text{d}s \\
&= \mathcal{H}\left(\frac{df(x)}{dx}\right)
\end{aligned}$$

■

We will also rely on the following two results. The first is a formulation of the Fourier transform applied to the Hilbert transform, the proof of which can be found in [40, pp.252-255].

Theorem 2.6.2 (Fourier transform applied to Hilbert transform) *For $f \in L^2(\mathbb{R})$,*

$$\widehat{(\mathcal{H}f)}(\omega) = -i\,\text{sgn}(\omega)\hat{f}(\omega). \tag{2.6.2}$$

The second is referred to as the *Hilbert transform product theorem* or *Bedrosian's theorem* [3].

Theorem 2.6.3 (Bedrosian) *Let $f, g \in L^2(\mathbb{R})$. If the Fourier transform $\hat{f}(\omega)$ of $f(x)$ vanishes for $|\omega| > a$, with $a > 0$, and the Fourier transform $\hat{g}(\omega)$ of $g(x)$ vanishes for $|\omega| < a$, then*

$$\mathcal{H}\left(f(x)g(x)\right) = f(x)(\mathcal{H}g)(x). \tag{2.6.3}$$

Example 2.6.1

(a) For $a \in \mathbb{R}$,

$$\mathcal{H}a = 0; \tag{2.6.4}$$

(b) For $f(x) = \cos 2\pi cx$ with $c > 0$,

$$(\mathcal{H}f)(x) = \sin 2\pi cx. \tag{2.6.5}$$

Solution:

(a) From the definition of the Hilbert transform in (2.6.1), we have

$$\begin{aligned}(\mathcal{H}a)(x) &= \frac{1}{\pi}\text{p.v.}\int_{-\infty}^{\infty}\frac{a}{x-s}\mathrm{d}s \\ &= \frac{a}{\pi}\lim_{A\to\infty}\left[-\ln|x-s|\right]_{-A}^{A} \\ &= \frac{a}{\pi}\lim_{A\to\infty}\ln\left|\frac{x+A}{x-A}\right| = 0.\end{aligned}$$

(b) Let $f(x) = \cos 2\pi cx$. Using (2.6.2) in Theorem 2.6.2 and (2.2.11)-(2.2.12) in Example 2.2.1, we know that

$$\begin{aligned}\mathcal{F}\left((\mathcal{H}f)(x)\right) &= -i\,\mathrm{sgn}(\omega)\hat{f}(\omega) \\ &= \frac{-i}{2}\,\mathrm{sgn}(\omega)\left[\delta(\omega-c)+\delta(\omega+c)\right] \\ &= \frac{1}{2i}\left[\delta(\omega-c)-\delta(\omega+c)\right] \\ &= \mathcal{F}\left(\sin 2\pi cx\right).\end{aligned}$$

Therefore,

$$(\mathcal{H}f)(x) = \sin 2\pi cx.$$

■

In this dissertation, we will be using the Hilbert transform to extend a given signal f to its *analytic signal representation* $f^\star$, given by

$$f^\star(t) = f(t) + i(\mathcal{H}f)(t). \tag{2.6.6}$$

This approach is commonly used in the area of signal processing and analysis to analyze a signal's instantaneous frequency information, and was first proposed by Dennis Gabor [26]. By taking the real part of the polar formulation of $f^\star$ in (2.6.6),the given signal $f(t)$ has the representation

$$f(t) = A(t)\cos 2\pi\theta(t), \tag{2.6.7}$$

where

$$A(t) = |f^\star(t)| = \left((f(t))^2 + ((\mathcal{H}f)(t))^2\right)^{\frac{1}{2}} \tag{2.6.8}$$

is called the *instantaneous amplitude* (IA) of f, and

$$\theta(t) = \frac{1}{2\pi}\tan^{-1}\left(\frac{\mathcal{H}f(t)}{f(t)}\right) \tag{2.6.9}$$

denotes the *instantaneous phase* of f. The instantaneous frequency ω is simply defined to be the time-derivative of the instantaneous phase; that is,

$$\omega(t) = \frac{d\theta(t)}{dt}, \tag{2.6.10}$$

as already mentioned in Chapter 1. (This terminology will be considered in general in Section 5.2 in Chapter 5.) This method of finding a signal's amplitude, frequency and phase information is called Hilbert spectral analysis in the current signal processing literature.

Since a negative IF is not physically meaningful, we include the following condition:

Theorem 2.6.4 (Non-negative IF) *The IF $\omega(t)$ in (2.6.10) is non-negative if and only if*

$$f(t)\left(\mathcal{H}f\right)'(t) - \left(\mathcal{H}f\right)(t)f'(t) \geq 0. \tag{2.6.11}$$

Proof:

From (2.6.10) and (2.6.9), we know that

$$\begin{aligned}\omega(t) &= \frac{1}{2\pi}\frac{d}{dt}\tan^{-1}\left(\frac{\mathcal{H}f(t)}{f(t)}\right) \\ &= \frac{1}{2\pi}\cdot\frac{1}{1+\left(\frac{(\mathcal{H}f)(t)}{f(t)}\right)^2}\cdot\frac{f(t)(\mathcal{H}f)'(t)-(\mathcal{H}f)(t)f'(t)}{(f(t))^2} \\ &= \frac{1}{2\pi}\frac{f(t)(\mathcal{H}f)'(t)-(\mathcal{H}f)(t)f'(t)}{(f(t))^2+((\mathcal{H}f)(t))^2}.\end{aligned}$$

Therefore, $\omega(t) \geq 0$ if and only if

$$f(t)\left(\mathcal{H}f\right)'(t) - \left(\mathcal{H}f\right)(t)f'(t) \geq 0.$$

■

As mentioned in Chapter 1, the empirical mode decomposition is one approach to signal decomposition and analysis that relies on the HSA technique described above. We will discuss this method in detail in Chapter 6.

Chapter 3

Quasi-interpolation

In this chapter, we define and describe a quasi-interpolation scheme (as introduced in Section 2.4 in Chapter 2) based on the m^{th} order B-splines (defined in (2.3.6) in Chapter 2). Our idea is to use this scheme, together with a local interpolation scheme (to be described in Chapter 4) to create a so-called blending operator (which will also be defined in Chapter 4). This operator is developed in such a way that it preserves the properties of both its constituent parts – it will therefore have a local formulation, preserve polynomials up to a certain degree, and satisfy certain interpolation conditions. This interpolation scheme may then be used in applications such as constructing upper and lower envelopes in the empirical mode decomposition algorithm (to be described in Section 6.1 of Chapter 6).

In Section 3.1, we start by developing a quasi-interpolation operator, in terms of the m^{th} order B-splines, that preserves polynomials p of degree $\leq m-1$. Our quasi-interpolation operator is based on a quasi-interpolation scheme for real-time application described in [9] – however, the method in [9] is derived for data values on an unbounded interval, and is adapted here (in a non-trivial way) for a bounded interval.

In Section 3.2, we develop a variation on the quasi-interpolation scheme described in Section 3.1 (where the spline knots are chosen to be equal to the sampling points) by adapting this scheme for the case where the knots are chosen to lie midway between every two consecutive sampling points. This setup facilitates a more symmetric formulation of the quasi-interpolation scheme.

The quasi-interpolation schemes in Sections 3.1 and 3.2 are exact on π_{m-1}; that is, when it is applied to a polynomial of degree $\leq m-1$, this exact polynomial is returned. In Section 3.3, we provide error bounds that describe how well a general, real-valued function f (that is not a polynomial) is approximated by these schemes.

3.1 Quasi-interpolation: Scheme E

For $m \geq 3$, let

$$\mathbf{y}: \quad a = y_0 < y_1 < \cdots < y_{N+1} = b \tag{3.1.1}$$

be a given sequence of (non-uniform) sampling points, and let f be a real-valued function. In this section, we develop a spline quasi-interpolation operator $\mathcal{Q}_m^E$, under the assumption that the B-spline knot sequence $\mathbf{x}$ is equal to the sampling point sequence $\mathbf{y}$. We append the $m-1$ stacked knots $x_{-m+1} = \cdots = x_{-1} = a$ and $b = x_{N+2} = \cdots = x_{N+m}$ on either side, so that the (non-uniform) knot sequence $\mathbf{x}$ is given by

$$\mathbf{x}: x_{-m+1} = \cdots = a = x_0 < x_1 < \cdots < x_{N+1} = b = \cdots = x_{N+m}. \tag{3.1.2}$$

In this section, we will therefore denote the sampling points $\mathbf{y}$ by $\mathbf{x}$ also, for convenience. This setup facilitates easy implementation in real-time applications in practice.

We will need the following notations.

First, $D(x_j, \ldots, x_{j+m-1})$ denotes the Vandermonde determinant of $x_j, \ldots, x_{j+m-1}$; that is,

$$D(x_j, \ldots, x_{j+m-1}) = \begin{vmatrix} 1 & 1 & \cdots & 1 \\ x_j & x_{j+1} & \cdots & x_{j+m-1} \\ \vdots & \vdots & & \vdots \\ x_j^{m-1} & x_{j+1}^{m-1} & \cdots & x_{j+m-1}^{m-1} \end{vmatrix}; \tag{3.1.3}$$

and $D(x_j, \ldots, x_{j+k-1}, \xi_{\mathbf{x},m,\ell}, x_{j+k+1}, \ldots, x_{j+m-1})$ is obtained from $D(x_j, \ldots, x_{j+m-1})$ by replacing its $(k+1)^{\text{th}}$ column with the vector

$$\xi_{\mathbf{x},m,\ell} := [\xi_{\mathbf{x}}^0(\ell), \ldots, \xi_{\mathbf{x}}^{m-1}(\ell)]^T, \tag{3.1.4}$$

with

$$\begin{cases} \xi_{\mathbf{x}}^0(\ell) = 1; \\ \xi_{\mathbf{x}}^n(\ell) = \dfrac{\sigma^n(x_{\ell+1}, \ldots, x_{\ell+m-1})}{\binom{m-1}{n}}, \quad n = 1, \ldots, m-1; \end{cases} \tag{3.1.5}$$

and where $\sigma^n(x_{\ell+1}, \ldots, x_{\ell+m-1})$ denotes the classical symmetric function, defined by

$$\begin{cases} \sigma^0(x_{\ell+1}, \ldots, x_{\ell+m-1}) = 1; \\ \sigma^n(x_{\ell+1}, \ldots, x_{\ell+m-1}) = \displaystyle\sum_{\ell+1 \le t_1 < t_2 < \cdots < t_n \le \ell+m-1} x_{t_1} x_{t_2} \cdots x_{t_n}, \\ \qquad\qquad\qquad\qquad\qquad\qquad\qquad\qquad n = 1, \ldots, m-1, \end{cases} \tag{3.1.6}$$

with the definition that $\sigma^n(x_{\ell+1}, \ldots, x_{\ell+m-1}) = 0$ if $n \ge m$.

Furthermore, $D_C(x_j, \ldots, x_{j+p}, x_{j+p}^{(1)}, \ldots, x_{j+p}^{(q)}, x_{j+p+1}, \ldots, x_{j+m-q-1})$ denotes the confluent Vandermonde determinant; that is, for $\ell = 1, \ldots, q$, the $(p+1+\ell)^{\text{th}}$ column of D_C is given by

$$(D_C)_{k,p+1+\ell} = \begin{cases} 0, & \text{if } k \le \ell; \\ \frac{(k-1)!}{(k-1-\ell)!} x_{j+p}^{k-1-\ell}, & \text{if } k > \ell. \end{cases} \tag{3.1.7}$$

(In other words, confluent columns are derivatives of the original Vandermonde columns.) The remaining $m-q$ columns of D_C are regular Vandermonde columns corresponding to $x_j, \ldots, x_{j+m-q-1}$ (as in (3.1.3)). Similar as above,
$D_C(x_j, \ldots, x_{j+p}, x_{j+p}^{(1)}, \ldots, x_{j+p}^{(k-1)}, \xi_{\mathbf{x},m,\ell}, x_{j+p}^{(k+1)}, \ldots, x_{j+p}^{(q)}, x_{j+p+1}, \ldots, x_{j+m-q-1})$ is obtained from $D_C(x_j, \ldots, x_{j+p}, x_{j+p}^{(1)}, \ldots, x_{j+p}^{(q)}, x_{j+p+1}, \ldots, x_{j+m-q-1})$ by replacing its $(p+k+1)^{\text{th}}$ column with $\xi_{\mathbf{x},m,\ell}$.

Definition 3.1.1 (Quasi-interpolation operator) *For an integer $m \ge 3$, the quasi-interpolation operator $\mathcal{Q}_m^E$ is defined by*

$$(\mathcal{Q}_m^E f)(x) := \sum_{\ell=1}^{m-1} f^{(\ell)}(a) M_{m,-\ell}^E(x) + \sum_{i=0}^{N+1} f(y_i) M_{m,i}^E(x) + \sum_{r=1}^{m-2} f^{(r)}(b) M_{m,N+1+r}^E(x), \tag{3.1.8}$$

in terms of the spline molecules

$$\begin{cases} M^E_{m,-\ell}(x) := \sum_{j=0}^{m-1-\ell} a^E_{m,-\ell,j} N_{\mathbf{x},m,j-m+1}(x), \quad \ell = 1,\dots,m-1; \\ M^E_{m,i}(x) := \sum_{j=0}^{m-1} a^E_{m,i,j} N_{\mathbf{x},m,i+j-m+1}(x), \quad i = 0,\dots,N; \\ M^E_{m,N+1+r}(x) := \sum_{j=r}^{m-2} a^E_{m,N+1+r,j} N_{\mathbf{x},m,N+j-m+2}(x), \quad r = 0,\dots,m-2, \end{cases} \tag{3.1.9}$$

where the coefficients are given by:

- *For* $i = 0,\dots,m-2,\ j = m-1-i,\dots,m-1,$ *and* $i = m-1,\dots,N+1-m,\ j = 0,\dots,m-1,$ *and* $i = N-m+2,\dots,N,\ j = 0,\dots,N-i$*:*

$$a^E_{m,i,j} = \frac{D(x_{i+j-m+1},\dots,x_{i-1},\xi_{\mathbf{x},m,i+j-m+1},x_{i+1},\dots,x_{i+j})}{D(x_{i+j-m+1},\dots,x_{i+j})}; \tag{3.1.10}$$

- *For* $i = 0,\dots,m-2,\ j = 0,\dots,m-2-i$*:*

$$a^E_{m,i,j} = \frac{D_C(x_0,x_0^{(1)},\dots,x_0^{(m-1-i-j)},x_1,\dots,x_{i-1},\xi_{\mathbf{x},m,i+j-m+1},x_{i+1},\dots,x_{i+j})}{D_C(x_0,x_0^{(1)},\dots,x_0^{(m-1-i-j)},x_1,\dots,x_{i+j})}; \tag{3.1.11}$$

- *For* $\ell = 1,\dots,m-1,\ j = 0,\dots,m-1-\ell$*:*

$$a^E_{m,-\ell,j} = \frac{D_C(x_0,x_0^{(1)},\dots,x_0^{(\ell-1)},\xi_{\mathbf{x},m,j-m+1},x_0^{(\ell+1)},\dots,x_0^{(m-1-j)},x_1,\dots,x_j)}{D_C(x_0,x_0^{(1)},\dots,x_0^{(m-1-j)},x_1,\dots,x_j)}; \tag{3.1.12}$$

- *For* $i = N-m+2,\dots,N,\ j = N-i+1,\dots,m-1$*:*

$$\begin{aligned} &a^E_{m,i,j} \\ &= \frac{D_C(x_{i+j-m+1},\dots,x_{i-1},\xi_{\mathbf{x},m,i+j-m+1},x_{i+1},\dots,x_{N+1},x_{N+1}^{(1)},\dots,x_{N+1}^{(i+j-N-1)})}{D_C(x_{i+j-m+1},\dots,x_{N+1},x_{N+1}^{(1)},\dots,x_{N+1}^{(i+j-N-1)})}; \end{aligned} \tag{3.1.13}$$

- *For* $r = 0, \ldots, m-2,\ j = r, \ldots, m-2$*:*

$$a^E_{m,N+1+r,j} = \frac{D_C(x_{N+j-m+2}, \ldots, x_{N+1}, x^{(1)}_{N+1}, \ldots, x^{(r-1)}_{N+1}, \xi_{\mathbf{x},m,N+j-m+2}, x^{(r+1)}_{N+1}, \ldots, x^{(j)}_{N+1})}{D_C(x_{N+j-m+2}, \ldots, x_{N+1}, x^{(1)}_{N+1}, \ldots, x^{(j)}_{N+1})}. \tag{3.1.14}$$

We note that the molecules in the definition above are compactly supported, with

$$\begin{cases} \text{supp} M^E_{m,-\ell} = [x_0, x_{m-\ell}], \quad \ell = 1, \ldots, m-1; \\ \text{supp} M^E_{m,i} = [x_{i-m+1}, x_{i+m}], \quad i = 0, \ldots, N; \\ \text{supp} M^E_{m,N+1+r} = [x_{N-m+2+r}, x_{N+1}], \quad r = 0, \ldots, m-2. \end{cases} \tag{3.1.15}$$

With these definitions, we can show that polynomials of degree $\leq m-1$ are indeed preserved, as follows.

Theorem 3.1.1 (Polynomial preservation) *For* $N \geq 3m-3$*, the quasi-interpolation operator* $\mathcal{Q}^E_m$*, formulated in (3.1.8) in Definition 3.1.1, satisfies the condition*

$$(\mathcal{Q}^E_m p)(x) = p(x), \tag{3.1.16}$$

for all $x \in [a, b]$ *and* $p \in \pi_{m-1}$*.*

Proof:

We divide the proof into three parts.

(a) Let $x \in [x_{2m-2}, x_{N-2m+3}]$, so that (3.1.8) becomes simply

$$(\mathcal{Q}^E_m f)(x) = \sum_{i=m-1}^{N+1-m} f(x_i) M^E_{m,i}(x), \tag{3.1.17}$$

from the support properties of $M^E_{m,i}$ in (3.1.15). We proceed to show that the constants $a^E_{m,i,j},\ i = m-1, \ldots, N+1-m,\ j = 0, \ldots, m-1$, satisfy the formulation (3.1.10) in Definition 3.1.1 if $\mathcal{Q}^E_m$ satisfies (3.1.16), for $p(x) = x^t,\ t = 0, \ldots, m-1$.

To this end, by using (3.1.17) and the second equation in (3.1.9), the left hand side of (3.1.16) becomes

$$\begin{aligned}(\mathcal{Q}_m^E p)(x) &= \sum_{i=m-1}^{N+1-m} x_i^t \sum_{j=0}^{m-1} a_{m,i,j}^E N_{\mathbf{x},m,i+j-m+1}(x) \\ &= \sum_{j=0}^{m-1} \sum_{k=j}^{N+2-2m+j} x_{k-j+m-1}^t a_{m,k-j+m-1,j}^E N_{\mathbf{x},m,k}(x) \\ &= \sum_{k=0}^{N+1-m} \sum_{j=\max\{0,k-N-2+2m\}}^{\min\{m-1,k\}} x_{k-j+m-1}^t a_{m,k-j+m-1,j}^E N_{\mathbf{x},m,k}(x),\end{aligned} \tag{3.1.18}$$

for $p(x) = x^t,\ t = 0, \ldots, m-1$. Next, from Marsden's identity on the interval $[x_{2m-2}, x_{N-2m+3}]$, we have

$$x^t = \sum_{k=m-1}^{N-2m+2} \xi_{\mathbf{x}}^t(k) N_{\mathbf{x},m,k}(x), \quad t = 0, \ldots, m-1, \tag{3.1.19}$$

where $\xi_{\mathbf{x}}^t(k)$ is defined in terms of the classical symmetric functions as in (3.1.4)-(3.1.6). By substituting (3.1.18) and (3.1.19) in (3.1.16), we obtain

$$\sum_{j=\max\{0,k-N-2+2m\}}^{\min\{m-1,k\}} x_{k-j+m-1}^t a_{m,k-j+m-1,j}^E = \xi_{\mathbf{x}}^t(k), \quad t = 0, \ldots, m-1,$$

for $k = m-1, \ldots, N-2m+2$, yielding (for $N \geq 3m-3$)

$$\sum_{j=0}^{m-1} x_{k-j+m-1}^t a_{m,k-j+m-1,j}^E = \xi_{\mathbf{x}}^t(k), \quad t = 0, \ldots, m-1.$$

The formulation (3.1.10) in Definition 3.1.1 then follows by using Cramer's rule.

(b) Next, let $x \in [a, x_{2m-2}]$, so that (3.1.8) becomes

$$(\mathcal{Q}_m^E f)(x) = \sum_{\ell=1}^{m-1} f^{(\ell)}(a) M_{m,-\ell}^E(x) + \sum_{i=0}^{3m-4} f(x_i) M_{m,i}^E(x), \tag{3.1.20}$$

from the support properties of $M_{m,i}^E$ in (3.1.15). As in the first part, we show that the constants $a_{m,i,j}^E,\ i=-m+1,\ldots,m-2$, satisfy the formulation (3.1.10)-(3.1.12) in Definition 3.1.1 if $\mathcal{Q}_m^E$ satisfies (3.1.16), for $p(x)=x^t,\ t=0,\ldots,m-1$.

By using (3.1.20) and the first two equations in (3.1.9), the left hand side of (3.1.16) becomes

$$\begin{aligned}(\mathcal{Q}_m^E p)(x) &= \sum_{\ell=1}^{m-1}\tbinom{t}{\ell}\ell! x_0^{t-\ell}\sum_{j=0}^{m-1-\ell} a_{m,-\ell,j}^E N_{\mathbf{x},m,j-m+1}(x)\\ &\qquad + \sum_{i=0}^{3m-4} x_i^t \sum_{j=0}^{m-1} a_{m,i,j}^E N_{\mathbf{x},m,i+j-m+1}(x)\\ &= \sum_{\ell=1}^{m-1}\sum_{k=-m+1}^{-\ell}\tbinom{t}{\ell}\ell! x_0^{t-\ell} a_{m,-\ell,k+m-1}^E N_{\mathbf{x},m,k}(x)\\ &\qquad + \sum_{j=0}^{m-1}\sum_{k=j-m+1}^{2m+j-3} x_{k-j+m-1}^t a_{m,k-j+m-1,j}^E N_{\mathbf{x},m,k}(x)\\ &= \sum_{k=-m+1}^{-1}\sum_{\ell=1}^{-k}\tbinom{t}{\ell}\ell! x_0^{t-\ell} a_{m,-\ell,k+m-1}^E N_{\mathbf{x},m,k}(x)\\ &\qquad + \sum_{k=-m+1}^{3m-4}\sum_{j=\max\{0,k-2m+3\}}^{\min\{m-1,k+m-1\}} x_{k-j+m-1}^t a_{m,k-j+m-1,j}^E N_{\mathbf{x},m,k}(x).\end{aligned} \tag{3.1.21}$$

Combining (3.1.16) and (3.1.21) with Marsden's identity on the interval $[a, x_{2m-2}]$, given by

$$x^t = \sum_{k=-m+1}^{2m-3} \xi_{\mathbf{x}}^t(k) N_{\mathbf{x},m,k}(x), \quad t=0,\ldots,m-1,$$

we have

$$\sum_{k=-m+1}^{-1}\left[\sum_{\ell=1}^{-k}\tbinom{t}{\ell}\ell! x_0^{t-\ell} a_{m,-\ell,k+m-1}^E\right.$$

$$+\sum_{j=0}^{k+m-1} x_{k-j+m-1}^t a_{m,k-j+m-1,j}^E \Bigg] N_{\mathbf{x},m,k}(x)$$
$$+\sum_{k=0}^{m-2}\left[\sum_{j=0}^{m-1} x_{k-j+m-1}^t a_{m,k-j+m-1,j}^E\right] N_{\mathbf{x},m,k}(x)$$
$$= \sum_{k=-m+1}^{m-2} \xi_{\mathbf{x}}^t(k) N_{\mathbf{x},m,k}(x).$$

The result follows by comparing the left hand side and right hand side for $k = -m+1, \ldots, m-2$, and using Cramer's rule. The formulation (3.1.10) corresponds to $k = 0, \ldots, m-2$, while (3.1.11) and (3.1.12) (in terms of confluent Vandermonde determinants) correspond to $k = -m+1, \ldots, -1$.

(c) Lastly, let $x \in [x_{N+3-2m}, b]$, so that (3.1.8) becomes

$$(\mathcal{Q}_m^E f)(x) = \sum_{i=N+4-3m}^{N} f(x_i) M_{m,i}^E(x) + \sum_{r=0}^{m-2} f^{(r)}(b) M_{m,N+1+r}^E(x), \tag{3.1.22}$$

from the support properties of $M_{m,i}^E$ in (3.1.15). We proceed to show that the constants $a_{m,i,j}^E,\ i = N-m+2, \ldots, N+m-1$, satisfy the formulation (3.1.10), (3.1.13) and (3.1.14) in Definition 3.1.1 if $\mathcal{Q}_m^E$ satisfies (3.1.16), for $p(x) = x^t,\ t = 0, \ldots, m-1$.

By using (3.1.22) and the first two equations in (3.1.9), the left hand side of (3.1.16) becomes

$$(\mathcal{Q}_m^E p)(x) = \sum_{i=N+4-3m}^{N} x_i^t \sum_{j=0}^{m-1} a_{m,i,j}^E N_{\mathbf{x},m,i+j-m+1}(x)$$
$$+\sum_{r=0}^{m-2} \tbinom{t}{r} r! x_{N+1}^{t-r} \sum_{j=r}^{m-2} a_{m,N+1+r,j}^E N_{\mathbf{x},m,N+j-m+2}(x)$$
$$= \sum_{j=0}^{m-1} \sum_{k=N+j-4m+5}^{N+j-m+1} x_{k-j+m-1}^t a_{m,k-j+m-1,j}^E N_{\mathbf{x},m,k}(x)$$
$$+\sum_{r=0}^{m-2} \sum_{k=N+r-m+2}^{N} \tbinom{t}{r} r! x_{N+1}^{t-r} a_{m,N+1+r,k-N+m-2}^E N_{\mathbf{x},m,k}(x)$$

$$= \sum_{k=N-4m+5}^{N} \sum_{j=\max\{0,k-N+m-1\}}^{\min\{m-1,k-N+4m-5\}} x_{k-j+m-1}^{t} a_{m,k-j+m-1,j}^{E} N_{\mathbf{x},m,k}(x) + \sum_{k=N-m+2}^{N} \sum_{r=0}^{k-N+m-2} \binom{t}{r} r! x_{N+1}^{t-r} a_{m,N+1+r,k-N+m-2}^{E} N_{\mathbf{x},m,k}(x). \tag{3.1.23}$$

Combining (3.1.16) and (3.1.23) with Marsden's identity on the interval $[x_{N+3-2m}, b]$, namely

$$x^t = \sum_{k=N+3-2m}^{N} \xi_{\mathbf{x}}^t(k) N_{\mathbf{x},m,k}(x), \quad t = 0, \ldots, m-1,$$

we have

$$\sum_{k=N+3-2m}^{N-m+1} \left[\sum_{j=0}^{m-1} x_{k-j+m-1}^{t} a_{m,k-j+m-1,j}^{E} \right] N_{\mathbf{x},m,k}(x) + \sum_{k=N-m+2}^{N} \left[\sum_{j=k-N+m-1}^{m-1} x_{k-j+m-1}^{t} a_{m,k-j+m-1,j}^{E} + \sum_{r=0}^{k-N+m-2} \binom{t}{r} r! x_0^{t-r} a_{m,N+1+r,k-N+m-2}^{E} \right] N_{\mathbf{x},m,k}(x) = \sum_{k=N+3-2m}^{N} \xi_{\mathbf{x}}^t(k) N_{\mathbf{x},m,k}(x).$$

The result follows by comparing the left hand side and right hand side for $k = N+3-2m, \ldots, N$, and using Cramer's rule. The formulation (3.1.10) corresponds to $k = N+3-2m, \ldots, N-m+1$, while (3.1.13) and (3.1.14) (in terms of confluent Vandermonde determinants) correspond to $k = N-m+2, \ldots, N$. ■

3.2 Quasi-interpolation: Scheme H

For the sampling points

$$\mathbf{y} : a = y_0 < y_1 < \cdots < y_N = b \tag{3.2.1}$$

and a real-valued function f, we proceed in this section to adapt the spline quasi-interpolation scheme of Section 3.1 (where the spline knots were chosen to coincide with the sampling points) for the case where we define the spline knots to lie midway between consecutive sampling points. More precisely, we define the knot sequence $\mathbf{x}$ by

$$\mathbf{x} : x_{-m+1} = \cdots = a = x_0 < x_1 < \cdots < x_{N+1} = b = \cdots = x_{N+m},$$

with

$$\begin{cases} x_0 := y_0; \\ x_i := \frac{1}{2}\left(y_{i-1} + y_i\right), \ i = 1, \ldots, N; \\ x_{N+1} := y_N. \end{cases} \tag{3.2.2}$$

Using the definitions (3.1.3)-(3.1.7), we have the following:

Definition 3.2.1 (Quasi-interpolation operator) *The quasi-interpolation operator $\mathcal{Q}_m^H$ is defined by*

$$(\mathcal{Q}_m^H f)(x) := \sum_{\ell=1}^{m-1} f^{(\ell)}(a) M_{m,-\ell}^H(x) + \sum_{i=0}^{N} f(y_i) M_{m,i}^H(x) + \sum_{r=1}^{m-1} f^{(r)}(b) M_{m,N+r}^H(x), \tag{3.2.3}$$

in terms of the spline molecules

$$\begin{cases} M_{m,-\ell}^H(x) := \displaystyle\sum_{j=0}^{m-1-\ell} a_{m,-\ell,j}^H N_{\mathbf{x},m,j-m+1}(x), \quad \ell = 1, \ldots, m-1; \\ M_{m,i}^H(x) := \displaystyle\sum_{j=0}^{m-1} a_{m,i,j}^H N_{\mathbf{x},m,i+j-m+1}(x), \quad i = 0, \ldots, N; \\ M_{m,N+r}^H(x) := \displaystyle\sum_{j=r}^{m-1} a_{m,N+r,j}^H N_{\mathbf{x},m,N+j-m+1}(x), \quad r = 1, \ldots, m-1, \end{cases} \tag{3.2.4}$$

where the coefficients are given by:

- *For $i = 0, \ldots, m-2$, $j = m-1-i, \ldots, m-1$, and $i = m-1, \ldots, N+1-m$, $j = 0, \ldots, m-1$, and $i = N-m+2, \ldots, N$, $j = 0, \ldots, N-i$:*

$$a_{m,i,j}^H = \frac{D(y_{i+j-m+1}, \ldots, y_{i-1}, \xi_{\mathbf{x},m,i+j-m+1}, y_{i+1}, \ldots, y_{i+j})}{D(y_{i+j-m+1}, \ldots, y_{i+j})}; \tag{3.2.5}$$

- *For* $i = 0, \ldots, m-2,\ j = 0, \ldots, m-2-i$*:*

$$a^H_{m,i,j} = \frac{D_C(y_0, y_0^{(1)}, \ldots, y_0^{(m-1-i-j)}, y_1, \ldots, y_{i-1}, \xi_{\mathbf{x},m,i+j-m+1}, y_{i+1}, \ldots, y_{i+j})}{D_C(y_0, y_0^{(1)}, \ldots, y_0^{(m-1-i-j)}, y_1, \ldots, y_{i+j})}; \tag{3.2.6}$$

- *For* $\ell = 1, \ldots, m-1,\ j = 0, \ldots, m-1-\ell$*:*

$$a^H_{m,-\ell,j} = \frac{D_C(y_0, y_0^{(1)}, \ldots, y_0^{(\ell-1)}, \xi_{\mathbf{x},m,j-m+1}, y_0^{(\ell+1)}, \ldots, y_0^{(m-1-j)}, y_1, \ldots, y_j)}{D_C(y_0, y_0^{(1)}, \ldots, y_0^{(m-1-j)}, y_1, \ldots, y_j)}; \tag{3.2.7}$$

- *For* $i = N-m+2, \ldots, N,\ j = N-i+1, \ldots, m-1$*:*

$$\begin{aligned} &a^H_{m,i,j} \\ &= \frac{D_C(y_{i+j-m+1}, \ldots, y_{i-1}, \xi_{\mathbf{x},m,i+j-m+1}, y_{i+1}, \ldots, y_N, y_N^{(1)}, \ldots, y_N^{(i+j-N)})}{D_C(y_{i+j-m+1}, \ldots, y_N, y_N^{(1)}, \ldots, y_N^{(i+j-N)})}; \end{aligned} \tag{3.2.8}$$

- *For* $r = 1, \ldots, m-1,\ j = r, \ldots, m-1$*:*

$$\begin{aligned} &a^H_{m,N+r,j} \\ &= \frac{D_C(y_{N+j-m+1}, \ldots, y_N, y_N^{(1)}, \ldots, y_N^{(r-1)}, \xi_{\mathbf{x},m,N+j-m+1}, y_N^{(r+1)}, \ldots, y_N^{(j)})}{D_C(y_{N+j-m+1}, \ldots, y_N, y_N^{(1)}, \ldots, y_N^{(j)})}. \end{aligned} \tag{3.2.9}$$

The molecules in the definition above are compactly supported, with

$$\begin{cases} \text{supp} M^H_{m,-\ell} = [x_0, x_{m-\ell}], \quad \ell = 1, \ldots, m-1; \\ \text{supp} M^H_{m,i} = [x_{i-m+1}, x_{i+m}], \quad i = 0, \ldots, N; \\ \text{supp} M^H_{m,N+r} = [x_{N-m+1+r}, x_{N+1}], \quad r = 1, \ldots, m-1. \end{cases} \tag{3.2.10}$$

We remark that, in contrast to the quasi-interpolant described in (3.1.8) in Section 3.1, each sampling point $y_0, \ldots, y_N$, is located precisely in the center of the support interval of each corresponding molecule $M^H_{m,i},\ i = 0, \ldots, N$.

With these definitions, we can show that $\mathcal{Q}_m^H$ preserves polynomials of degree $\leq m-1$:

Theorem 3.2.1 (Polynomial preservation) *For $N \geq 3m-3$, the quasi-interpolation operator $\mathcal{Q}_m^H$, formulated in (3.2.3) in Definition 3.2.1, satisfies the condition*

$$(\mathcal{Q}_m^H p)(x) = p(x), \tag{3.2.11}$$

for all $x \in [a,b]$ and $p \in \pi_{m-1}$.

The proof follows a similar pattern as the proof of Theorem 3.1.1 and is omitted here. ■

3.3 Approximation order

Lastly in this chapter, we analyze the order of approximation of the quasi-interpolation operators $\mathcal{Q}_m^E$ and $\mathcal{Q}_m^H$.

In this regard, since $\mathcal{Q}_m^E$ and $\mathcal{Q}_m^H$ are expressed in terms of the spline molecules $M_{m,i}^E$ and $M_{m,i}^H$, respectively, it is a key requirement to find upper bounds on these spline molecules on the interval $[a,b]$. These upper bounds will be given in Theorem 3.3.1. Our first task in developing these upper bounds is to bound the spline coefficients $a_{m,i,j}^E$ and $a_{m,i,j}^H$.

To this end, we start by noting that, for an integer $m \geq 3$ and a sequence of real numbers $\{x_1, \ldots, x_{m-1}\}$,

$$\begin{cases} \displaystyle\sum_{i=1}^{m-1} \sigma^{\ell}(x_1, \ldots, x_{i-1}, x_{i+1}, \ldots, x_{m-1}) = (m-1-\ell)\sigma^{\ell}(x_1, \ldots, x_{m-1}); \\ \displaystyle\sum_{i=1}^{m-1} x_i \sigma^{\ell}(x_1, \ldots, x_{i-1}, x_{i+1}, \ldots, x_{m-1}) = (\ell+1)\sigma^{\ell+1}(x_1, \ldots, x_{m-1}), \end{cases} \tag{3.3.1}$$

for $\ell = 0, \ldots, m-2$, and

$$x_{m-1}\sigma^{m-2-\ell}(x_1, \ldots, x_{m-2}) + \sigma^{m-1-\ell}(x_1, \ldots, x_{m-2}) = \sigma^{m-1-\ell}(x_1, \ldots, x_{m-1}), \tag{3.3.2}$$

for $\ell = 0, \ldots, m-1$, all of which follow directly from the definition of the symmetric polynomials in (3.1.6).

We will rely on the following lemma, which originally appeared in [9, Lemma 2.1]. It is given here with a modified proof.

Lemma 3.3.1 (Symmetric polynomials) *For an integer $m \geq 3$, let $\{x_1, \ldots, x_{m-1}\}$ and $\{y_1, \ldots, y_{m-1}\}$ denote two sequences of real numbers. Then*

$$\sum_{\ell=0}^{m-1} (-1)^{\ell} \frac{\sigma^{m-1-\ell}(x_1, \ldots, x_{m-1})}{\binom{m-1}{\ell}} \sigma^{\ell}(y_1, \ldots, y_{m-1}) = \frac{1}{(m-1)!} \left[\sum_{1 \leq t_1, \ldots, t_{m-1} \leq m-1} \prod_{k=1}^{m-1} (x_{t_k} - y_k) \right]. \quad (3.3.3)$$

Proof:

Our proof is by induction on m. It can be verified directly, using the definition (3.1.6) of the symmetric polynomials, that the result holds for $m = 3$. We now assume the result holds for an integer $m-1$ and proceed to prove (3.3.3). Using the induction hypothesis, (3.3.1) and (3.3.2), we have that

$$\frac{1}{(m-1)!} \left[\sum_{1 \leq t_1, \ldots, t_{m-1} \leq m-1} \prod_{k=1}^{m-1} (x_{t_k} - y_k) \right]$$

$$= \frac{1}{(m-1)!} \left[\sum_{\substack{1 \leq t_2, \ldots, t_{m-1} \leq m-2 \\ t_1 = m-1}} \prod_{k=1}^{m-1} (x_{t_k} - y_k) + \sum_{\substack{1 \leq t_1, t_3 \ldots, t_{m-1} \leq m-2 \\ t_2 = m-1}} \prod_{k=1}^{m-1} (x_{t_k} - y_k) \right.$$

$$\left. + \cdots + \sum_{\substack{1 \leq t_1, \ldots, t_{m-2} \leq m-2 \\ t_{m-1} = m-1}} \prod_{k=1}^{m-1} (x_{t_k} - y_k) \right]$$

$$= \frac{1}{(m-1)!} \left[(x_{m-1} - y_1) \sum_{1 \leq t_2, \ldots, t_{m-1} \leq m-2} \prod_{k=1}^{m-1} (x_{t_k} - y_k) \right.$$

$$
\begin{aligned}
&\quad + (x_{m-1} - y_2) \sum_{1 \le t_1, t_3 \ldots, t_{m-1} \le m-2} \prod_{k=1}^{m-1} (x_{t_k} - y_k) \\
&\qquad + \cdots + (x_{m-1} - y_{m-1}) \sum_{1 \le t_1, \ldots, t_{m-2} \le m-2} \prod_{k=1}^{m-1} (x_{t_k} - y_k) \Bigg] \\
&= \frac{1}{m-1} \Bigg[(x_{m-1} - y_1) \sum_{\ell=0}^{m-2} (-1)^\ell \frac{\sigma^{m-2-\ell}(x_1, \ldots, x_{m-2})}{\binom{m-2}{\ell}} \sigma^\ell(y_2, \ldots, y_{m-1}) \\
&\qquad + (x_{m-1} - y_2) \sum_{\ell=0}^{m-2} (-1)^\ell \frac{\sigma^{m-2-\ell}(x_1, \ldots, x_{m-2})}{\binom{m-2}{\ell}} \sigma^\ell(y_1, y_3, \ldots, y_{m-1}) \\
&\quad + \cdots + (x_{m-1} - y_{m-1}) \sum_{\ell=0}^{m-2} (-1)^\ell \frac{\sigma^{m-2-\ell}(x_1, \ldots, x_{m-2})}{\binom{m-2}{\ell}} \sigma^\ell(y_1, \ldots, y_{m-2}) \Bigg] \\
&= \frac{1}{m-1} \Bigg[\sum_{\ell=0}^{m-2} (-1)^\ell \frac{x_{m-1} \sigma^{m-2-\ell}(x_1, \ldots, x_{m-2})}{\binom{m-2}{\ell}} \times \\
&\qquad \big(\sigma^\ell(y_2, \ldots, y_{m-1}) + \sigma^\ell(y_1, y_3, \ldots, y_{m-1}) + \cdots + \sigma^\ell(y_1, \ldots, y_{m-2}) \big) \\
&\qquad - \sum_{\ell=0}^{m-2} (-1)^\ell \frac{\sigma^{m-2-\ell}(x_1, \ldots, x_{m-2})}{\binom{m-2}{\ell}} \times \\
&\big(y_1 \sigma^\ell(y_2, \ldots, y_{m-1}) + y_2 \sigma^\ell(y_1, y_3, \ldots, y_{m-1}) + \cdots + y_{m-1} \sigma^\ell(y_1, \ldots, y_{m-2}) \big) \Bigg] \\
&= \frac{1}{m-1} \Bigg[\sum_{\ell=0}^{m-1} (-1)^\ell \frac{x_{m-1} \sigma^{m-2-\ell}(x_1, \ldots, x_{m-2})}{\binom{m-2}{\ell}} (m-1-\ell) \sigma^\ell(y_1, \ldots, y_{m-1}) \\
&\qquad + \sum_{\ell=-1}^{m-2} (-1)^{\ell+1} \frac{\sigma^{m-2-\ell}(x_1, \ldots, x_{m-2})}{\binom{m-2}{\ell}} (\ell+1) \sigma^{\ell+1}(y_1, \ldots, y_{m-1}) \Bigg] \\
&= \sum_{\ell=0}^{m-1} (-1)^\ell \frac{x_{m-1} \sigma^{m-2-\ell}(x_1, \ldots, x_{m-2})}{\binom{m-1}{\ell}} \sigma^\ell(y_1, \ldots, y_{m-1}) \\
&\qquad + \sum_{\ell=0}^{m-1} (-1)^\ell \frac{\sigma^{m-1-\ell}(x_1, \ldots, x_{m-2})}{\binom{m-1}{\ell}} \sigma^\ell(y_1, \ldots, y_{m-1})
\end{aligned}
$$

$$= \sum_{\ell=0}^{m-1} \frac{(-1)^\ell}{\binom{m-1}{\ell}} \left[x_{m-1}\sigma^{m-2-\ell}(x_1,\ldots,x_{m-2}) + \sigma^{m-1-\ell}(x_1,\ldots,x_{m-2})\right] \times$$

$$\sigma^\ell(y_1,\ldots,y_{m-1})$$

$$= \sum_{\ell=0}^{m-1}(-1)^\ell \frac{\sigma^{m-1-\ell}(x_1,\ldots,x_{m-1})}{\binom{m-1}{\ell}}\sigma^\ell(y_1,\ldots,y_{m-1}),$$

completing our inductive proof of (3.3.3). ■

Next, we derive an upper bound on the spline coefficients $a^E_{m,i,j}$, $a^H_{m,i,j}$, $i = -m+1,\ldots,N+m-1$, $j = 0,\ldots,m-1$. To this end, we recall the standard formula for the expansion of a linear factorization of a monomial in terms of the symmetric polynomials in (3.1.6): for a sequence of real numbers $\{t_1,\ldots,t_n\}$ and some $r \in \mathbb{R}$ and $n \in \mathbb{N}$,

$$\prod_{j=1}^{n}(r-t_j) = \sum_{j=0}^{n}(-1)^j r^{n-j}\sigma^j(t_1,\ldots,t_n). \tag{3.3.4}$$

The following lemma originally appeared in [9, Theorem 2.2], where the result was proved only for an unbounded interval. Our lemma below is a non-trivial extension that include upper bounds on the spline coefficients near the boundaries $x = a$ and $x = b$.

Lemma 3.3.2 (Upper bound on spline coefficients) *For an integer $m \geq 3$, let $\mathbf{x}$ and $\mathbf{y}$ be the sequences defined in (3.1.2) and (3.2.1), respectively. Suppose that*

$$\begin{cases} \gamma^E := \sup\limits_{n=0,\ldots,N+m-1} |x_n - x_{n-m+1}|; \\ \delta^E := \min\left\{1, \inf\limits_{n=0,\ldots,N} |x_{n+1}-x_n|\right\}, \end{cases} \tag{3.3.5}$$

and

$$\begin{cases} \gamma^H := \sup\limits_{n=0,\ldots,N+m-1} |x_n - y_{n-m+1}|; \\ \delta^H := \min\left\{1, \inf\limits_{n=0,\ldots,N-1} |y_{n+1}-y_n|\right\}, \end{cases} \tag{3.3.6}$$

with the definition that $y_{-m+1} = \cdots = y_0$. Then

$$|a^E_{m,i,j}| \leq \frac{1}{(m-2)!}\left(\frac{\gamma^E}{\delta^E}\right)^{m-1} \tag{3.3.7}$$

and

$$|a^H_{m,i,j}| \leq \frac{1}{(m-2)!}\left(\frac{\gamma^H}{\delta^H}\right)^{m-1}, \tag{3.3.8}$$

for $i = -m+1, \ldots, N+m-1,\ j = 0, \ldots, m-1$.

Proof:

We provide the proof of (3.3.8); the proof of (3.3.7) is similar.

First, let $i \in \{m-1, \ldots, N+1-m\}$ and $j \in \{0, \ldots, m-1\}$ be fixed. From a standard result in linear algebra, we have an explicit formulation of the Vandermonde determinant $D(y_{i+j-m+1}, \ldots, y_{i+j})$, namely

$$D(y_{i+j-m+1}, \ldots, y_{i+j}) = \prod_{i+j-m+1 \leq k < \ell \leq i+j} (y_\ell - y_k) \tag{3.3.9}$$

(see, for example, [32]). Therefore,

$$\begin{aligned}
&D(y_{i+j-m+1}, \ldots, y_{i-1}, \xi_{\mathbf{x},m,i+j-m+1}, y_{i+1}, \ldots, y_{i+j}) \\
&= \prod_{\substack{i+j-m+1 \leq k < \ell \leq i+j \\ k,\ell \neq i}} (y_\ell - y_k) \times \\
&\qquad \prod_{k=i+j-m+1}^{i-1} (\xi_{\mathbf{x},m,i+j-m+1} - y_k) \prod_{k=i+1}^{i+j} (y_k - \xi_{\mathbf{x},m,i+j-m+1}) \\
&= \prod_{\substack{i+j-m+1 \leq k < \ell \leq i+j \\ k,\ell \neq i}} (y_\ell - y_k) \prod_{\substack{k=0 \\ k \neq m-j-1}}^{m-1} (-1)^j \left(\xi_{\mathbf{x},m,i+j-m+1} - y_{k+i+j-m+1}\right) \\
&= (-1)^j \prod_{\substack{i+j-m+1 \leq k < \ell \leq i+j \\ k,\ell \neq i}} (y_\ell - y_k) \times \\
&\qquad \sum_{n=0}^{m-1} (-1)^n \xi_{\mathbf{x}}^{m-1-n} (i+j-m+1) \sigma^n(y_{i+j-m+1}, \ldots, y_{i-1}, y_{i+1}, \ldots, y_{i+j}) \\
&= (-1)^j \prod_{\substack{i+j-m+1 \leq k < \ell \leq i+j \\ k,\ell \neq i}} (y_\ell - y_k) \times \\
&\sum_{n=0}^{m-1} (-1)^n \frac{\sigma^{m-1-n}(x_{i+j-m+2}, \ldots, x_{i+j})}{\binom{m-1}{n}} \sigma^n(y_{i+j-m+1}, \ldots, y_{i-1}, y_{i+1}, \ldots, y_{i+j})
\end{aligned}$$

$$= (-1)^j \prod_{\substack{i+j-m+1 \le k < \ell \le i+j \\ k,\ell \neq i}} (y_\ell - y_k) \times$$
$$\frac{1}{(m-1)!} \left[\sum_{i+j-m+2 \le t_{i+j-m+1}, \ldots, t_{i-1}, t_{i+1}, \ldots, t_{i+j} \le i+j} \prod_{\substack{n=i+j-m+1 \\ n \neq i}}^{i+j} (x_{t_n} - y_n) \right], \tag{3.3.10}$$

from the definition (3.1.4)-(3.1.5), together with (3.3.4) and (3.3.3) in Lemma 3.3.1. It therefore follows from the definition of $a^H_{m,i,j}$ in (3.2.5), as well as (3.3.9)-(3.3.10), that

$$\begin{aligned} |a^H_{m,i,j}| &\le \frac{1}{(m-1)!} \prod_{\substack{k=i+j-m+1 \\ k \neq i}}^{i+j} |y_i - y_k|^{-1} \times \\ &\qquad \sum_{i+j-m+2 \le t_{i+j-m+1}, \ldots, t_{i-1}, t_{i+1}, \ldots, t_{i+j} \le i+j} \prod_{\substack{n=i+j-m+1 \\ n \neq i}}^{i+j} |x_{t_n} - y_n| \\ &\le \frac{1}{(m-2)!} \left(\frac{\gamma^H}{\delta^H} \right)^{m-1}. \end{aligned}$$

Next, we prove (3.3.8) for the spline coefficients near the left hand side boundary $x = a$; the proof for the spline coefficients near the right hand side boundary is similar.

Let $i \in \{1, \ldots, m-2\}$ and $j \in \{0, \ldots, m-2-i\}$ be fixed. An explicit formulation of the confluent Vandermonde determinant $D_C(y_0, y_0^{(1)}, \ldots, y_0^{(m-1-j-i)}, y_1, \ldots, y_{i+j})$ is given in [32, 43], namely

$$D_C(y_0, y_0^{(1)}, \ldots, y_0^{(m-1-j-i)}, y_1, \ldots, y_{i+j}) = \prod_{\ell=1}^{i+j} (y_\ell - y_0)^{m-j-i} \prod_{1 \le k < \ell \le i+j} (y_\ell - y_k). \tag{3.3.11}$$

Therefore, with $y_{-m+1} = \cdots = y_0$, we have

$$D_C(y_0, y_0^{(1)}, \ldots, y_0^{(m-1-j-i)}, y_1, \ldots, y_{i-1}, \xi_{\mathbf{x},m,i+j-m+1}, y_{i+1}, \ldots, y_{i+j})$$

$$= \prod_{\substack{\ell=1 \\ \ell\neq i}}^{i+j}(y_\ell - y_0)^{m-j-i} \prod_{\substack{1\leq k<\ell\leq i+j \\ k,\ell\neq i}} (y_\ell - y_k)\times$$

$$(\xi_{\mathbf{x},m,i+j-m+1} - y_0)^{m-j-i} \prod_{k=1}^{i-1}(\xi_{\mathbf{x},m,i+j-m+1} - y_k) \prod_{k=i+1}^{i+j}(y_k - \xi_{\mathbf{x},m,i+j-m+1})$$

$$= \prod_{\substack{\ell=1 \\ \ell\neq i}}^{i+j}(y_\ell - y_0)^{m-j-i} \prod_{\substack{1\leq k<\ell\leq i+j \\ k,\ell\neq i}} (y_\ell - y_k) \prod_{\substack{k=i+j-m+1 \\ k\neq i}}^{i+j} (-1)^j\,(\xi_{\mathbf{x},m,i+j-m+1} - y_k)$$

$$= (-1)^j \prod_{\substack{\ell=1 \\ \ell\neq i}}^{i+j}(y_\ell - y_0)^{m-j-i} \prod_{\substack{1\leq k<\ell\leq i+j \\ k,\ell\neq i}} (y_\ell - y_k)\times$$

$$\prod_{\substack{k=0 \\ k\neq m-1-j}}^{m-1} (\xi_{\mathbf{x},m,i+j-m+1} - y_{k+i+j-m+1})$$

$$= (-1)^j \prod_{\substack{\ell=1 \\ \ell\neq i}}^{i+j}(y_\ell - y_0)^{m-j-i} \prod_{\substack{1\leq k<\ell\leq i+j \\ k,\ell\neq i}} (y_\ell - y_k)\times$$

$$\sum_{n=0}^{m-1}(-1)^n \xi_{\mathbf{x}}^{m-1-n}(i+j-m+1)\sigma^n(y_{i+j-m+1},\ldots,y_{i-1},y_{i+1},\ldots,y_{i+j})$$

$$= (-1)^j \prod_{\substack{\ell=1 \\ \ell\neq i}}^{i+j}(y_\ell - y_0)^{m-j-i} \prod_{\substack{1\leq k<\ell\leq i+j \\ k,\ell\neq i}} (y_\ell - y_k)\times$$

$$\sum_{n=0}^{m-1}(-1)^n \frac{\sigma^{m-1-n}(x_{i+j-m+2},\ldots,x_{i+j})}{\binom{m-1}{n}}\sigma^n(y_{i+j-m+1},\ldots,y_{i-1},y_{i+1},\ldots,y_{i+j})$$

$$= (-1)^j \prod_{\substack{\ell=1 \\ \ell\neq i}}^{i+j}(y_\ell - y_0)^{m-j-i} \prod_{\substack{1\leq k<\ell\leq i+j \\ k,\ell\neq i}} (y_\ell - y_k)\times$$

$$\frac{1}{(m-1)!}\left[\sum_{i+j-m+2\leq t_{i+j-m+1},\ldots,t_{i-1},t_{i+1},\ldots,t_{i+j}\leq i+j} \prod_{\substack{n=i+j-m+1 \\ n\neq i}}^{i+j}(x_{t_n} - y_n)\right],$$

(3.3.12)

from the definition (3.1.4)-(3.1.5), together with (3.3.4) and (3.3.3) in Lemma 3.3.1. It therefore follows from the definition of $a^H_{m,i,j}$ in (3.2.6), as well as (3.3.11)-(3.3.12), that

$$\begin{aligned}|a^H_{m,i,j}| &\leq \frac{1}{(m-1)!}|y_i - y_0|^{-(m-j-i)} \prod_{\substack{k=1\\k\neq i}}^{i+j} |y_i - y_k|^{-1} \times \\ &\qquad \sum_{i+j-m+2\leq t_{i+j-m+1},\ldots,t_{i-1},t_{i+1},\ldots,t_{i+j}\leq i+j} \prod_{\substack{n=i+j-m+1\\n\neq i}}^{i+j} |x_{t_n} - y_n| \\ &\leq \frac{1}{(m-2)!}\left(\frac{\gamma^H}{\delta^H}\right)^{m-1}.\end{aligned}$$

Lastly, let $i = 0,\ j \in \{0,\ldots,m-2\}$ or $i = 0,\ \ell \in \{1,\ldots,m-1\},\ j \in \{0,\ldots,m-1-\ell\}$ be fixed. Then, with the definition $y_{-m+1} = \cdots = y_0$, we have, from (3.3.11) with $i = 0$,

$$\begin{aligned}&D_C(y_0, y_0^{(1)},\ldots,y_0^{(\ell-1)}, \xi_{\mathbf{x},m,j-m+1}, y_0^{(\ell+1)},\ldots,y_0^{(m-1-j)}, y_1,\ldots,y_j) \\ &= \prod_{s=1}^{j}(y_s - y_0)^{m-j-1} \prod_{1\leq k<s\leq j}(y_s - y_k)\times \\ &\qquad\qquad (\xi_{\mathbf{x},m,j-m+1} - y_0)^{m-j-1} \prod_{k=1}^{j}(y_k - \xi_{\mathbf{x},m,j-m+1}) \\ &= \prod_{s=1}^{j}(y_s - y_0)^{m-j-1} \prod_{1\leq k<s\leq j}(y_s - y_k) \prod_{k=j-m+2}^{j}(-1)^j(\xi_{\mathbf{x},m,j-m+1} - y_k) \\ &= (-1)^j \prod_{s=1}^{j}(y_s - y_0)^{m-j-1} \prod_{1\leq k<s\leq j}(y_s - y_k) \prod_{k=0}^{m-2}(\xi_{\mathbf{x},m,j-m+1} - y_{k+j-m+2}) \\ &= (-1)^j \prod_{s=1}^{j}(y_s - y_0)^{m-j-1} \prod_{1\leq k<s\leq j}(y_s - y_k)\times \\ &\qquad\qquad \sum_{n=0}^{m-1}(-1)^n \xi_{\mathbf{x}}^{m-1-n}(j-m+1)\sigma^n(y_{j-m+2},\ldots,y_j)\end{aligned}$$

$$= (-1)^j \prod_{s=1}^{j} (y_s - y_0)^{m-j-1} \prod_{1 \le k < s \le j} (y_s - y_k) \times \sum_{n=0}^{m-1} (-1)^n \frac{\sigma^{m-1-n}(x_{j-m+2}, \ldots, x_j)}{\binom{m-1}{n}} \sigma^n(y_{j-m+2}, \ldots, y_j)$$

$$= (-1)^j \prod_{s=1}^{j} (y_s - y_0)^{m-j-1} \prod_{1 \le k < s \le j} (y_s - y_k) \times \frac{1}{(m-1)!} \left[\sum_{j-m+2 \le t_{j-m+2}, \ldots, t_j \le j} \prod_{n=j-m+2}^{j} (x_{t_n} - y_n) \right], \tag{3.3.13}$$

from (3.1.4)-(3.1.5), and (3.3.4) and (3.3.3) in Lemma 3.3.1. It therefore follows from the definition of $a^H_{m,i,j}$ in (3.2.6)-(3.2.7), as well as (3.3.13), that

$$\begin{aligned} |a^H_{m,i,j}| &\le \frac{1}{(m-1)!} \prod_{s=1}^{j} |y_s - y_0|^{-1} \sum_{j-m+2 \le t_{j-m+2}, \ldots, t_j \le j} \prod_{n=j-m+2}^{j} |x_{t_n} - y_n| \\ &\le \frac{1}{(m-2)!} \left(\frac{\gamma^H}{\delta^H} \right)^{m-1}. \end{aligned}$$

■

From Lemma 3.3.2, and the fact that the B-splines $\{N_{\mathbf{x},m,j} : j = -m+1, \ldots, N\}$ provide a partition of unity, the result on the upper bound on the spline molecules $M^E_{m,i}$ and $M^H_{m,i}$ follows easily:

Theorem 3.3.1 (Upper bound on spline molecules) *For an integer $m \ge 3$, let $M^E_{m,i}$ and $M^H_{m,i}$, $i = -m+1, \ldots, N+m-1$, be the spline molecules defined in (3.1.9) and (3.2.4), respectively. Then*

$$|M^E_{m,i}(x)| \le \frac{1}{(m-2)!} \left(\frac{\gamma^E}{\delta^E} \right)^{m-1} \tag{3.3.14}$$

and

$$|M^H_{m,i}(x)| \le \frac{1}{(m-2)!} \left(\frac{\gamma^H}{\delta^H} \right)^{m-1}, \tag{3.3.15}$$

for all $i = -m+1, \ldots, N+m-1$, *and* $x \in [a,b]$, *where the constants* γ^E, δ^E *and* γ^H, δ^H *are defined in (3.3.5) and (3.3.6), respectively.*

Proof:

We provide the proof of (3.3.15); the proof of (3.3.14) is similar.

Using the spline molecule definition (3.2.4) and (3.3.8) in Lemma 3.3.2, and the properties (2.3.10)-(2.3.14) in Theorem 2.3.2, we have, for $i = -m+1, \ldots, N+m-1$,

$$\begin{aligned} |M^H_{m,i}(x)| &\leq \sum_{j=0}^{m-1} |a^H_{m,i,j} N_{\mathbf{x},m,i+j-m+1}(x)| \\ &\leq \frac{1}{(m-2)!} \left(\frac{\gamma^H}{\delta^H}\right)^{m-1} \sum_{j=0}^{m-1} N_{\mathbf{x},m,i+j-m+1}(x) \\ &= \frac{1}{(m-2)!} \left(\frac{\gamma^H}{\delta^H}\right)^{m-1}. \end{aligned}$$

■

We are now ready to provide error estimates for the quasi-interpolation operators $\mathcal{Q}^E_m$ and $\mathcal{Q}^H_m$. In the following, $||\cdot||_{\infty,[x_i,x_{i+1}]}$ denotes the uniform (or supremum) norm on the interval $[x_i, x_{i+1}]$; that is,

$$||g||_{\infty,[x_i,x_{i+1}]} = \sup\{|g(x)| : \ x \in [x_i, x_{i+1}]\}.$$

Theorem 3.3.2 (Error of quasi-interpolation) *For a function* $f \in C^m[a,b]$, *let* $\mathcal{Q}^E_m$ *and* $\mathcal{Q}^H_m$ *be the quasi-interpolation operators defined in Definitions 3.1.1 and 3.2.1, respectively. Define*

$$\varepsilon := \sup_{n=0,\ldots,N} |x_{n+1} - x_n|, \tag{3.3.16}$$

and let γ^E, δ^E *and* γ^H, δ^H *be defined by (3.3.5) and (3.3.6), respectively. Then the supremum norm approximation error of quasi-interpolation is*

given by

$$||f-\mathcal{Q}_m^E||_{\infty,[x_i,x_{i+1}]} \leq \begin{cases} A_m^E||f^{(m)}||_{\infty,[x_i,x_{i+1}]}R_m^E, & i=0; \\ B_m^E||f^{(m)}||_{\infty,[x_i,x_{i+1}]}S_m^E, & i=1,\ldots,N-m+2; \\ C_m^E||f^{(m)}||_{\infty,[x_i,x_{i+1}]}T_m^E, & i=N-m+3,\ldots,N, \end{cases} \tag{3.3.17}$$

where A_m^E, B_m^E *and* C_m^E *are constants independent of* ε, γ^E *and* δ^E, *and*

$$\begin{cases} R_m^E := \varepsilon^m + \varepsilon^m\left(\frac{\gamma^E}{\delta^E}\right)^{m-1} + \varepsilon\left(\frac{\gamma^E}{\delta^E}\right)^{m-1}; \\ S_m^E := \varepsilon^m + \varepsilon^m\left(\frac{\gamma^E}{\delta^E}\right)^{m-1}; \\ T_m^E := \varepsilon^m + \varepsilon^m\left(\frac{\gamma^E}{\delta^E}\right)^{m-1} + \varepsilon\left(\frac{\gamma^E}{\delta^E}\right)^{m-1}\left(\frac{1-\varepsilon^{m-2}}{1-\varepsilon}\right), \end{cases}$$

whereas

$$||f-\mathcal{Q}_m^H||_{\infty,[x_i,x_{i+1}]} \leq \begin{cases} A_m^H||f^{(m)}||_{\infty,[x_i,x_{i+1}]}R_m^H, & i=0; \\ B_m^H||f^{(m)}||_{\infty,[x_i,x_{i+1}]}S_m^H, & i=1,\ldots,N-m+1; \\ C_m^H||f^{(m)}||_{\infty,[x_i,x_{i+1}]}T_m^H, & i=N-m+2,\ldots,N, \end{cases} \tag{3.3.18}$$

where A_m^H, B_m^H *and* C_m^H *are constants independent of* ε, γ^H *and* δ^H, *and*

$$\begin{cases} R_m^H := \varepsilon^m + \varepsilon^m\left(\frac{\gamma^H}{\delta^H}\right)^{m-1} + \varepsilon\left(\frac{\gamma^H}{\delta^H}\right)^{m-1}; \\ S_m^H := \varepsilon^m + \varepsilon^m\left(\frac{\gamma^H}{\delta^H}\right)^{m-1}; \\ T_m^H := \varepsilon^m + \varepsilon^m\left(\frac{\gamma^H}{\delta^H}\right)^{m-1} + \varepsilon\left(\frac{\gamma^H}{\delta^H}\right)^{m-1}\left(\frac{1-\varepsilon^{m-1}}{1-\varepsilon}\right). \end{cases}$$

Proof:

We proceed to prove (3.3.18); the proof of (3.3.17) is similar. In the following, we suppress the superscript H to simplify notation.

Let $i \in \{0,\ldots,N\}$ be fixed, and let $x \in [x_i, x_{i+1}]$. Then, with the definition

$$h(x,y) := (x-y)_+^{m-1}, \tag{3.3.19}$$

the Taylor expansion of f at x_i is given by

$$f(x) = \sum_{j=0}^{m-1} \frac{f^{(j)}(x_i)}{j!}(x - x_i)^j + \int_{x_i}^{x_{i+1}} \frac{f^{(m)}(y)}{(m-1)!} h(x, y)\mathrm{d}y,$$

whereas the Taylor expansion of $\mathcal{Q}_m f$ is given by

$$(\mathcal{Q}_m f)(x) = \sum_{j=0}^{m-1} \frac{f^{(j)}(x_i)}{j!}(x - x_i)^j + \int_{x_i}^{x_{i+1}} \frac{f^{(m)}(y)}{(m-1)!} (\mathcal{Q}_m h(\cdot, y))(x)\mathrm{d}y,$$

since the quasi-interpolation operator $\mathcal{Q}_m$ preserves polynomials in π_{m-1}. It therefore follows that

$$f(x) - (\mathcal{Q}_m f)(x) = \int_{x_i}^{x_{i+1}} \frac{f^{(m)}(y)}{(m-1)!} \left[h(x, y) - (\mathcal{Q}_m h(\cdot, y))(x)\right] \mathrm{d}y. \quad (3.3.20)$$

The rest of the proof is divided into three parts.

Proof of second inequality in (3.3.18):

We first derive the second inequality in (3.3.18). To this end, let $i \in \{m-1, \ldots, N-m+1\}$ (with $x \in [x_i, x_{i+1}]$). In the following, we suppress the variable of integration y, so that $h(x, y) = h(x)$.

By using the definition (3.2.3) of $\mathcal{Q}_m$ and keeping in mind the support conditions (3.2.10) of the spline molecules constituting $\mathcal{Q}_m$, it follows that

$$h(x) - (\mathcal{Q}_m h)(x) = h(x) - \sum_{j=i+1-m}^{i+m-1} h(y_j) M_{m,j}(x). \quad (3.3.21)$$

Next, we observe that

$$h(y_j) = (y_j - y)_+^{m-1} = 0, \quad y \geq y_j,$$

from the definition of h in (3.3.19), so that, since $y \in [x_i, x_{i+1}]$ and $x_j < y_j < x_{j+1}$ for all $j = 1, \ldots, N-1$ (from (3.2.1)),

$$h(y_j) = 0, \quad j \leq i - 1. \quad (3.3.22)$$

Therefore, with ε defined in (3.3.16) and the upper bound on the spline molecules $M_{m,j}$ given in (3.3.15) in Theorem 3.3.1, (3.3.21) becomes

$$\begin{aligned}
&|h(x) - (\mathcal{Q}_m h)(x)| \\
&\leq |h(x)| + \frac{1}{(m-2)!}\left(\frac{\gamma}{\delta}\right)^{m-1} \sum_{j=i}^{i+m-1} |h(y_j)| \\
&\leq \varepsilon^{m-1} + \frac{1}{(m-2)!}\left(\frac{\gamma}{\delta}\right)^{m-1} \left(\varepsilon^{m-1} + 2\varepsilon^{m-1} + \cdots + m\varepsilon^{m-1}\right) \\
&= \varepsilon^{m-1} + \frac{\varepsilon^{m-1}}{(m-2)!}\left(\frac{\gamma}{\delta}\right)^{m-1} \frac{m(m+1)}{2}.
\end{aligned}$$

Therefore, (3.3.20) becomes

$$\begin{aligned}
&|f(x) - (\mathcal{Q}_m f)(x)| \\
&\leq \int_{x_i}^{x_{i+1}} \frac{f^{(m)}(y)}{(m-1)!}\left[\varepsilon^{m-1} + \frac{m(m+1)\varepsilon^{m-1}}{2(m-2)!}\left(\frac{\gamma}{\delta}\right)^{m-1}\right] \mathrm{d}y \\
&\leq ||f^{(m)}||_{\infty,[x_i,x_{i+1}]}\left[\frac{\varepsilon^m}{(m-1)!} + \frac{m(m+1)\varepsilon^m}{2(m-1)!(m-2)!}\left(\frac{\gamma}{\delta}\right)^{m-1}\right],
\end{aligned}$$

from which our result follows.

Next, for a fixed $i \in \{1, \ldots, m-2\}$, let $x \in [x_i, x_{i+1}]$. In this case, from the definition (3.2.3) and the support properties (3.2.10), we have

$$h(x) - (\mathcal{Q}_m h)(x) = h(x) - \sum_{j=i+1-m}^{-1} h^{(-j)}(a) M_{m,j}(x) - \sum_{j=0}^{i+m-1} h(y_j) M_{m,j}(x).$$

Now, we deduce from the definition of h in (3.3.19) that

$$h^{(n)}(x) = (m-1)(m-2)\cdots(m-n)(x-y)_+^{m-1-n}, \quad n = 0, \ldots, m-1, \tag{3.3.23}$$

so that

$$h^{(n)}(a) = \begin{cases} (m-1)!, & n = m-1; \\ 0, & n = 0, \ldots, m-2. \end{cases} \tag{3.3.24}$$

Therefore, using also the upper bound (3.3.15) and (3.3.22), we have

$|h(x) - (\mathcal{Q}_m h)(x)|$

$$\leq |h(x)| + \frac{1}{(m-2)!}\left(\frac{\gamma}{\delta}\right)^{m-1}\sum_{j=1}^{m-i-1}|h^{(j)}(a)| + \frac{1}{(m-2)!}\left(\frac{\gamma}{\delta}\right)^{m-1}\sum_{j=i}^{i+m-1}|h(y_j)|$$
$$\leq \varepsilon^{m-1} + \frac{1}{(m-2)!}\left(\frac{\gamma}{\delta}\right)^{m-1}\left(\varepsilon^{m-1} + 2\varepsilon^{m-1} + \cdots + m\varepsilon^{m-1}\right)$$
$$= \varepsilon^{m-1} + \frac{\varepsilon^{m-1}}{(m-2)!}\left(\frac{\gamma}{\delta}\right)^{m-1}\frac{m(m+1)}{2}.$$

Therefore, (3.3.20) yields

$$\begin{aligned}
&|f(x) - (\mathcal{Q}_m f)(x)| \\
&\leq \int_{x_i}^{x_{i+1}} \frac{f^{(m)}(y)}{(m-1)!}\left[\varepsilon^{m-1} + \frac{m(m+1)\varepsilon^{m-1}}{2(m-2)!}\left(\frac{\gamma}{\delta}\right)^{m-1}\right]\mathrm{d}y \\
&\leq ||f^{(m)}||_{\infty,[x_i,x_{i+1}]}\left[\frac{\varepsilon^m}{(m-1)!} + \frac{m(m+1)\varepsilon^m}{2(m-1)!(m-2)!}\left(\frac{\gamma}{\delta}\right)^{m-1}\right],
\end{aligned}$$

producing the same result as before.

Proof of first inequality in (3.3.18):

Next, we proceed to show the first inequality in (3.3.18). To this end, let $x \in [x_0, x_1]$. In this case, we have

$$h(x) - (\mathcal{Q}_m h)(x) = h(x) - \sum_{j=1-m}^{-1} h^{(-j)}(a)M_{m,j}(x) - \sum_{j=0}^{m-1} h(y_j)M_{m,j}(x),$$

from (3.2.3) and (3.2.10). Keeping in mind that $x_0 = y_0 < x_1 < y_1 < x_2 < \cdots$ from (3.2.1), we have, using also (3.3.19), (3.3.22), (3.3.24) and the upper bound (3.3.15),

$$\begin{aligned}
&|h(x) - (\mathcal{Q}_m h)(x)| \\
&\leq |h(x)| + \frac{1}{(m-2)!}\left(\frac{\gamma}{\delta}\right)^{m-1}\sum_{j=1}^{m-1}|h^{(j)}(a)| + \frac{1}{(m-2)!}\left(\frac{\gamma}{\delta}\right)^{m-1}\sum_{j=1}^{m-1}|h(y_j)| \\
&\leq \varepsilon^{m-1} + \frac{1}{(m-2)!}\left(\frac{\gamma}{\delta}\right)^{m-1}(m-1)! \\
&\qquad\qquad + \frac{1}{(m-2)!}\left(\frac{\gamma}{\delta}\right)^{m-1}\left(2\varepsilon^{m-1} + 3\varepsilon^{m-1} + \cdots + m\varepsilon^{m-1}\right)
\end{aligned}$$

$$\leq \varepsilon^{m-1} + \frac{(m-1)!}{(m-2)!}\left(\frac{\gamma}{\delta}\right)^{m-1} + \frac{\varepsilon^{m-1}}{(m-2)!}\left(\frac{\gamma}{\delta}\right)^{m-1}\frac{m(m+1)}{2}.$$

Therefore, (3.3.20) yields

$$\begin{aligned}
&|f(x) - (\mathcal{Q}_m f)(x)| \\
&\leq \int_{x_i}^{x_{i+1}} \frac{f^{(m)}(y)}{(m-1)!}\left[\varepsilon^{m-1} + \frac{m(m+1)\varepsilon^{m-1}}{2(m-2)!}\left(\frac{\gamma}{\delta}\right)^{m-1} + \frac{(m-1)!}{(m-2)!}\left(\frac{\gamma}{\delta}\right)^{m-1}\right]\mathrm{d}y \\
&\leq ||f^{(m)}||_{\infty,[x_i,x_{i+1}]}\left[\frac{\varepsilon^m}{(m-1)!} + \frac{m(m+1)\varepsilon^m}{2(m-1)!(m-2)!}\left(\frac{\gamma}{\delta}\right)^{m-1}\right. \\
&\qquad\qquad \left. + \frac{\varepsilon}{(m-2)!}\left(\frac{\gamma}{\delta}\right)^{m-1}\right],
\end{aligned}$$

from which our result follows.

Proof of third inequality in (3.3.18):

Lastly, we let $i \in \{N-m+2, \ldots, N\}$ be fixed, and let $x \in [x_i, x_{i+1}]$. This time, we have

$$h(x) - (\mathcal{Q}_m h)(x) = h(x) - \sum_{j=i+1-m}^{N} h(y_j)M_{m,j}(x) - \sum_{j=N+1}^{i+m-1} h^{(j-N)}(b)M_{m,j}(x),$$

from the definition (3.2.3) and the support properties (3.2.10). Using (3.3.22) and the upper bound (3.3.15), we have

$$\begin{aligned}
&|h(x) - (\mathcal{Q}_m h)(x)| \\
&\leq |h(x)| + \frac{1}{(m-2)!}\left(\frac{\gamma}{\delta}\right)^{m-1}\sum_{j=i}^{N}|h(y_j)| + \frac{1}{(m-2)!}\left(\frac{\gamma}{\delta}\right)^{m-1}\sum_{j=1}^{i+m-1-N}|h^{(j)}(b)|.
\end{aligned} \tag{3.3.25}$$

Now, from (3.3.19) and (3.3.23), we have

$$\begin{aligned}
&\sum_{j=1}^{i+m-1-N}|h^{(j)}(b)| \\
&= \sum_{j=1}^{i+m-1-N}|(m-1)(m-2)\cdots(m-j)(b-y)_+^{m-1-j}|
\end{aligned}$$

$$\begin{aligned}
&\leq (N+1-i)\left[(m-1)\varepsilon^{m-2}+(m-1)(m-2)\varepsilon^{m-3}+\cdots\right.\\
&\qquad \left.+(m-1)(m-2)\cdots(m-(i+m-1-N))\varepsilon^{m-1-(i+m-1-N)}\right]\\
&\leq (m-1)\sum_{k=1}^{m-1}\left[\prod_{\ell=1}^{k}(m-\ell)\right]\varepsilon^{m-1-k}\\
&\leq (m-1)(m-1)!\sum_{k=0}^{m-2}\varepsilon^{k}=(m-1)(m-1)!\frac{1-\varepsilon^{m-1}}{1-\varepsilon}. \qquad (3.3.26)
\end{aligned}$$

Therefore, (3.3.25) becomes

$$\begin{aligned}
&|h(x)-(\mathcal{Q}_m h)(x)|\\
&\leq \varepsilon^{m-1}+\frac{1}{(m-2)!}\left(\frac{\gamma}{\delta}\right)^{m-1}\left(\varepsilon^{m-1}+2\varepsilon^{m-1}+\cdots+(N+1-i)\varepsilon^{m-1}\right)\\
&\quad +\frac{1}{(m-2)!}\left(\frac{\gamma}{\delta}\right)^{m-1}(m-1)(m-1)!\frac{1-\varepsilon^{m-1}}{1-\varepsilon}\\
&\leq \varepsilon^{m-1}+\frac{1}{(m-2)!}\left(\frac{\gamma}{\delta}\right)^{m-1}\left(\varepsilon^{m-1}+2\varepsilon^{m-1}+\cdots+(m-1)\varepsilon^{m-1}\right)\\
&\quad +\frac{(m-1)(m-1)!}{(m-2)!}\left(\frac{\gamma}{\delta}\right)^{m-1}\frac{1-\varepsilon^{m-1}}{1-\varepsilon}\\
&\leq \varepsilon^{m-1}+\frac{\varepsilon^{m-1}}{(m-2)!}\left(\frac{\gamma}{\delta}\right)^{m-1}\frac{m(m-1)}{2}+\frac{(m-1)(m-1)!}{(m-2)!}\left(\frac{\gamma}{\delta}\right)^{m-1}\frac{1-\varepsilon^{m-1}}{1-\varepsilon}.
\end{aligned}$$

Therefore, (3.3.20) becomes

$$\begin{aligned}
&|f(x)-(\mathcal{Q}_m f)(x)|\\
&\leq \int_{x_i}^{x_{i+1}}\frac{f^{(m)}(y)}{(m-1)!}\left[\varepsilon^{m-1}+\frac{m(m-1)\varepsilon^{m-1}}{2(m-2)!}\left(\frac{\gamma}{\delta}\right)^{m-1}\right.\\
&\qquad\qquad \left.+\frac{(m-1)(m-1)!}{(m-2)!}\left(\frac{\gamma}{\delta}\right)^{m-1}\left(\frac{1-\varepsilon^{m-1}}{1-\varepsilon}\right)\right]\mathrm{d}y\\
&\leq ||f^{(m)}||_{\infty,[x_i,x_{i+1}]}\left[\frac{\varepsilon^{m}}{(m-1)!}+\frac{m(m-1)\varepsilon^{m}}{2(m-1)!(m-2)!}\left(\frac{\gamma}{\delta}\right)^{m-1}\right.\\
&\qquad\qquad \left.+\frac{(m-1)\varepsilon}{(m-2)!}\left(\frac{\gamma}{\delta}\right)^{m-1}\left(\frac{1-\varepsilon^{m-1}}{1-\varepsilon}\right)\right],
\end{aligned}$$

which completes our proof. ■

Chapter 4

Blending interpolation

Given a real-valued function f and a strictly increasing sequence of sampling points $\{y_i\} \subseteq [a, b]$, our objective in this chapter is to construct a spline interpolation operator $\mathcal{P}_m$ in terms of the m^{th} order B-splines (defined in (2.3.6) in Chapter 2) such that the following conditions are satisfied:

(i) $\mathcal{P}_m$ is local in the sense that the value of $\mathcal{P}_m f$ at any $y^* \in [a, b]$ only depends on the values of f in a small neighborhood of y^*;

(ii) $\mathcal{P}_m$ preserves polynomials of degree $\leq m - 1$; that is,

$$(\mathcal{P}_m p)(x) = p(x), \quad p \in \pi_{m-1},\ x \in [a, b]; \tag{4.0.1}$$

(iii) $\mathcal{P}_m f$ interpolates f at the interpolation points $\{y_i\}$; that is,

$$(\mathcal{P}_m f)(y_i) = f(y_i), \tag{4.0.2}$$

for all i in $\{y_i\}$;

(iv) $\mathcal{P}_m$ preserves derivatives of f of order ℓ (for some ℓ) at a and b, so that

$$\begin{cases} (\mathcal{P}_m f)^{(\ell)}(a) = f^{(\ell)}(a); \\ (\mathcal{P}_m f)^{(\ell)}(b) = f^{(\ell)}(b). \end{cases} \tag{4.0.3}$$

In (iv), since the derivatives of the function f might not be known in practice, we approximate the ℓ^{th} derivative of f at a and b by the ℓ^{th} order divided difference of f at a and b, respectively, when applying our method.

Our idea is to apply the spline quasi-interpolation operator $\mathcal{Q}_m$ (specifically, $\mathcal{Q}_m^E$ or $\mathcal{Q}_m^H$), developed in Chapter 3, to satisfy properties (i) and (ii). Then, to satisfy the interpolation conditions (iii) and the Hermite interpolation conditions (iv) above (while preserving local support), we will apply a local interpolation operator $\mathcal{R}_m$ as well, leading to the blending operator $\mathcal{P}_m$, as introduced in [13], defined by

$$\mathcal{P}_m := \mathcal{R}_m \oplus \mathcal{Q}_m, \tag{4.0.4}$$

where

$$\mathcal{R}_m \oplus \mathcal{Q}_m := \mathcal{Q}_m + \mathcal{R}_m(\mathcal{I}_m - \mathcal{Q}_m) = \mathcal{Q}_m + \mathcal{R}_m - \mathcal{R}_m\mathcal{Q}_m, \tag{4.0.5}$$

with $\mathcal{I}_m$ denoting the identity operator. From this formulation, it becomes clear that the idea of the blending operation is to first apply the local quasi-interpolation operator $\mathcal{Q}_m$ to f to ensure desired smoothness and high approximation order, and then to apply the local interpolation operator $\mathcal{R}_m$ to the error produced by $\mathcal{Q}_m$ to achieve interpolation at the interpolation points $\{y_i\}$ and preservation of the ℓ^{th} order derivatives at the boundaries $x = a$ and $x = b$. (Note that the operators $\mathcal{Q}_m$ and $\mathcal{R}_m$ are not commutative.)

In Section 4.1, we develop a local interpolation operator $\mathcal{R}_m^E$ that will achieve properties (iii) and (iv) when the knot sequence $\mathbf{x}$ is chosen to coincide with the interpolation point sequence $\mathbf{y}$. Our local interpolation operator is inspired by a method in [15]. However, we note that, in contrast to the scheme in [15], our method is defined for a bounded interval and accommodates the Hermite interpolation conditions in (iv).

Similar to our approach in Chapter 3, we also develop a variation on the local interpolation scheme in Section 4.1 by considering a spline knot sequence $\mathbf{x}$ where each knot x_i is defined to lie midway between the interpolation points y_{i-1} and y_i in $\mathbf{y}$. This gives rise to the local interpolation operator $\mathcal{R}_m^H$, and is described in Section 4.2.

In Section 4.3, we combine the quasi-interpolation operators $\mathcal{Q}_m^E$ and $\mathcal{Q}_m^H$ of Chapter 3 with the local interpolation operators $\mathcal{R}_m^E$ and $\mathcal{R}_m^H$, respectively, in the blending operator, defined in (4.0.4)-(4.0.5). We also show in this section that the blending operator preserves the properties of both

the quasi-interpolation and local interpolation operators.

Lastly, in Section 4.4, we investigate the error bounds for the blending interpolation operator applied to a general real-valued function f.

4.1 Local interpolation: Scheme E

For $m \geq 3$, let $\mathbf{y} = \{y_0, \ldots, y_{N+1}\}$ in (3.1.1) be a given sequence of (non-uniform) sampling points in $[a, b]$, and let f be a real-valued function. We proceed to define the local spline interpolation operator $\mathcal{R}_m^E$, which will facilitate the interpolation conditions (iii) and Hermite interpolation conditions (iv) on p.63. This operator will accompany the spline quasi-interpolation operator $\mathcal{Q}_m^E$, described in Section 3.1 in Chapter 3, in the formation of the blending operator $\mathcal{P}_m$ in (4.0.4). Therefore, the B-spline knot sequence $\mathbf{x}$ is chosen to coincide with the interpolation point sequence $\mathbf{y}$, and we denote both by $\mathbf{x}$ in this section.

To construct $\mathcal{R}_m^E$, we also consider a knot sequence $\mathbf{t} \supset \mathbf{x}$, which is constructed as follows:

- First, let m be even.

  With the definition
  $$q_m := \frac{m}{2}, \tag{4.1.1}$$
  we insert $q_m - 1$ equally spaced knots in between every two (interior) knots of $\mathbf{x}$, so that
  $$t_{m+(j-1)q_m} = x_j, \quad j = 1, \ldots, N.$$
  Furthermore, to facilitate the Hermite interpolation conditions at the boundaries $x = a$ and $x = b$, we also insert $m-1$ evenly spaced knots $t_1, \ldots, t_{m-1}$ in the interval (x_0, x_1), with $t_0 := x_0$, as well as $m-2$ evenly spaced knots $t_{m+(N-1)q_m+1}, \ldots, t_{2m+(N-1)q_m-2}$ in the interval (x_N, x_{N+1}), with $t_{2m+(N-1)q_m-1} := x_{N+1}$. The knot sequence $\mathbf{t}$ is also extended with stacked knots in the same way as $\mathbf{x}$, with $t_j = x_j,\ j =$

$-1, \ldots, -m+1$, and $t_{2m+(N-1)q_m-1+j} = x_{N+1+j},\ j = 1, \ldots, m-1$.

With this setup, we define the knot sequences $\mathbf{t}_{-k},\ k = 0, \ldots, m-1$, and $\mathbf{t}_{N+1+k},\ k = 0, \ldots, m-2$, by

$$\begin{cases} \mathbf{t}_{-k} = \left\{ t_{-k}, \ldots, \underbrace{t_0, \ldots, t_m}_{m+1-k \text{ knots}} \right\}, \quad k = 0, \ldots, m-1; \\ \mathbf{t}_{N+1+k} = \left\{ \underbrace{t_{m+(N-1)q_m}, \ldots, t_{2m+(N-1)q_m-1}}_{m-k \text{ knots}}, \ldots, t_{2m+(N-1)q_m-1+k+1} \right\}, \\ \qquad\qquad\qquad\qquad\qquad\qquad\qquad\qquad\qquad\qquad k = 0, \ldots, m-2, \end{cases} \tag{4.1.2}$$

where the $m+1-k$ knots in $[t_0, t_m]$ are chosen to be evenly spread out among $t_0, \ldots, t_m$; and the $m-k$ knots in $[t_{m+(N-1)q_m}, t_{2m+(N-1)q_m-1}]$ are chosen to be evenly spread out among $t_{m+(N-1)q_m}, \ldots, t_{2m+(N-1)q_m-1}$.

Lastly, the knot sequence $\mathbf{t}_1$ is defined by

$$\mathbf{t}_1 = \{t_{m-q_m}, \ldots, t_{m+q_m}\}.$$

We note that, with the above definitions, each $\mathbf{t}_k,\ k = -m+1, \ldots, 1;\ N+1, \ldots, N+m-1$, contain exactly $m+1$ knots.

- Second, suppose m is odd.

With the definition

$$r_m := \frac{m+1}{2}, \tag{4.1.3}$$

we insert $r_m - 1$ equally spaced knots in (x_j, x_{j+1}) if j is even, and $r_m - 2$ equally spaced knots in (x_j, x_{j+1}) if j is odd, so that

$$t_{m+(j-1)r_m-\lfloor j/2 \rfloor} = x_j, \quad j = 1, \ldots, N.$$

Furthermore, to facilitate the Hermite interpolation conditions at the boundaries $x = a$ and $x = b$, we also insert $m-1$ evenly spaced knots $t_1, \ldots, t_{m-1}$ in the interval (x_0, x_1), with $t_0 := x_0$, as well as

$m-2$ evenly spaced knots $t_{m+(N-1)r_m-\lfloor N/2\rfloor+1},\ldots,t_{2m+(N-1)r_m-\lfloor N/2\rfloor-2}$ in the interval (x_N, x_{N+1}), with $t_{2m+(N-1)r_m-\lfloor N/2\rfloor-1} := x_{N+1}$. The knot sequence $\mathbf{t}$ is also extended with stacked knots in the same way as $\mathbf{x}$, with $t_j = x_j,\ j=-1,\ldots,-m+1$, and $t_{2m+(N-1)r_m-\lfloor N/2\rfloor-1+j} = x_{N+1+j},\ j=1,\ldots,m-1$.

With this setup, we define the knot sequences $\mathbf{t}_{-k},\ k=0,\ldots,m-1$, and $\mathbf{t}_{N+1+k},\ k=0,\ldots,m-2$, by

$$\begin{cases} \mathbf{t}_{-k} = \left\{ t_{-k},\ldots,\ \underbrace{t_0,\ldots,t_m}_{m+1-k \text{ knots}} \right\}, \quad k=0,\ldots,m-1; \\ \mathbf{t}_{N+1+k} = \left\{ \underbrace{t_{m+(N-1)r_m-\lfloor N/2\rfloor},\ldots,t_{2m+(N-1)r_m-\lfloor N/2\rfloor-1}}_{m-k \text{ knots}}, \right. \\ \qquad\qquad \left. \ldots, t_{2m+(N-1)r_m-\lfloor N/2\rfloor-1+k+1} \right\}, \quad k=0,\ldots,m-2, \end{cases} \tag{4.1.4}$$

where the $m+1-k$ knots in $[t_0, t_m]$ are chosen to be evenly spread out among $t_0,\ldots,t_m$; and the $m-k$ knots in $[t_{m+(N-1)r_m-\lfloor N/2\rfloor}, t_{2m+(N-1)r_m-\lfloor N/2\rfloor-1}]$ are chosen to be evenly spread out among $t_{m+(N-1)r_m-\lfloor N/2\rfloor},\ldots,t_{2m+(N-1)r_m-\lfloor N/2\rfloor-1}$.

Lastly, the knot sequence $\mathbf{t}_1$ is defined by

$$\mathbf{t}_1 = \{t_{m-r_m},\ldots,t_{m+r_m-1}\}.$$

Again, we note that with the above definitions, each $\mathbf{t}_k,\ k=-m+1,\ldots,1;\ N+1,\ldots,N+m-1$, contain exactly $m+1$ knots.

Definition 4.1.1 (Local interpolation operator) *With the definitions (4.1.1) and (4.1.3), the local interpolation operator $\mathcal{R}_m^E$ is defined by*

$$(\mathcal{R}_m^E f)(x) := \sum_{\ell=1}^{m-1} f^{(\ell)}(a) L_{m,-\ell}^E(x) + \sum_{i=0}^{N+1} f(x_i) L_{m,i}^E(x) + \sum_{r=1}^{m-2} f^{(r)}(b) L_{m,N+1+r}^E(x), \tag{4.1.5}$$

in terms of the spline molecules

$$\begin{cases} L^E_{m,-\ell}(x) := \sum_{k=0}^{m-1} b^E_{m,-\ell,k} N_{\mathbf{t}_{-m+1+k},m}(x), \quad \ell = 0,\dots,m-1; \\ L^E_{m,1}(x) := \dfrac{N_{\mathbf{t}_1,m}(x)}{N_{\mathbf{t}_1,m}(x_1)}; \\ L^E_{m,i}(x) := \dfrac{N_{\mathbf{t},m,m+(i-2)q_m}(x)}{N_{\mathbf{t},m,m+(i-2)q_m}(x_i)}, \quad i = 2,\dots,N, \quad \text{if } m \text{ is even}; \\ L^E_{m,i}(x) := \dfrac{N_{\mathbf{t},m,m+(i-2)r_m-\lfloor (i-1)/2 \rfloor}(x)}{N_{\mathbf{t},m,m+(i-2)r_m-\lfloor (i-1)/2 \rfloor}(x_i)}, \quad i = 2,\dots,N, \quad \text{if } m \text{ is odd}; \\ L^E_{m,N+1+r}(x) := \sum_{k=0}^{m-2} b^E_{m,N+1+r,k} N_{\mathbf{t}_{N+1+k},m}(x), \quad r = 0,\dots,m-2, \end{cases} \tag{4.1.6}$$

with the coefficients $b^E_{m,-\ell,k}$, $k,\ell = 0,\dots,m-1$, *and* $b^E_{m,N+1+r,k}$, $k,r = 0,\dots,m-2$, *determined by the conditions*

$$\begin{cases} L^{E(n)}_{m,-\ell}(a) = \delta_{\ell-n}, \ \ell, \ n = 0,\dots,m-1; \\ L^{E(n)}_{m,N+1+r}(b) = \delta_{r-n}, \ r, \ n = 0,\dots,m-2. \end{cases} \tag{4.1.7}$$

The above molecules are compactly supported, with

$$\begin{cases} \text{supp} L^E_{m,-\ell} = [x_0, x_1], \quad \ell = 0,\dots,m-1; \\ \text{supp} L^E_{m,1} = [t_{m-q_m}, x_2], \quad \text{if } m \text{ is even}; \\ \text{supp} L^E_{m,1} = [t_{m-r_m}, x_2], \quad \text{if } m \text{ is odd}; \\ \text{supp} L^E_{m,i} = [x_{i-1}, x_{i+1}], \quad i = 2,\dots,N; \\ \text{supp} L^E_{m,N+1+r} = [x_N, x_{N+1}], \quad r = 0,\dots,m-2. \end{cases} \tag{4.1.8}$$

From the construction in (4.1.6), it is clear that

$$L^E_{m,i}(x_j) = \delta_{i-j}, \quad i = 1,\dots,N; \ j = 0,\dots,N+1. \tag{4.1.9}$$

By using also (4.1.7), the following result follows immediately.

Theorem 4.1.1 (Interpolation conditions) *The local interpolation operator* $\mathcal{R}^E_m$, *formulated in (4.1.5) of Definition 4.1.1, satisfies the Hermite interpolation conditions*

$$(\mathcal{R}^E_m f)(x_i) = f(x_i), \quad i = 0,\dots,N+1,$$

and

$$\begin{cases} (\mathcal{R}_m^E f)^{(n)}(a) = f^{(n)}(a), & n = 1, \ldots, m-1; \\ (\mathcal{R}_m^E f)^{(n)}(b) = f^{(n)}(b), & n = 1, \ldots, m-2. \end{cases}$$

4.2 Local interpolation: Scheme H

For $m \geq 3$, let $\mathbf{y} = \{y_0, \ldots, y_N\}$ in (3.2.1) be a given sequence of (non-uniform) sampling points in $[a, b]$, and let f be a real-valued function. In this section, we define the local spline interpolation operator $\mathcal{R}_m^H$ to satisfy the interpolation conditions (iii) and Hermite interpolation conditions (iv) on p.63. This operator will accompany the spline quasi-interpolation operator $\mathcal{Q}_m^H$, described in Section 3.2 in Chapter 3, in the construction of the blending operator $\mathcal{P}_m$ in (4.0.4). We therefore construct the spline knots to lie midway between consecutive sampling points, as in (3.2.2) in Section 3.2.

To construct $\mathcal{R}_m^H$, we again consider a knot sequence $\mathbf{t} \supset \mathbf{y}$, which is constructed following a similar approach as in Section 4.1:

- First, suppose m is even.

  With q_m defined in (4.1.1), that is,

  $$q_m := \frac{m}{2},$$

  we insert $q_m - 1$ equally spaced knots in between every two (interior) knots of $\mathbf{y}$, so that

  $$t_{m+(j-1)q_m} = y_j, \quad j = 1, \ldots, N-1.$$

  Furthermore, to facilitate the Hermite interpolation conditions at the boundaries $x = a$ and $x = b$, we also insert $m - 1$ evenly spaced knots $t_1, \ldots, t_{m-1}$ in the interval (y_0, y_1), with $t_0 := x_0$, as well as $m - 1$ evenly spaced knots $t_{m+(N-2)q_m+1}, \ldots, t_{2m+(N-2)q_m-1}$ in the interval (y_{N-1}, y_N), with $t_{2m+(N-2)q_m} := y_N$. The knot sequence $\mathbf{t}$ is also extended with stacked knots, with $t_{-m+1} = \cdots = t_0$ and $t_{2m+(N-2)q_m} = \cdots = t_{3m+(N-2)q_m-1}$.

With this setup, we define the knot sequences $\mathbf{t}_{-k},\ k = 0, \ldots, m-1$, and $\mathbf{t}_{N+k},\ k = 0, \ldots, m-1$, by

$$\begin{cases} \mathbf{t}_{-k} = \left\{ t_{-k}, \ldots, \underbrace{t_0, \ldots, t_m}_{m+1-k \text{ knots}} \right\}, \quad k = 0, \ldots, m-1; \\ \mathbf{t}_{N+k} = \left\{ \underbrace{t_{m+(N-2)q_m}, \ldots, t_{2m+(N-2)q_m}}_{m+1-k \text{ knots}}, \ldots, t_{2m+(N-2)q_m+k} \right\}, \\ \qquad\qquad\qquad\qquad\qquad\qquad\qquad\qquad k = 0, \ldots, m-1, \end{cases} \tag{4.2.1}$$

where the $m+1-k$ knots in $[t_0, t_m]$ are chosen to be evenly spread out among $t_0, \ldots, t_m$; and the $m+1-k$ knots in $[t_{m+(N-2)q_m}, t_{2m+(N-2)q_m}]$ are chosen to be evenly spread out in among $t_{m+(N-2)q_m}, \ldots, t_{2m+(N-2)q_m}$.

Lastly, the knot sequences $\mathbf{t}_1$ and $\mathbf{t}_{N-1}$ are defined by

$$\begin{aligned} \mathbf{t}_1 &= \{t_{m-q_m}, \ldots, t_{m+q_m}\}; \\ \mathbf{t}_{N-1} &= \left\{t_{m+(N-3)q_m}, \ldots, t_{m+(N-1)q_m}\right\}. \end{aligned}$$

We note that, with the above definitions, each $\mathbf{t}_k,\ k = -m+1, \ldots, 1;\ N-1, \ldots, N+m-1$, contain exactly $m+1$ knots.

- Second, let m be odd.

  With r_m defined in (4.1.3), that is,

  $$r_m := \frac{m+1}{2},$$

  we insert $r_m - 1$ equally spaced knots in (y_j, y_{j+1}) if j is even, and $r_m - 2$ equally spaced knots in (y_j, y_{j+1}) if j is odd, so that

  $$t_{m+(j-1)r_m-\lfloor j/2 \rfloor} = y_j, \quad j = 1, \ldots, N-1.$$

  Furthermore, to facilitate the Hermite interpolation conditions at the boundaries $x = a$ and $x = b$, we also insert $m-1$ evenly spaced knots $t_1, \ldots, t_{m-1}$ in the interval (y_0, y_1), with $t_0 := y_0$, as well as $m-1$

evenly spaced knots $t_{m+(N-2)r_m-\lfloor (N-1)/2\rfloor+1},\ldots,t_{2m+(N-2)r_m-\lfloor (N-1)/2\rfloor-1}$ in the interval (y_N, y_{N+1}), with $t_{2m+(N-2)r_m-\lfloor (N-1)/2\rfloor} := y_N$. The knot sequence $\mathbf{t}$ is also extended with stacked knots, with $t_{-m+1} = \cdots = t_0$ and $t_{2m+(N-2)r_m-\lfloor (N-1)/2\rfloor} = \cdots = t_{3m+(N-2)r_m-\lfloor (N-1)/2\rfloor-1}$.

With this setup, we define the knot sequences $\mathbf{t}_{-k},\ k = 0,\ldots,m-1$, and $\mathbf{t}_{N+k},\ k = 0,\ldots,m-1$, by

$$\begin{cases} \mathbf{t}_{-k} = \left\{ t_{-k},\ldots,\ \underbrace{t_0,\ldots,t_m}_{m+1-k \text{ knots}} \right\}, \quad k = 0,\ldots,m-1; \\ \mathbf{t}_{N+k} = \left\{ \underbrace{t_{m+(N-2)r_m-\lfloor (N-1)/2\rfloor},\ldots,t_{2m+(N-2)r_m-\lfloor (N-1)/2\rfloor}}_{m+1-k \text{ knots}}, \right. \\ \qquad\qquad \left. \ldots, t_{2m+(N-2)r_m-\lfloor (N-1)/2\rfloor+k} \right\}, \quad k = 0,\ldots,m-1, \end{cases} \tag{4.2.2}$$

where the $m+1-k$ knots in $[t_0, t_m]$ are chosen to be evenly spread out among $t_0,\ldots,t_m$; and the $m+1-k$ knots in $[t_{m+(N-2)r_m-\lfloor (N-1)/2\rfloor}, t_{2m+(N-2)r_m-\lfloor (N-1)/2\rfloor}]$ are chosen to be evenly spread out among $t_{m+(N-2)r_m-\lfloor (N-1)/2\rfloor},\ldots,t_{2m+(N-2)r_m-\lfloor (N-1)/2\rfloor}$.

Lastly, the knot sequences $\mathbf{t}_1$ and $\mathbf{t}_{N-1}$ are defined by

$$\mathbf{t}_1 = \left\{ t_{m-r_m},\ldots,t_{m+r_m-1} \right\},$$

and

$$\begin{cases} \mathbf{t}_{N-1} = \left\{ t_{m+(N-3)r_m-\lfloor (N-2)/2\rfloor},\ldots,t_{m+(N-1)r_m-\lfloor (N-1)/2\rfloor-1} \right\}, \\ \qquad\qquad\qquad\qquad\qquad\qquad\qquad\qquad \text{if } N \text{ is even}; \\ \mathbf{t}_{N-1} = \left\{ t_{m+(N-3)r_m-\lfloor (N-2)/2\rfloor},\ldots,t_{m+(N-1)r_m-\lfloor (N-1)/2\rfloor} \right\}, \\ \qquad\qquad\qquad\qquad\qquad\qquad\qquad\qquad \text{if } N \text{ is odd}. \end{cases}$$

Again, we note that with the above definitions, each $\mathbf{t}_k,\ k = -m+1,\ldots,1;\ N-1,\ldots,N+m-1$, contain exactly $m+1$ knots.

Definition 4.2.1 (Local interpolation operator) *With the definitions (4.1.1) and (4.1.3), the local interpolation operator $\mathcal{R}_m^H$ is defined by*

$$(\mathcal{R}_m^H f)(x) := \sum_{\ell=1}^{m-1} f^{(\ell)}(a) L_{m,-\ell}^H(x) + \sum_{i=0}^{N} f(y_i) L_{m,i}^H(x) + \sum_{r=1}^{m-1} f^{(r)}(b) L_{m,N+r}^H(x), \tag{4.2.3}$$

in terms of the spline molecules

$$\begin{cases} L_{m,-\ell}^H(x) := \displaystyle\sum_{k=0}^{m-1} b_{m,-\ell,k}^H N_{\mathbf{t}_{-m+1+k},m}(x), \quad \ell = 0,\dots,m-1; \\ L_{m,1}^H(x) := \dfrac{N_{\mathbf{t}_1,m}(x)}{N_{\mathbf{t}_1,m}(y_1)}; \\ L_{m,i}^H(x) := \dfrac{N_{\mathbf{t},m,m+(i-2)q_m}(x)}{N_{\mathbf{t},m,m+(i-2)q_m}(y_i)}, \quad i = 2,\dots,N-2, \quad \text{if } m \text{ is even}; \\ L_{m,i}^H(x) := \dfrac{N_{\mathbf{t},m,m+(i-2)r_m-\lfloor (i-1)/2 \rfloor}(x)}{N_{\mathbf{t},m,m+(i-2)r_m-\lfloor (i-1)/2 \rfloor}(y_i)}, \quad i = 2,\dots,N-2, \quad \text{if } m \text{ is odd}; \\ L_{m,N-1}^H(x) := \dfrac{N_{\mathbf{t}_{N-1,m}}(x)}{N_{\mathbf{t}_{N-1,m}}(y_{N-1})}; \\ L_{m,N+r}^H(x) := \displaystyle\sum_{k=0}^{m-1} b_{m,N+r,k}^H N_{\mathbf{t}_{N+k},m}(x), \quad r = 0,\dots,m-1, \end{cases} \tag{4.2.4}$$

with the coefficients $b_{m,-\ell,k}^H$, $k,\ell = 0,\dots,m-1$, and $b_{m,N+r,k}^H$, $k,r = 0,\dots,m-1$, determined by the conditions

$$\begin{cases} L_{m,-\ell}^{H(n)}(a) = \delta_{\ell-n}, \ \ell, \ n = 0,\dots,m-1; \\ L_{m,N+r}^{H(n)}(b) = \delta_{r-n}, \ r, \ n = 0,\dots,m-1. \end{cases} \tag{4.2.5}$$

The above molecules are compactly supported, with

$$\begin{cases} \text{supp}L_{m,-\ell}^H = [y_0, y_1], \quad \ell = 0, \ldots, m-1; \\ \text{supp}L_{m,1}^H = [t_{m-q_m}, y_2], \quad \text{if } m \text{ is even}; \\ \text{supp}L_{m,1}^H = [t_{m-r_m}, y_2], \quad \text{if } m \text{ is odd}; \\ \text{supp}L_{m,i}^H = [y_{i-1}, y_{i+1}], \quad i = 2, \ldots, N-2; \\ \text{supp}L_{m,N-1}^H = [y_{N-2}, t_{m+(N-1)q_m}], \quad \text{if } m \text{ is even}; \\ \text{supp}L_{m,N-1}^H = [y_{N-2}, t_{m+(N-1)r_m-\lfloor (N-1)/2 \rfloor -1}], \quad \text{if } m \text{ is odd, } N \text{ is even}; \\ \text{supp}L_{m,N-1}^H = [y_{N-2}, t_{m+(N-1)r_m-\lfloor (N-1)/2 \rfloor}], \quad \text{if } m \text{ is odd, } N \text{ is odd}; \\ \text{supp}L_{m,N+r}^H = [y_{N-1}, y_N], \quad r = 0, \ldots, m-1. \end{cases} \tag{4.2.6}$$

From the construction in (4.2.4), it is clear that

$$L_{m,i}^H(y_j) = \delta_{i-j}, \quad i = 1, \ldots, N-1; \ j = 0, \ldots, N. \tag{4.2.7}$$

By using also (4.2.5), the following result follows immediately.

Theorem 4.2.1 (Interpolation conditions) *The local interpolation operator $\mathcal{R}_m^H$, formulated in (4.2.3) in Definition 4.2.1, satisfies the Hermite interpolation conditions*

$$(\mathcal{R}_m^H f)(y_i) = f(y_i), \quad i = 0, \ldots, N,$$

and

$$\begin{cases} (\mathcal{R}_m^H f)^{(n)}(a) = f^{(n)}(a), \quad n = 1, \ldots, m-1; \\ (\mathcal{R}_m^H f)^{(n)}(b) = f^{(n)}(b), \quad n = 1, \ldots, m-1. \end{cases}$$

4.3 Blending interpolation

With $\mathcal{Q}_m^E$ and $\mathcal{R}_m^E$ formulated in Definitions 3.1.1 and 4.1.1, respectively, and $\mathcal{Q}_m^H$ and $\mathcal{R}_m^H$ formulated in Definitions 3.2.1 and 4.2.1, respectively, we can now derive the blending operator as in (4.0.4), (4.0.5). More specifically, we have

$$\begin{aligned} &\mathcal{P}_m^E \\ &= \mathcal{Q}_m^E + \mathcal{R}_m^E - \mathcal{R}_m^E \mathcal{Q}_m^E \end{aligned}$$

$$
\begin{aligned}
&= \sum_{\ell=1}^{m-1} f^{(\ell)}(a) M^E_{m,-\ell}(x) + \sum_{\ell=1}^{m-1} \left[f^{(\ell)}(a) - (\mathcal{Q}^E_m f)^{(\ell)}(a) \right] L^E_{m,-\ell}(x) \\
&\quad + \sum_{i=0}^{N+1} f(x_i) M^E_{m,i}(x) + \sum_{i=0}^{N+1} \left[f(x_i) - (\mathcal{Q}^E_m f)(x_i) \right] L^E_{m,i}(x) \\
&\quad + \sum_{r=1}^{m-2} f^{(r)}(b) M^E_{m,N+1+r}(x) + \sum_{r=1}^{m-2} \left[f^{(r)}(b) - (\mathcal{Q}^E_m f)^{(r)}(b) \right] L^E_{m,N+1+r}(x),
\end{aligned}
\tag{4.3.1}
$$

and

$$
\begin{aligned}
&\mathcal{P}^H_m \\
&= \mathcal{Q}^H_m + \mathcal{R}^H_m - \mathcal{R}^H_m \mathcal{Q}^H_m \\
&= \sum_{\ell=1}^{m-1} f^{(\ell)}(a) M^H_{m,-\ell}(x) + \sum_{\ell=1}^{m-1} \left[f^{(\ell)}(a) - (\mathcal{Q}^H_m f)^{(\ell)}(a) \right] L^H_{m,-\ell}(x) \\
&\quad + \sum_{i=0}^{N} f(y_i) M^H_{m,i}(x) + \sum_{i=0}^{N} \left[f(y_i) - (\mathcal{Q}^H_m f)(y_i) \right] L^H_{m,i}(x) \\
&\quad + \sum_{r=1}^{m-1} f^{(r)}(b) M^H_{m,N+r}(x) + \sum_{r=1}^{m-1} \left[f^{(r)}(b) - (\mathcal{Q}^H_m f)^{(r)}(b) \right] L^H_{m,N+r}(x).
\end{aligned}
\tag{4.3.2}
$$

We can then show that $\mathcal{P}^E_m$ and $\mathcal{P}^H_m$ satisfy all four conditions (i)-(iv) on p.63, as follows:

Theorem 4.3.1 (Blending operator) *The blending operators $\mathcal{P}^E_m$ and $\mathcal{P}^H_m$, defined by (4.3.1) and (4.3.2), respectively, are local and satisfy the polynomial preservation property of the quasi-interpolation operators $\mathcal{Q}^E_m$ and $\mathcal{Q}^H_m$, respectively, as well as the Hermite interpolation conditions of the local interpolation operators $\mathcal{R}^E_m$ and $\mathcal{R}^H_m$, respectively; that is, $\mathcal{P}^E_m$ and $\mathcal{P}^H_m$ satisfy (4.0.1)-(4.0.3).*

Proof:

We proceed to prove Theorem 4.3.1 for the blending operator $\mathcal{P}^H_m$; the proof for $\mathcal{P}^E_m$ is similar.

(i) First, from the support properties (3.2.10) and (4.2.6), it is clear that $\mathcal{P}_m^H$ is local.

(ii) To verify the polynomial preservation property (4.0.1), let p be a polynomial in π_{m-1}. Then, from Theorem 3.2.1,

$$\begin{aligned}(\mathcal{P}_m^H p)(x) &= (\mathcal{Q}_m^H p)(x) + (\mathcal{R}_m^H p)(x) - (\mathcal{R}_m^H(\mathcal{Q}_m^H p))(x)\\ &= p(x) + (\mathcal{R}_m^H p)(x) - (\mathcal{R}_m^H p)(x) = p(x),\end{aligned}$$

for all $x \in [a, b]$.

(iii) To show that $\mathcal{P}_m^H f$ interpolates f at y_i, $i = 0, \ldots, N$, we may use Theorem 4.2.1 together with (4.2.3), (4.2.7) and (4.2.5) to deduce that

$$\begin{aligned}(\mathcal{P}_m^H f)(y_i) &= (\mathcal{Q}_m^H f)(y_i) + (\mathcal{R}_m^H f)(y_i) - (\mathcal{R}_m^H(\mathcal{Q}_m^H f))(y_i)\\ &= (\mathcal{Q}_m^H f)(y_i) + f(y_i) - (\mathcal{Q}_m^H f)(y_i) = f(y_i),\end{aligned}$$

for $i = 0, \ldots, N$, yielding (4.0.2).

(iv) Lastly, we observe that

$$\begin{aligned}(\mathcal{R}_m^H(\mathcal{Q}_m^H f))^{(n)}(a) &= (\mathcal{Q}_m^H f)^{(n)}(a); \quad n = 1, \ldots, m-1;\\ (\mathcal{R}_m^H(\mathcal{Q}_m^H f))^{(n)}(b) &= (\mathcal{Q}_m^H f)^{(n)}(b), \quad n = 1, \ldots, m-1,\end{aligned}$$

from the construction of $\mathcal{R}_m^H$ and the spline molecules $L_{m,i}^H$ in Definition 4.2.1. Therefore, using also Theorem 4.2.1, we have

$$\begin{aligned}&(\mathcal{P}_m^H f)^{(n)}(a)\\ &= (\mathcal{Q}_m^H f)^{(n)}(a) + (\mathcal{R}_m^H f)^{(n)}(a) - (\mathcal{R}_m^H(\mathcal{Q}_m^H f))^{(n)}(a)\\ &= (\mathcal{Q}_m^H f)^{(n)}(a) + f^{(n)}(a) - (\mathcal{Q}_m^H f)^{(n)}(a) = f^{(n)}(a),\end{aligned}$$

for $n = 1, \ldots, m-1$, and

$$\begin{aligned}&(\mathcal{P}_m^H f)^{(n)}(b)\\ &= (\mathcal{Q}_m^H f)^{(n)}(b) + (\mathcal{R}_m^H f)^{(n)}(b) - (\mathcal{R}_m^H(\mathcal{Q}_m^H f))^{(n)}(b)\\ &= (\mathcal{Q}_m^H f)^{(n)}(b) + f^{(n)}(b) - (\mathcal{Q}_m^H f)^{(n)}(b) = f^{(n)}(b),\end{aligned}$$

for $n = 1, \ldots, m-1$, so that (4.0.3) follows. ■

4.4 Approximation order

Lastly in this chapter, we provide an error analysis of the blending interpolation operators $\mathcal{P}_m^E$ and $\mathcal{P}_m^H$.

From the definitions of $\mathcal{P}_m^E$ and $\mathcal{P}_m^H$ in (4.3.1) and (4.3.2), respectively, it is clear that, in order to bound the error of spline interpolation of these operators, we need upper bounds on the spline molecules $M_{m,i}^E,\ L_{m,i}^E,\ M_{m,i}^{E(n)}$ and $M_{m,i}^H,\ L_{m,i}^H,\ M_{m,i}^{H(n)}$, respectively. The upper bounds on $M_{m,i}^E$ and $M_{m,i}^H$ are given in Theorem 3.3.1 of Chapter 3. We now proceed to derive upper bounds on $L_{m,i}^E,\ M_{m,i}^{E(n)}$ and $L_{m,i}^H,\ M_{m,i}^{H(n)}$.

To this end, we start by obtaining an upper bound on the spline coefficients $b_{m,i,k}^E$ and $b_{m,i,k}^H$ in (4.1.6) and (4.2.4), respectively.

Lemma 4.4.1 (Upper bound on spline coefficients) *For an integer $m \geq 3$, let $\mathbf{x}$ and $\mathbf{y}$ be the sequences defined in (3.1.2) and (3.2.1), respectively, and let $\mathbf{t}$ be the fine knot sequence defined in (4.1.2), (4.1.4), (4.2.1) and (4.2.2). Suppose that*

$$\rho^E := \max\left\{1, |x_1 - x_0|, |x_{N+1} - x_N|\right\} \tag{4.4.1}$$

and

$$\rho^H := \max\left\{1, |y_1 - y_0|, |y_N - y_{N-1}|\right\}. \tag{4.4.2}$$

Then

$$\begin{cases} |b_{m,i,k}^E| = 1, \quad i = 0,\ k = 0, \ldots, m-1; \\ \qquad\qquad\qquad\qquad\qquad\qquad i = N+1,\ k = 0, \ldots, m-2; \\ |b_{m,i,k}^E| \leq \dfrac{\rho^E}{m-1}, \quad i = -m+1, \ldots, -1;\ k = 0, \ldots, m-1; \\ \qquad\qquad\qquad\qquad\qquad\qquad i = N+2, \ldots, N+m-1; \\ \qquad\qquad\qquad\qquad\qquad\qquad\quad k = 0, \ldots, m-2, \end{cases} \tag{4.4.3}$$

and

$$\begin{cases} |b_{m,i,k}^H| = 1, \quad i = 0,\ N;\ k = 0, \ldots, m-1; \\ |b_{m,i,k}^H| \leq \dfrac{\rho^H}{m-1}, \quad i = -m+1, \ldots, -1, N+1, \ldots, N+m-1; \\ \qquad\qquad\qquad\qquad\qquad\qquad\quad k = 0, \ldots, m-1. \end{cases} \tag{4.4.4}$$

Proof:

We provide the proof of (4.4.4); the proof of (4.4.3) follows the same pattern.

Let $-\ell := i \in \{-m+1, \ldots, 0\}$ and $k \in \{0, \ldots, m-1\}$ be fixed (the proof for the case when $i \in \{N, \ldots, N+m-1\}$, $k \in \{0, \ldots, m-1\}$ is similar). From the linear system in the first line of (4.2.4), we may obtain an explicit expression of $b^H_{m,-\ell,k}$ by using Cramer's rule; that is,

$$b^H_{m,-\ell,k} = \frac{\det S_{m,\ell}}{\det S_m},$$

where

$$S_m := \begin{bmatrix} N_{\mathbf{t}_{-m+1},m}(a) & N_{\mathbf{t}_{-m+2},m}(a) & \cdots & N_{\mathbf{t}_0,m}(a) \\ N'_{\mathbf{t}_{-m+1},m}(a) & N'_{\mathbf{t}_{-m+2},m}(a) & \cdots & N'_{\mathbf{t}_0,m}(a) \\ \vdots & \vdots & \ddots & \vdots \\ N^{(m-1)}_{\mathbf{t}_{-m+1},m}(a) & N^{(m-1)}_{\mathbf{t}_{-m+2},m}(a) & \cdots & N^{(m-1)}_{\mathbf{t}_0,m}(a) \end{bmatrix},$$

and $S_{m,\ell}$ is obtained from S_m by replacing its $(\ell+1)^{\text{th}}$ column with the column vector

$$\mathbf{d}_\ell := [\underbrace{0, \ldots, 0}_{\ell}, 1, \underbrace{0, \ldots, 0}_{m-\ell-1}]^T;$$

that is,

$$S_{m,\ell} := \begin{bmatrix} N_{\mathbf{t}_{-m+1},m}(a) & \cdots & N_{\mathbf{t}_{-m+\ell},m}(a) & 0 & N_{\mathbf{t}_{-m+\ell+2},m}(a) & \cdots & N_{\mathbf{t}_0,m}(a) \\ \vdots & \ddots & \vdots & \vdots & \vdots & \ddots & \vdots \\ N^{(\ell-1)}_{\mathbf{t}_{-m+1},m}(a) & \cdots & N^{(\ell-1)}_{\mathbf{t}_{-m+\ell},m}(a) & 0 & N^{(\ell-1)}_{\mathbf{t}_{-m+\ell+2},m}(a) & \cdots & N^{(\ell-1)}_{\mathbf{t}_0,m}(a) \\ N^{(\ell)}_{\mathbf{t}_{-m+1},m}(a) & \cdots & N^{(\ell)}_{\mathbf{t}_{-m+\ell},m}(a) & 1 & N^{(\ell)}_{\mathbf{t}_{-m+\ell+2},m}(a) & \cdots & N^{(\ell)}_{\mathbf{t}_0,m}(a) \\ N^{(\ell+1)}_{\mathbf{t}_{-m+1},m}(a) & \cdots & N^{(\ell+1)}_{\mathbf{t}_{-m+\ell},m}(a) & 0 & N^{(\ell+1)}_{\mathbf{t}_{-m+\ell+2},m}(a) & \cdots & N^{(\ell+1)}_{\mathbf{t}_0,m}(a) \\ \vdots & \ddots & \vdots & \vdots & \vdots & \ddots & \vdots \\ N^{(m-1)}_{\mathbf{t}_{-m+1},m}(a) & \cdots & N^{(m-1)}_{\mathbf{t}_{-m+\ell},m}(a) & 0 & N^{(m-1)}_{\mathbf{t}_{-m+\ell+2},m}(a) & \cdots & N^{(m-1)}_{\mathbf{t}_0,m}(a) \end{bmatrix}.$$

From the construction of the B-splines $N_{\mathbf{t}_{-m+1},m}, \ldots, N_{\mathbf{t}_0,m}$, it is clear that both S_m and $S_{m,\ell}$ are lower triangular matrices, so that their determinants are simply the products of the elements on the main diagonals. Therefore,

we have

$$b^H_{m,-\ell,k} = \frac{\prod_{\substack{j=0 \\ j\neq\ell}}^{m-1} N^{(j)}_{\mathbf{t}_{-m+1+j},m}(a)}{\prod_{j=0}^{m-1} N^{(j)}_{\mathbf{t}_{-m+1+j},m}(a)} = \frac{1}{N^{(\ell)}_{\mathbf{t}_{-m+1+\ell},m}(a)}. \tag{4.4.5}$$

If $\ell = 0$, it follows from the construction of $\mathbf{t}_{-m+1}$ in (4.2.1), (4.2.2), that

$$N_{\mathbf{t}_{-m+1},m}(a) = 1,$$

so that (4.4.5) yields

$$b^H_{m,0,k} = 1.$$

If $\ell \neq 0$, we deduce, by using the recursive formula for the derivative of a B-spline in (2.3.15) and the positivity property (2.3.13) in Theorem 2.3.2, together with the definitions of the knot sequences $\mathbf{t}_{-m+1}, \ldots, \mathbf{t}_0$ in (4.2.1) and (4.2.2), that

$$\begin{aligned}
&N^{(\ell)}_{\mathbf{t}_{-m+1+\ell},m}(a) \\
&= N^{(\ell)}_{\mathbf{t}_{-m+1+\ell},m,-m+1+\ell}(a) \\
&= (m-1)\left[\frac{1}{t_\ell - y_0} N^{(\ell-1)}_{\mathbf{t}_{-m+1+\ell},m-1,-m+1+\ell}(a)\right. \\
&\qquad\qquad \left. - \frac{1}{y_1 - t_{-m+2+\ell}} N^{(\ell-1)}_{\mathbf{t}_{-m+1+\ell},m-1,-m+2+\ell}(a)\right] \\
&= (m-1)(m-2)\left[\frac{1}{(t_\ell - y_0)}\left(\frac{1}{(t_{\ell-1} - y_0)} N^{(\ell-2)}_{\mathbf{t}_{-m+1+\ell},m-2,-m+1+\ell}(a)\right.\right. \\
&\qquad \left. - \frac{1}{(y_1 - t_{-m+2+\ell})} N^{(\ell-2)}_{\mathbf{t}_{-m+1+\ell},m-2,-m+2+\ell}(a)\right) \\
&\qquad - \frac{1}{(y_1 - t_{-m+2+\ell})}\left(\frac{1}{(t_\ell - y_0)} N^{(\ell-2)}_{\mathbf{t}_{-m+1+\ell},m-2,-m+2+\ell}(a)\right. \\
&\qquad\qquad \left.\left. - \frac{1}{(y_1 - t_{-m+3+\ell})} N^{(\ell-2)}_{\mathbf{t}_{-m+1+\ell},m-2,-m+3+\ell}(a)\right)\right] \\
&= (m-1)(m-2)\left[\frac{1}{(t_\ell - y_0)(t_{\ell-1} - y_0)} N^{(\ell-2)}_{\mathbf{t}_{-m+1+\ell},m-2,-m+1+\ell}(a)\right. \\
&\qquad - 2\frac{1}{(t_\ell - y_0)(y_1 - t_{-m+2+\ell})} N^{(\ell-2)}_{\mathbf{t}_{-m+1+\ell},m-2,-m+2+\ell}(a) \\
&\qquad \left. + \frac{1}{(y_1 - t_{-m+2+\ell})(y_1 - t_{-m+3+\ell})} N^{(\ell-2)}_{\mathbf{t}_{-m+1+\ell},m-2,-m+3+\ell}(a)\right]
\end{aligned}$$

$$
\begin{aligned}
&= \cdots \\
&= (m-1)(m-2)\cdots(m-\ell)\times \\
&\quad \left[\frac{1}{(t_\ell - y_0)\cdots(t_1 - y_0)} N_{\mathbf{t}_{-m+1+\ell},m-\ell,-m+1+\ell}(a) - \cdots \right. \\
&\quad \left. + \frac{1}{(y_1 - t_{-m+1+\ell+1})\cdots(y_1 - t_{-m+1+2\ell})} N_{\mathbf{t}_{-m+1+\ell},m-\ell,-m+1+2\ell}(a)\right].
\end{aligned}
$$

The only B-spline in this sum with a non-zero value at $x = a$ is $N_{\mathbf{t}_{-m+1+\ell},m-\ell,-m+1+\ell}(a) = 1$; that is, the only non-zero term in the sum above is the first term. Therefore, with ρ^H defined in (4.4.2), we have

$$
|N^{(\ell)}_{\mathbf{t}_{-m+1+\ell},m}(a)| \geq \frac{(m-1)(m-2)\cdots(m-\ell)}{(\rho^H)^\ell} \geq \frac{m-1}{\rho^H}.
$$

Therefore, (4.4.5) yields

$$
b^H_{m,-\ell,k} \leq \frac{\rho^H}{m-1}.
$$

■

Using Lemma 4.4.1, we may now obtain the following upper bounds on the spline molecules $L^E_{m,i}$ and $L^H_{m,i}$, as follows.

Theorem 4.4.1 (Upper bound on spline molecules) *For an integer $m \geq 3$, let $L^E_{m,i}$ and $L^H_{m,i}$, $i = -m+1, \ldots, N+m-1$, be the spline molecules defined in (4.1.6) and (4.2.4), respectively. Then*

$$
|L^E_{m,i}(x)| \leq \begin{cases} \dfrac{m\rho^E}{m-1}, & i = -m+1, \ldots, -1; \\ m, & i = 0,\ N+1; \\ 1, & i = 1, \ldots, N; \\ \rho^E, & i = N+2, \ldots, N+m-1, \end{cases} \tag{4.4.6}
$$

for all $x \in [a,b]$, and

$$
|L^H_{m,i}(x)| \leq \begin{cases} \dfrac{m\rho^H}{m-1}, & i = -m+1, \ldots, -1; \\ m, & i = 0,\ N; \\ 1, & i = 1, \ldots, N-1; \\ \dfrac{m\rho^H}{m-1}, & i = N+1, \ldots, N+m-1, \end{cases} \tag{4.4.7}
$$

for all $x \in [a, b]$.

Proof:

We show the proof of (4.4.7); the proof of (4.4.6) is similar.

First, if $i \in \{1, \ldots, N-1\}$, the result follows immediately from the construction of $L^H_{m,i}$ in (4.2.4).

For $i = 0$ and $i = N$, we have, from the spline molecule definition (4.2.4), (2.3.10)-(2.3.14) in Theorem 2.3.2, (4.4.4) in Lemma 4.4.1, and the construction of the knot sequences $\mathbf{t}_{-m+1}, \ldots, \mathbf{t}_0$ in (4.2.1) and (4.2.2),

$$|L^H_{m,i}(x)| \leq \sum_{k=0}^{m-1} |b^H_{m,i,k} N_{\mathbf{t}_{-m+1+k},m}(x)| \leq m.$$

Lastly, for $i \in \{-m+1, \ldots, -1\}$ or $i \in \{N+1, \ldots, N+m-1\}$, we have, again using the spline molecule definition (4.2.4) and (2.3.10)-(2.3.14) in Theorem 2.3.2 and (4.4.4) in Lemma 4.4.1 and the construction of the knot sequences $\mathbf{t}_{-m+1}, \ldots, \mathbf{t}_0$ in (4.2.1)-(4.2.2),

$$|L^H_{m,i}(x)| \leq \sum_{k=0}^{m-1} |b^H_{m,i,k} N_{\mathbf{t}_{-m+1+k},m}(x)| \leq \frac{m\rho^H}{m-1}.$$

■

Next, we find an upper bound on the spline molecule derivatives $M^{E(n)}_{m,i}$ and $M^{H(n)}_{m,i}$, as follows:

Theorem 4.4.2 (Upper bound on spline molecule derivatives) *For an integer* $m \geq 3$*, let* $M^E_{m,i}$ *and* $M^H_{m,i}$*,* $i = -m+1, \ldots, N+m-1$*, be defined by (3.1.9) and (3.2.4), respectively. Then*

$$\begin{cases} |M^{E(n)}_{m,i}(a)| \leq \dfrac{m}{(m-2)!} \left(\dfrac{\gamma^E}{\delta^E}\right)^{m-1} \left(\dfrac{2}{\delta^E}\right)^{m-1}, \\ \qquad\qquad i = -m+1, \ldots, m-1; \ n = 1, \ldots, m-1; \\ |M^{E(n)}_{m,i}(b)| \leq \dfrac{m}{(m-2)!} \left(\dfrac{\gamma^E}{\delta^E}\right)^{m-1} \left(\dfrac{2}{\delta^E}\right)^{m-2}, \\ \qquad i = N-m+3, \ldots, N+m-1; \ n = 1, \ldots, m-2; \end{cases} \tag{4.4.8}$$

and

$$\begin{cases} |M_{m,i}^{H(n)}(a)| \leq \dfrac{m}{(m-2)!}\left(\dfrac{\gamma^H}{\delta^H}\right)^{m-1}\left(\dfrac{2}{\delta^H}\right)^{m-1}, \\ \qquad\qquad i=-m+1,\ldots,m-1;\ n=1,\ldots,m-1; \\ |M_{m,i}^{H(n)}(b)| \leq \dfrac{m}{(m-2)!}\left(\dfrac{\gamma^H}{\delta^H}\right)^{m-1}\left(\dfrac{2}{\delta^H}\right)^{m-1}, \\ \qquad i=N-m+2,\ldots,N+m-1;\ n=1,\ldots,m-1. \end{cases} \tag{4.4.9}$$

Proof:

We provide the proof of (4.4.9); the proof of (4.4.8) is similar.

Let $i \in \{-m+1,\ldots,m-1\}$ be fixed (the proof for the right hand side boundary follows similarly). From the spline molecule definition (3.2.4), the upper bound (3.3.8), the recursive formulation of the derivative of a B-spline in (2.3.15), and the definition of δ^H in (3.3.6), we have, for any $n \in \{1,\ldots,m-1\}$,

$$\begin{aligned} |M_{m,i}^{H(n)}(a)| &\leq \sum_{j=0}^{m-1} |a_{m,i,j}^H N_{\mathbf{x},m,i+j-m+1}^{(n)}(a)| \\ &\leq \frac{1}{(\delta^H)^n}\frac{1}{(m-2)!}\left(\frac{\gamma^H}{\delta^H}\right)^{m-1}\sum_{j=0}^{m-1}\sum_{k=0}^{n}\binom{n}{k}N_{\mathbf{x},m-n,i+j-m+1+k}(a) \\ &\leq \frac{1}{(\delta^H)^n}\frac{1}{(m-2)!}\left(\frac{\gamma^H}{\delta^H}\right)^{m-1} m2^{m-1} \\ &\leq \frac{m}{(m-2)!}\left(\frac{\gamma^H}{\delta^H}\right)^{m-1}\left(\frac{2}{\delta^H}\right)^{m-1}. \end{aligned}$$

■

We are now in a position to analyze the approximation order of the blending interpolation operators $\mathcal{P}_m^E$ and $\mathcal{P}_m^H$.

Theorem 4.4.3 (Error of blending interpolation) *For a function $f \in C^m[a,b]$, let $\mathcal{P}_m^E$ and $\mathcal{P}_m^H$ be the spline interpolation operators defined in*

(4.3.1) and (4.3.2), respectively. Let ε *and* γ^E, δ^E *and* γ^H, δ^H *and* ρ^E, ρ^H *be defined as in (3.3.16), (3.3.5), (3.3.6), (4.4.1) and (4.4.2), respectively. Then the supremum norm approximation error of blending spline interpolation is given by*

$$||f-\mathcal{P}_m^E||_{\infty,[x_i,x_{i+1}]} \leq \begin{cases} A_m^E||f^{(m)}||_{\infty,[x_i,x_{i+1}]}U_m^E, & i=0; \\ B_m^E||f^{(m)}||_{\infty,[x_i,x_{i+1}]}V_m^E, & i=1,\ldots,N-m+2; \\ C_m^E||f^{(m)}||_{\infty,[x_i,x_{i+1}]}W_m^E, & i=N-m+3,\ldots,N-1; \\ D_m^E||f^{(m)}||_{\infty,[x_i,x_{i+1}]}X_m^E, & i=N, \end{cases} \tag{4.4.10}$$

where A_m^E, B_m^E *and* C_m^E *are constants independent of* ε, γ^E *and* δ^E, *and*

$$\begin{cases} U_m^E := \varepsilon^m + \varepsilon^m\left(\frac{\gamma^E}{\delta^E}\right)^{m-1} + \varepsilon\left(\frac{\gamma^E}{\delta^E}\right)^{m-1} + \varepsilon^m\rho^E\left(\frac{\gamma^E}{\delta^E}\right)^{m-1}\left(\frac{2}{\delta^E}\right)^{m-1} \\ \qquad\qquad +\varepsilon\rho^E\left(\frac{\gamma^E}{\delta^E}\right)^{m-1}\left(\frac{2}{\delta^E}\right)^{m-1} + \varepsilon\rho^E; \\ V_m^E := \varepsilon^m + \varepsilon^m\left(\frac{\gamma^E}{\delta^E}\right)^{m-1}; \\ W_m^E := \varepsilon^m + \varepsilon^m\left(\frac{\gamma^E}{\delta^E}\right)^{m-1} + \varepsilon\left(\frac{\gamma^E}{\delta^E}\right)^{m-1}\left(\frac{1-\varepsilon^{m-1}}{1-\varepsilon}\right); \\ X_m^E := \varepsilon^m + \varepsilon^m\left(\frac{\gamma^E}{\delta^E}\right)^{m-1} + \varepsilon\left(\frac{\gamma^E}{\delta^E}\right)^{m-1}\left(\frac{1-\varepsilon^{m-1}}{1-\varepsilon}\right) + \varepsilon^m\rho^E\left(\frac{\gamma^E}{\delta^E}\right)^{m-1}\left(\frac{2}{\delta^E}\right)^{m-2} \\ \qquad\qquad +\varepsilon\rho^E\left(\frac{1-\varepsilon^{m-1}}{1-\varepsilon}\right) + \varepsilon\rho^E\left(\frac{\gamma^E}{\delta^E}\right)^{m-1}\left(\frac{2}{\delta^E}\right)^{m-2}\left(\frac{1-\varepsilon^{m-1}}{1-\varepsilon}\right), \end{cases}$$

whereas

$$||f-\mathcal{P}_m^H||_{\infty,[x_i,x_{i+1}]} \leq \begin{cases} A_m^H||f^{(m)}||_{\infty,[x_i,x_{i+1}]}U_m^H, & i=0,\ 1; \\ B_m^H||f^{(m)}||_{\infty,[x_i,x_{i+1}]}V_m^H, & i=2,\ldots,N-m+1; \\ C_m^H||f^{(m)}||_{\infty,[x_i,x_{i+1}]}W_m^H, & i=N-m+2,\ldots,N-2; \\ D_m^H||f^{(m)}||_{\infty,[x_i,x_{i+1}]}X_m^H, & i=N-1,\ N, \end{cases} \tag{4.4.11}$$

where A_m^H, B_m^H *and* C_m^H *are constants independent of* ε, γ^H *and* δ^H, *and*

$$\begin{cases} U_m^H := \varepsilon^m + \varepsilon^m \left(\frac{\gamma^H}{\delta^H}\right)^{m-1} + \varepsilon \left(\frac{\gamma^H}{\delta^H}\right)^{m-1} + \varepsilon^m \rho^H \left(\frac{\gamma^H}{\delta^H}\right)^{m-1} \left(\frac{2}{\delta^H}\right)^{m-1} \\ \qquad\qquad + \varepsilon \rho^H \left(\frac{\gamma^H}{\delta^H}\right)^{m-1} \left(\frac{2}{\delta^H}\right)^{m-1} + \varepsilon \rho^H; \\ V_m^H := \varepsilon^m + \varepsilon^m \left(\frac{\gamma^H}{\delta^H}\right)^{m-1}; \\ W_m^H := \varepsilon^m + \varepsilon^m \left(\frac{\gamma^H}{\delta^H}\right)^{m-1} + \varepsilon \left(\frac{\gamma^H}{\delta^H}\right)^{m-1} \left(\frac{1-\varepsilon^{m-1}}{1-\varepsilon}\right); \\ X_m^H := \varepsilon^m + \varepsilon^m \left(\frac{\gamma^H}{\delta^H}\right)^{m-1} + \varepsilon \left(\frac{\gamma^H}{\delta^H}\right)^{m-1} \left(\frac{1-\varepsilon^{m-1}}{1-\varepsilon}\right) + \varepsilon^m \rho^H \left(\frac{\gamma^H}{\delta^H}\right)^{m-1} \left(\frac{2}{\delta^H}\right)^{m-1} \\ \qquad\qquad + \varepsilon \rho^H \left(\frac{1-\varepsilon^{m-1}}{1-\varepsilon}\right) + \varepsilon \rho^H \left(\frac{\gamma^H}{\delta^H}\right)^{m-1} \left(\frac{2}{\delta^H}\right)^{m-1} \left(\frac{1-\varepsilon^{m-1}}{1-\varepsilon}\right). \end{cases}$$

Proof:

We proceed to prove (4.4.11); the proof of (4.4.10) is similar. In the following, we suppress the superscript H to simplify notation.

Similar to our approach in Theorem 3.3.2, let $i \in \{0, \ldots, N\}$ be fixed, and let $x \in [x_i, x_{i+1}]$. Then, with

$$h(x, y) = (x - y)_+^{m-1},$$

as in (3.3.19), the Taylor expansion of f at x_i is given by

$$f(x) = \sum_{j=0}^{m-1} \frac{f^{(j)}(x_i)}{j!}(x - x_i)^j + \int_{x_i}^{x_{i+1}} \frac{f^{(m)}(y)}{(m-1)!} h(x, y) \mathrm{d}y,$$

whereas the Taylor expansion of $\mathcal{P}_m f$ is given by

$$(\mathcal{P}_m f)(x) = \sum_{j=0}^{m-1} \frac{f^{(j)}(x_i)}{j!}(x - x_i)^j + \int_{x_i}^{x_{i+1}} \frac{f^{(m)}(y)}{(m-1)!} (\mathcal{P}_m h(\cdot, y))(x) \mathrm{d}y,$$

since the blending interpolation operator $\mathcal{P}_m$ preserves polynomials in π_{m-1}. It therefore follows that

$$f(x) - (\mathcal{P}_m f)(x) = \int_{x_i}^{x_{i+1}} \frac{f^{(m)}(y)}{(m-1)!} \left[h(x, y) - (\mathcal{P}_m h(\cdot, y))(x)\right] \mathrm{d}y. \quad (4.4.12)$$

The rest of the proof is divided into three parts.

Proof of second inequality in (4.4.11):

Let $i \in \{m-1, \ldots, N-m+1\}$, with $x \in [x_i, x_{i+1}]$. In the following, we suppress the variable of integration y, so that $h(x,y) = h(x)$.

From the definition of $\mathcal{P}_m$ in (4.3.2), the support properties (3.2.10) and (4.2.6) of the spline molecules, and the definition of $\mathcal{Q}_m$ in (3.2.3), we have

$$\begin{aligned}
&h(x) - (\mathcal{P}_m h)(x) \\
&= h(x) - \sum_{j=i+1-m}^{i+m-1} h(y_j) M_{m,j}(x) - \sum_{j=i-1}^{i+1} h(y_j) L_{m,j}(x) + \sum_{j=i-1}^{i+1} (\mathcal{Q}_m h)(y_j) L_{m,j}(x) \\
&= h(x) - \sum_{j=i+1-m}^{i+m-1} h(y_j) M_{m,j}(x) - \sum_{j=i-1}^{i+1} h(y_j) L_{m,j}(x) \\
&\qquad + \sum_{j=i-1}^{i+1} \left[\sum_{k=j+1-m}^{j+m-1} h(y_k) M_{m,k}(y_j) \right] L_{m,j}(x).
\end{aligned}$$

Next, we use the upper bounds (3.3.15) in Theorem 3.3.1 and (4.4.7) in Theorem 4.4.1, together with (3.3.22), to deduce that

$$\begin{aligned}
&|h(x) - (\mathcal{P}_m h)(x)| \\
&\leq |h(x)| + \frac{1}{(m-2)!} \left(\frac{\gamma}{\delta}\right)^{m-1} \sum_{j=i}^{i+m-1} |h(y_j)| + \sum_{j=i}^{i+1} |h(y_j)| \\
&\quad + \frac{1}{(m-2)!} \left(\frac{\gamma}{\delta}\right)^{m-1} \sum_{j=i-1}^{i+1} \sum_{k=j+1-m}^{j+m-1} |h(y_k)| \\
&\leq \varepsilon^{m-1} + \frac{1}{(m-2)!} \left(\frac{\gamma}{\delta}\right)^{m-1} \left(\varepsilon^{m-1} + 2\varepsilon^{m-1} + \cdots + m\varepsilon^{m-1}\right) + \left(\varepsilon^{m-1} + 2\varepsilon^{m-1}\right) \\
&\quad + \frac{1}{(m-2)!} \left(\frac{\gamma}{\delta}\right)^{m-1} \left[\sum_{k=i}^{i+m-2} |h(y_k)| + \sum_{k=i}^{i+m-1} |h(y_k)| + \sum_{k=i}^{i+m} |h(y_k)| \right] \\
&\leq 4\varepsilon^{m-1} + \frac{1}{(m-2)!} \left(\frac{\gamma}{\delta}\right)^{m-1} \left[\left(\varepsilon^{m-1} + \cdots + (m-1)\varepsilon^{m-1}\right) \right. \\
&\quad \left. + 2\left(\varepsilon^{m-1} + \cdots + m\varepsilon^{m-1}\right) + \left(\varepsilon^{m-1} + \cdots + (m+1)\varepsilon^{m-1}\right) \right]
\end{aligned}$$

$$= 4\varepsilon^{m-1} + \frac{\varepsilon^{m-1}}{(m-2)!}\left(\frac{\gamma}{\delta}\right)^{m-1}\left[\frac{m(m-1)}{2} + \frac{2m(m+1)}{2} + \frac{(m+1)(m+2)}{2}\right]$$
$$= 4\varepsilon^{m-1} + \frac{(2m^2+2m+1)\varepsilon^{m-1}}{(m-2)!}\left(\frac{\gamma}{\delta}\right)^{m-1}.$$

Therefore, (4.4.12) becomes

$$\begin{aligned}
&|f(x) - (\mathcal{P}_m f)(x)| \\
&\leq \int_{x_i}^{x_{i+1}} \frac{f^{(m)}(y)}{(m-1)!}\left[4\varepsilon^{m-1} + \frac{(2m^2+2m+1)\varepsilon^{m-1}}{(m-2)!}\left(\frac{\gamma}{\delta}\right)^{m-1}\right] \mathrm{d}y \\
&\leq ||f^{(m)}||_{\infty,[x_i,x_{i+1}]}\left[\frac{4\varepsilon^m}{(m-1)!} + \frac{(2m^2+2m+1)\varepsilon^m}{(m-1)!(m-2)!}\left(\frac{\gamma}{\delta}\right)^{m-1}\right],
\end{aligned}$$

from which our result follows.

Next, for a fixed $i \in \{2, \ldots, m-2\}$, let $x \in [x_i, x_{i+1}]$. By applying the definition of $\mathcal{P}_m$ in (4.3.2), the support properties (3.2.10) and (4.2.6) of the spline molecules, and the definition of $\mathcal{Q}_m$ in (3.2.3), we deduce that

$$\begin{aligned}
&h(x) - (\mathcal{P}_m h)(x) \\
&= h(x) - \sum_{j=i+1-m}^{-1} h^{(-j)}(a) M_{m,j}(x) - \sum_{j=0}^{i+m-1} h(y_j) M_{m,j}(x) \\
&\quad - \sum_{j=i-1}^{i+1} h(y_j) L_{m,j}(x) + \sum_{j=i-1}^{i+1} (\mathcal{Q}_m h)(y_j) L_{m,j}(x) \\
&= h(x) - \sum_{j=i+1-m}^{-1} h^{(-j)}(a) M_{m,j}(x) - \sum_{j=0}^{i+m-1} h(y_j) M_{m,j}(x) - \sum_{j=i-1}^{i+1} h(y_j) L_{m,j}(x) \\
&\quad + \sum_{j=i-1}^{i+1}\left[\sum_{k=j+1-m}^{-1} h^{(-k)}(a) M_{m,k}(y_j) + \sum_{k=0}^{j+m-1} h(y_k) M_{m,k}(y_j)\right] L_{m,j}(x).
\end{aligned}$$

Next, we use the upper bounds (3.3.15) in Theorem 3.3.1 and (4.4.7) in Theorem 4.4.1, together with (3.3.22) and (3.3.24), to obtain

$$\begin{aligned}
&|h(x) - (\mathcal{P}_m h)(x)| \\
&\leq |h(x)| + \frac{1}{(m-2)!}\left(\frac{\gamma}{\delta}\right)^{m-1} \sum_{j=1}^{m-1-i} |h^{(j)}(a)| + \frac{1}{(m-2)!}\left(\frac{\gamma}{\delta}\right)^{m-1} \sum_{j=i}^{i+m-1} |h(y_j)|
\end{aligned}$$

$$
\begin{aligned}
&+\sum_{j=i}^{i+1}|h(y_j)|+\frac{1}{(m-2)!}\left(\frac{\gamma}{\delta}\right)^{m-1}\sum_{j=i-1}^{i+1}\left[\sum_{k=1}^{m-1-j}|h^{(k)}(a)|+\sum_{k=i}^{j+m-1}|h(y_k)|\right]\\
&\leq \varepsilon^{m-1}+\frac{1}{(m-2)!}\left(\frac{\gamma}{\delta}\right)^{m-1}\left(\varepsilon^{m-1}+2\varepsilon^{m-1}+\cdots+m\varepsilon^{m-1}\right)+\left(\varepsilon^{m-1}+2\varepsilon^{m-1}\right)\\
&\quad+\frac{1}{(m-2)!}\left(\frac{\gamma}{\delta}\right)^{m-1}\left[\sum_{k=1}^{m-i}|h^{(k)}(a)|+\sum_{k=1}^{m-1-i}|h^{(k)}(a)|+\sum_{k=1}^{m-2-i}|h^{(k)}(a)|\right.\\
&\quad\left.+\sum_{k=i}^{i+m-2}|h(y_k)|+\sum_{k=i}^{i+m-1}|h(y_k)|+\sum_{k=i}^{i+m}|h(y_k)|\right]\\
&\leq 4\varepsilon^{m-1}+\frac{1}{(m-2)!}\left(\frac{\gamma}{\delta}\right)^{m-1}\left[\left(\varepsilon^{m-1}+\cdots+(m-1)\varepsilon^{m-1}\right)\right.\\
&\quad\left.+2\left(\varepsilon^{m-1}+\cdots+m\varepsilon^{m-1}\right)+\left(\varepsilon^{m-1}+\cdots+(m+1)\varepsilon^{m-1}\right)\right]\\
&=4\varepsilon^{m-1}+\frac{\varepsilon^{m-1}}{(m-2)!}\left(\frac{\gamma}{\delta}\right)^{m-1}\left[\frac{m(m-1)}{2}+\frac{2m(m+1)}{2}+\frac{(m+1)(m+2)}{2}\right]\\
&=4\varepsilon^{m-1}+\frac{(2m^2+2m+1)\varepsilon^{m-1}}{(m-2)!}\left(\frac{\gamma}{\delta}\right)^{m-1}.
\end{aligned}
$$

Therefore, (4.4.12) becomes

$$
\begin{aligned}
&|f(x)-(\mathcal{P}_m f)(x)|\\
&\leq\int_{x_i}^{x_{i+1}}\frac{f^{(m)}(y)}{(m-1)!}\left[4\varepsilon^{m-1}+\frac{(2m^2+2m+1)\varepsilon^{m-1}}{(m-2)!}\left(\frac{\gamma}{\delta}\right)^{m-1}\right]\mathrm{d}y\\
&\leq||f^{(m)}||_{\infty,[x_i,x_{i+1}]}\left[\frac{4\varepsilon^m}{(m-1)!}+\frac{(2m^2+2m+1)\varepsilon^m}{(m-1)!(m-2)!}\left(\frac{\gamma}{\delta}\right)^{m-1}\right],
\end{aligned}
$$

which is the same result as before.

Proof of first inequality in (4.4.11):

Next, let $x\in[x_i,x_{i+1}],\ i\in\{0,1\}$. In this case, we have

$$
\begin{aligned}
&h(x)-(\mathcal{P}_m h)(x)\\
&=h(x)-\sum_{j=i+1-m}^{-1}h^{(-j)}(a)M_{m,j}(x)-\sum_{j=0}^{i+m-1}h(y_j)M_{m,j}(x)\\
&\quad-\sum_{j=1-m}^{-1}h^{(-j)}(a)L_{m,j}(x)-\sum_{j=0}^{i+1}h(y_j)L_{m,j}(x)
\end{aligned}
$$

$$
\begin{aligned}
&+\sum_{j=1-m}^{-1}(\mathcal{Q}_m h)^{(-j)}(a)L_{m,j}(x)+\sum_{j=0}^{i+1}(\mathcal{Q}_m h)(y_j)L_{m,j}(x)\\
&=h(x)-\sum_{j=i+1-m}^{-1}h^{(-j)}(a)M_{m,j}(x)-\sum_{j=0}^{i+m-1}h(y_j)M_{m,j}(x)\\
&\quad-\sum_{j=1-m}^{-1}h^{(-j)}(a)L_{m,j}(x)-\sum_{j=0}^{i+1}h(y_j)L_{m,j}(x)\\
&\quad+\sum_{j=1-m}^{-1}\left[\sum_{k=j+1-m}^{-1}h^{(-k)}(a)M_{m,k}^{(-j)}(a)+\sum_{k=0}^{j+m-1}h(y_k)M_{m,k}^{(-j)}(a)\right]L_{m,j}(x)\\
&\quad+\sum_{j=0}^{i+1}\left[\sum_{k=j+1-m}^{-1}h^{(-k)}(a)M_{m,k}(y_j)+\sum_{k=0}^{j+m-1}h(y_k)M_{m,k}(y_j)\right]L_{m,j}(x),
\end{aligned}
$$

from the definition of $\mathcal{P}_m$ in (4.3.2), the support properties (3.2.10) and (4.2.6) of the spline molecules, and the definition of $\mathcal{Q}_m$ in (3.2.3). Now, we use the upper bounds (3.3.15) in Theorem 3.3.1 and (4.4.7) in Theorem 4.4.1 and (4.4.9) in Theorem 4.4.2, together with (3.3.22) and (3.3.23), to obtain

$$
\begin{aligned}
&|h(x)-(\mathcal{P}_m h)(x)|\\
&\le |h(x)|+\frac{1}{(m-2)!}\left(\frac{\gamma}{\delta}\right)^{m-1}\sum_{j=1}^{m-1-i}|h^{(j)}(a)|+\frac{1}{(m-2)!}\left(\frac{\gamma}{\delta}\right)^{m-1}\sum_{j=1}^{i+m-1}|h(y_j)|\\
&\quad+\frac{m\rho}{m-1}\sum_{j=1}^{m-1}|h^{(j)}(a)|+m\sum_{j=1}^{i+1}|h(y_j)|\\
&\quad+\frac{m\rho}{m-1}\frac{1}{(m-2)!}\left(\frac{\gamma}{\delta}\right)^{m-1}m\left(\frac{2}{\delta}\right)^{m-1}\sum_{j=1}^{m-1}\left[\sum_{k=1}^{m-1}|h^{(k)}(a)|+\sum_{k=1}^{m-1-j}|h(y_k)|\right]\\
&\quad+m\frac{1}{(m-2)!}\left(\frac{\gamma}{\delta}\right)^{m-1}\sum_{j=0}^{i+1}\left[\sum_{k=1}^{m-1-j}|h^{(k)}(a)|+\sum_{k=1}^{j+m-1}|h(y_k)|\right]\\
&\le \varepsilon^{m-1}+\frac{1}{(m-2)!}\left(\frac{\gamma}{\delta}\right)^{m-1}(m-1)!\\
&\quad+\frac{1}{(m-2)!}\left(\frac{\gamma}{\delta}\right)^{m-1}\left(2\varepsilon^{m-1}+\cdots+(m+1)\varepsilon^{m-1}\right)
\end{aligned}
$$

$$
\begin{aligned}
&+\frac{m\rho}{m-1}(m-1)!+m\left(2\varepsilon^{m-1}+3\varepsilon^{m-1}\right)\\
&+\frac{m\rho}{m-1}\frac{1}{(m-2)!}\left(\frac{\gamma}{\delta}\right)^{m-1}m\left(\frac{2}{\delta}\right)^{m-1}\times\\
&\qquad\qquad\left[(m-1)(m-1)!+\left(2\varepsilon^{m-1}+\cdots+(m-1)\varepsilon^{m-1}\right)\right]\\
&+\frac{m}{(m-2)!}\left(\frac{\gamma}{\delta}\right)^{m-1}\left[(m-1)!+3\left(2\varepsilon^{m-1}+\cdots+(m+2)\varepsilon^{m-1}\right)\right]\\
&\leq(5m+1)\varepsilon^{m-1}+\frac{(m+1)(m-1)!}{(m-2)!}\left(\frac{\gamma}{\delta}\right)^{m-1}\\
&+\frac{\varepsilon^{m-1}}{(m-2)!}\left(\frac{\gamma}{\delta}\right)^{m-1}\left[\frac{(m+1)(m+2)}{2}+\frac{3m(m+2)(m+3)}{2}\right]\\
&+\frac{m\rho(m-1)!}{m-1}+\frac{m^2\rho(m-1)!}{(m-2)!}\left(\frac{\gamma}{\delta}\right)^{m-1}\left(\frac{2}{\delta}\right)^{m-1}\\
&+\frac{m^2\rho\varepsilon^{m-1}}{(m-1)(m-2)!}\left(\frac{\gamma}{\delta}\right)^{m-1}\left(\frac{2}{\delta}\right)^{m-1}\frac{m(m-1)}{2}\\
&\leq(5m+1)\varepsilon^{m-1}+\frac{(m+1)(m-1)!}{(m-2)!}\left(\frac{\gamma}{\delta}\right)^{m-1}\\
&\quad+\frac{\varepsilon^{m-1}(m+2)(3m^2+10m+1)}{2(m-2)!}\left(\frac{\gamma}{\delta}\right)^{m-1}+\frac{m\rho(m-1)!}{m-1}\\
&\quad+\frac{m^2\rho(m-1)!}{(m-2)!}\left(\frac{\gamma}{\delta}\right)^{m-1}\left(\frac{2}{\delta}\right)^{m-1}+\frac{m^3\rho\varepsilon^{m-1}}{2(m-2)!}\left(\frac{\gamma}{\delta}\right)^{m-1}\left(\frac{2}{\delta}\right)^{m-1}.
\end{aligned}
$$

Therefore, (4.4.12) yields

$$
\begin{aligned}
&|f(x)-(\mathcal{P}_mf)(x)|\\
&\leq\int_{x_i}^{x_{i+1}}\frac{f^{(m)}(y)}{(m-1)!}\left[(5m+1)\varepsilon^{m-1}+\frac{(m+1)(m-1)!}{(m-2)!}\left(\frac{\gamma}{\delta}\right)^{m-1}\right.\\
&\quad+\frac{(m+2)(3m^2+10m+1)\varepsilon^{m-1}}{2(m-2)!}\left(\frac{\gamma}{\delta}\right)^{m-1}+\frac{m\rho(m-1)!}{m-1}\\
&\quad\left.+\frac{m^2\rho(m-1)!}{(m-2)!}\left(\frac{\gamma}{\delta}\right)^{m-1}\left(\frac{2}{\delta}\right)^{m-1}+\frac{m^3\rho\varepsilon^{m-1}}{2(m-2)!}\left(\frac{\gamma}{\delta}\right)^{m-1}\left(\frac{2}{\delta}\right)^{m-1}\right]\mathrm{d}y\\
&\leq||f^{(m)}||_{\infty,[x_i,x_{i+1}]}\left[\frac{(5m+1)\varepsilon^m}{(m-1)!}+\frac{(m+1)\varepsilon}{(m-2)!}\left(\frac{\gamma}{\delta}\right)^{m-1}\right.\\
&\quad\left.+\frac{(m+2)(3m^2+10m+1)\varepsilon^m}{2(m-1)!(m-2)!}\left(\frac{\gamma}{\delta}\right)^{m-1}+\frac{m\rho\varepsilon}{m-1}\right.
\end{aligned}
$$

$$+\frac{m^2\rho\varepsilon}{(m-2)!}\left(\frac{\gamma}{\delta}\right)^{m-1}\left(\frac{2}{\delta}\right)^{m-1}+\frac{m^3\rho\varepsilon^m}{2(m-1)!(m-2)!}\left(\frac{\gamma}{\delta}\right)^{m-1}\left(\frac{2}{\delta}\right)^{m-1}\Bigg],$$

from which our result follows.

Proof of third inequality in (4.4.11):

Next, let $i \in \{N-m+2,\ldots,N-2\}$, with $x \in [x_i, x_{i+1}]$. In this case, we have, from the definition of $\mathcal{P}_m$ in (4.3.2), the spline molecule support properties in (3.2.10) and (4.2.6), and the definition of $\mathcal{Q}_m$ in (3.2.3),

$$\begin{aligned}
&h(x)-(\mathcal{P}_m h)(x)\\
&=h(x)-\sum_{j=i+1-m}^{N}h(y_j)M_{m,j}(x)-\sum_{j=N+1}^{i+m-1}h^{(j-N)}(b)M_{m,j}(x)\\
&\quad-\sum_{j=i-1}^{i+1}h(y_j)L_{m,j}(x)+\sum_{j=i-1}^{i+1}(\mathcal{Q}_m h)(y_j)L_{m,j}(x)\\
&=h(x)-\sum_{j=i+1-m}^{N}h(y_j)M_{m,j}(x)-\sum_{j=N+1}^{i+m-1}h^{(j-N)}(b)M_{m,j}(x)-\sum_{j=i-1}^{i+1}h(y_j)L_{m,j}(x)\\
&\quad+\sum_{j=i-1}^{i+1}\left[\sum_{k=j+1-m}^{N}h(y_k)M_{m,k}(y_j)+\sum_{k=N+1}^{j+m-1}h^{(k-N)}(b)M_{m,k}(y_j)\right]L_{m,j}(x).
\end{aligned}$$

Now, we apply the upper bounds (3.3.15) and (4.4.7) together with (3.3.22), (3.3.23) and (3.3.26), to deduce that

$$\begin{aligned}
&|h(x)-(\mathcal{P}_m h)(x)|\\
&\le|h(x)|+\frac{1}{(m-2)!}\left(\frac{\gamma}{\delta}\right)^{m-1}\sum_{j=i}^{N}|h(y_j)|+\frac{1}{(m-2)!}\left(\frac{\gamma}{\delta}\right)^{m-1}\sum_{j=1}^{i+m-1-N}|h^{(j)}(b)|\\
&\quad+\sum_{j=i}^{i+1}|h(y_j)|+\frac{1}{(m-2)!}\left(\frac{\gamma}{\delta}\right)^{m-1}\sum_{j=i-1}^{i+1}\left[\sum_{k=j+1-m}^{N}|h(y_k)|+\sum_{k=1}^{j+m-1-N}|h^{(k)}(b)|\right]\\
&\le\varepsilon^{m-1}+\frac{1}{(m-2)!}\left(\frac{\gamma}{\delta}\right)^{m-1}\left(\varepsilon^{m-1}+\cdots+(m-1)\varepsilon^{m-1}\right)\\
&\quad+\frac{1}{(m-2)!}\left(\frac{\gamma}{\delta}\right)^{m-1}\left[(m-1)(m-1)!\frac{1-\varepsilon^{m-1}}{1-\varepsilon}\right]+\left(\varepsilon^{m-1}+2\varepsilon^{m-1}\right)
\end{aligned}$$

$$+\frac{1}{(m-2)!}\left(\frac{\gamma}{\delta}\right)^{m-1}\left[3\sum_{k=i}^{N}|h(y_k)|+\sum_{k=1}^{i+m-2-N}|h^{(k)}(b)|\right.$$
$$\left.+\sum_{k=1}^{i+m-1-N}|h^{(k)}(b)|+\sum_{k=1}^{i+m-N}|h^{(k)}(b)|\right]$$
$$\leq 4\varepsilon^{m-1}+\frac{4}{(m-2)!}\left(\frac{\gamma}{\delta}\right)^{m-1}\left(\varepsilon^{m-1}+\cdots+(m-1)\varepsilon^{m-1}\right)$$
$$+\frac{4}{(m-2)!}\left(\frac{\gamma}{\delta}\right)^{m-1}\left[(m-1)(m-1)!\frac{1-\varepsilon^{m-1}}{1-\varepsilon}\right]$$
$$=4\varepsilon^{m-1}+\frac{4\varepsilon^{m-1}}{(m-2)!}\left(\frac{\gamma}{\delta}\right)^{m-1}\frac{m(m-1)}{2}+\frac{4(m-1)(m-1)!}{(m-2)!}\left(\frac{\gamma}{\delta}\right)^{m-1}\frac{1-\varepsilon^{m-1}}{1-\varepsilon}.$$

Therefore, (4.4.12) becomes

$$|f(x)-(\mathcal{P}_m f)(x)|$$
$$\leq\int_{x_i}^{x_{i+1}}\frac{f^{(m)}(y)}{(m-1)!}\left[4\varepsilon^{m-1}+\frac{4m(m-1)\varepsilon^{m-1}}{2(m-2)!}\left(\frac{\gamma}{\delta}\right)^{m-1}\right.$$
$$\left.+\frac{4(m-1)(m-1)!}{(m-2)!}\left(\frac{\gamma}{\delta}\right)^{m-1}\left(\frac{1-\varepsilon^{m-1}}{1-\varepsilon}\right)\right]\mathrm{d}y$$
$$\leq||f^{(m)}||_{\infty,[x_i,x_{i+1}]}\left[\frac{4\varepsilon^m}{(m-1)!}+\frac{4m(m-1)\varepsilon^m}{2(m-1)!(m-2)!}\left(\frac{\gamma}{\delta}\right)^{m-1}\right.$$
$$\left.+\frac{4(m-1)\varepsilon}{(m-2)!}\left(\frac{\gamma}{\delta}\right)^{m-1}\left(\frac{1-\varepsilon^{m-1}}{1-\varepsilon}\right)\right],$$

and our result follows.

Proof of fourth inequality in (4.4.11):

Lastly, let $i\in\{N-1,N\}$, with $x\in[x_i,x_{i+1}]$. In this case, we have, from the definition of $\mathcal{P}_m$ in (4.3.2), the spline molecule support properties in (3.2.10) and (4.2.6), and the definition of $\mathcal{Q}_m$ in (3.2.3),

$$h(x)-(\mathcal{P}_m h)(x)$$
$$=h(x)-\sum_{j=i+1-m}^{N}h(y_j)M_{m,j}(x)-\sum_{j=N+1}^{i+m-1}h^{(j-N)}(b)M_{m,j}(x)$$

$$
\begin{aligned}
&\quad - \sum_{j=i-1}^{N} h(y_j) L_{m,j}(x) - \sum_{j=N+1}^{N+m-1} h^{(j-N)}(b) L_{m,j}(x) \\
&\quad + \sum_{j=i-1}^{N} (\mathcal{Q}_m h)(y_j) L_{m,j}(x) + \sum_{j=N+1}^{N+m-1} (\mathcal{Q}_m h)^{(j-N)}(b) L_{m,j}(x) \\
&= h(x) - \sum_{j=i+1-m}^{N} h(y_j) M_{m,j}(x) - \sum_{j=N+1}^{i+m-1} h^{(j-N)}(b) M_{m,j}(x) \\
&\quad - \sum_{j=i-1}^{N} h(y_j) L_{m,j}(x) - \sum_{j=N+1}^{N+m-1} h^{(j-N)}(b) L_{m,j}(x) \\
&\quad + \sum_{j=i-1}^{N} \left[\sum_{k=j+1-m}^{N} h(y_k) M_{m,k}(y_j) + \sum_{k=N+1}^{j+m-1} h^{(k-N)}(b) M_{m,k}(y_j) \right] L_{m,j}(x) \\
&\quad + \sum_{j=N+1}^{N+m-1} \left[\sum_{k=j+1-m}^{N} h(y_k) M_{m,k}^{(j-N)}(b) + \sum_{k=N+1}^{j+m-1} h^{(k-N)}(b) M_{m,k}^{(j-N)}(b) \right] L_{m,j}(x).
\end{aligned}
$$

Next, we apply the upper bounds (3.3.15), (4.4.7) and (4.4.9), together with (3.3.22), (3.3.23) and (3.3.26), to deduce that

$$
\begin{aligned}
&|h(x) - (\mathcal{P}_m h)(x)| \\
&\leq |h(x)| + \frac{1}{(m-2)!} \left(\frac{\gamma}{\delta}\right)^{m-1} \sum_{j=i}^{N} |h(y_j)| + \frac{1}{(m-2)!} \left(\frac{\gamma}{\delta}\right)^{m-1} \sum_{j=1}^{i+m-1-N} |h^{(j)}(b)| \\
&\quad + m \sum_{j=i}^{N} |h(y_j)| + \frac{m\rho}{m-1} \sum_{j=1}^{m-1} |h^{(j)}(b)| \\
&\quad + m \frac{1}{(m-2)!} \left(\frac{\gamma}{\delta}\right)^{m-1} \sum_{j=i-1}^{N} \left[\sum_{k=j+1-m}^{N} |h(y_k)| + \sum_{k=1}^{j+m-1-N} |h^{(k)}(b)| \right] \\
&\quad + \frac{m\rho}{m-1} \frac{1}{(m-2)!} \left(\frac{\gamma}{\delta}\right)^{m-1} m \left(\frac{2}{\delta}\right)^{m-1} \times \\
&\qquad\qquad \sum_{j=1}^{m-1} \left[\sum_{k=j+1-m+N}^{N} |h(y_k)| + \sum_{k=1}^{m-1} |h^{(k)}(b)| \right] \\
&\leq \varepsilon^{m-1} + \frac{1}{(m-2)!} \left(\frac{\gamma}{\delta}\right)^{m-1} \left(\varepsilon^{m-1} + 2\varepsilon^{m-1}\right)
\end{aligned}
$$

$$
\begin{aligned}
&+\frac{1}{(m-2)!}\left(\frac{\gamma}{\delta}\right)^{m-1}2(m-1)!\frac{1-\varepsilon^{m-1}}{1-\varepsilon}+m\left(\varepsilon^{m-1}+2\varepsilon^{m-1}\right)\\
&+\frac{m\rho}{m-1}2(m-1)!\frac{1-\varepsilon^{m-1}}{1-\varepsilon}\\
&+\frac{m}{(m-2)!}\left(\frac{\gamma}{\delta}\right)^{m-1}3\left[\left(\varepsilon^{m-1}+2\varepsilon^{m-1}\right)+2(m-1)!\frac{1-\varepsilon^{m-1}}{1-\varepsilon}\right]\\
&+\frac{m\rho}{m-1}\frac{1}{(m-2)!}\left(\frac{\gamma}{\delta}\right)^{m-1}m\left(\frac{2}{\delta}\right)^{m-1}(m-1)\times\\
&\qquad\qquad\left[\left(\varepsilon^{m-1}+2\varepsilon^{m-1}\right)+2(m-1)!\frac{1-\varepsilon^{m-1}}{1-\varepsilon}\right]\\
\leq\ &(3m+1)\varepsilon^{m-1}+\frac{(9m+3)\varepsilon^{m-1}}{(m-2)!}\left(\frac{\gamma}{\delta}\right)^{m-1}\\
&+\frac{(6m+2)(m-1)!}{(m-2)!}\left(\frac{\gamma}{\delta}\right)^{m-1}\frac{1-\varepsilon^{m-1}}{1-\varepsilon}\\
&+\frac{2m\rho(m-1)!}{m-1}\frac{1-\varepsilon^{m-1}}{1-\varepsilon}+\frac{3m^2\rho\varepsilon^{m-1}}{(m-2)!}\left(\frac{\gamma}{\delta}\right)^{m-1}\left(\frac{2}{\delta}\right)^{m-1}\\
&\qquad+\frac{2m^2\rho(m-1)!}{(m-2)!}\left(\frac{\gamma}{\delta}\right)^{m-1}\left(\frac{2}{\delta}\right)^{m-1}\frac{1-\varepsilon^{m-1}}{1-\varepsilon}.
\end{aligned}
$$

Therefore, (4.4.12) becomes

$$
\begin{aligned}
&|f(x)-(\mathcal{P}_m f)(x)|\\
&\leq\int_{x_i}^{x_{i+1}}\frac{f^{(m)}(y)}{(m-1)!}\left[(3m+1)\varepsilon^{m-1}+\frac{3(3m+1)\varepsilon^{m-1}}{(m-2)!}\left(\frac{\gamma}{\delta}\right)^{m-1}\right.\\
&\quad+\frac{2(3m+1)(m-1)!}{(m-2)!}\left(\frac{\gamma}{\delta}\right)^{m-1}\frac{1-\varepsilon^{m-1}}{1-\varepsilon}+\frac{2m\rho(m-1)!}{m-1}\left(\frac{1-\varepsilon^{m-1}}{1-\varepsilon}\right)\\
&\quad+\frac{3m^2\rho\varepsilon^{m-1}}{(m-2)!}\left(\frac{\gamma}{\delta}\right)^{m-1}\left(\frac{2}{\delta}\right)^{m-1}\\
&\qquad\left.+\frac{2m^2\rho(m-1)!}{(m-2)!}\left(\frac{\gamma}{\delta}\right)^{m-1}\left(\frac{2}{\delta}\right)^{m-1}\left(\frac{1-\varepsilon^{m-1}}{1-\varepsilon}\right)\right]\mathrm{d}y\\
&\leq||f^{(m)}||_{\infty,[x_i,x_{i+1}]}\left[\frac{(3m+1)\varepsilon^m}{(m-1)!}+\frac{3(3m+1)\varepsilon^m}{(m-1)!(m-2)!}\left(\frac{\gamma}{\delta}\right)^{m-1}\right.\\
&\quad\left.+\frac{2(3m+1)\varepsilon}{(m-2)!}\left(\frac{\gamma}{\delta}\right)^{m-1}\left(\frac{1-\varepsilon^{m-1}}{1-\varepsilon}\right)+\frac{2m\rho\varepsilon}{m-1}\left(\frac{1-\varepsilon^{m-1}}{1-\varepsilon}\right)\right.
\end{aligned}
$$

$$+\frac{3m^2\rho\varepsilon^m}{(m-1)!(m-2)!}\left(\frac{\gamma}{\delta}\right)^{m-1}\left(\frac{2}{\delta}\right)^{m-1}$$
$$+\frac{2m^2\rho\varepsilon}{(m-2)!}\left(\frac{\gamma}{\delta}\right)^{m-1}\left(\frac{2}{\delta}\right)^{m-1}\left(\frac{1-\varepsilon^{m-1}}{1-\varepsilon}\right)\Bigg],$$

thereby completing our proof of (4.4.11). ■

Chapter 5

Stationary and non-stationary signals

Signals with frequencies that do not change with time are called stationary signals. These types of signals are best analyzed by Fourier series methods or the Fourier transform. This is discussed in Section 5.1 of this chapter.

However, most real-life signals are non-stationary; that is, their frequencies may change with time. To analyze these types of signals, we need to expand the traditional Fourier signal model. In the current signal processing literature, this is done by the adaptive harmonic model, to be introduced and described in Section 5.2 of this chapter.

In Section 5.3, we give an overview of a few existing methods in the literature that analyze non-stationary signals, namely the short-time Fourier transform, the continuous wavelet transform, the Wigner distribution, and reassignment methods. Empirical mode decomposition and the synchrosqueezed wavelet transform are two more non-stationary signal analysis techniques – these will be studied in much more detail in Chapters 6 and 7, respectively.

5.1 Stationary signals

We have already seen in Section 2.1 in Chapter 2 that, by considering the Fourier series of even function extensions, every finite-energy signal f on the bounded interval $[0, \frac{L}{2}]$ (that is, f satisfies $\int_0^{L/2} |f(t)|^2 \mathrm{d}t < \infty$) has a

Fourier cosine series representation given by

$$f(t) = \frac{a_0}{2} + \sum_{j=1}^{\infty} a_j \cos\left(\frac{2\pi jt}{L}\right), \quad -\frac{L}{2} \leq t \leq \frac{L}{2}, \tag{5.1.1}$$

where

$$a_j = \frac{4}{L}\int_0^{\frac{L}{2}} f(t)\cos\left(\frac{2\pi jt}{L}\right), \quad j = 0, 1, 2, \ldots \tag{5.1.2}$$

(see Theorem 2.1.2 in Chapter 2). Therefore, every periodic signal f, with period L as in (5.1.1)-(5.1.2), has frequencies $\omega_j = \frac{j}{L}$Hz, for all positive integers j, provided that $a_j \neq 0$ (where "Hz" stands for the unit *Hertz*, for measuring the number of cycles of oscillation per second, when t represents the time variable).

On the other hand, to study the frequency content of a finite-energy signal f with time-domain $\mathbb{R}$, the Fourier transform, defined in (2.2.1) in Section 2.2 in Chapter 2, is commonly used instead. As an example, let us consider the signal

$$f(t) = a_0 + \sum_{j=1}^{N} a_j \cos 2\pi\omega_j t, \tag{5.1.3}$$

for arbitrary frequency values $\omega_j > 0$ and $a_j \in \mathbb{R}$, $j = 1, \ldots, N$. This signal is called a stationary signal, since the frequencies ω_j, $j = 1, \ldots, N$, are independent of the time variable $t \in \mathbb{R}$. Using (2.2.11) in Example 2.2.1, the Fourier transform of f in (5.1.3) is given by

$$\hat{f}(\omega) = a_0\delta(\omega) + \frac{1}{2}\sum_{j=1}^{N} a_j \left(\delta\left(\omega - \omega_j\right) + \delta\left(\omega + \omega_j\right)\right). \tag{5.1.4}$$

Therefore, the frequencies of a stationary signal f with time domain $\mathbb{R}$ can be easily determined by applying the Fourier transform.

We remark that the stationary signal in (5.1.3) is a special case of the general stationary signal model

$$f(t) = a_0 + \sum_{j=1}^{N} a_j \cos 2\pi(\omega_j t + b_j), \tag{5.1.5}$$

with $b_j = 0$. This general model allows for the use of sine functions and negative amplitudes for stationary signals. Of course, every f in (5.1.5) has the same frequencies $\omega_j,\ j = 1, \ldots, N$, as the corresponding f in (5.1.3), since

$$\hat{f}(\omega) = a_0\delta(\omega) + \frac{1}{2}\sum_{j=1}^{N} a_j e^{i2\pi\omega b_j/\omega_j}\left(\delta(\omega-\omega_j) + \delta(\omega+\omega_j)\right),$$

as in (5.1.4), using also (2.2.8) in Theorem 2.2.1.

It is clear that the Fourier transform is useful to discover the frequency contents of a stationary signal. However, since the Fourier transform does not display the time instants at which specific frequency values are assumed, it becomes problematic to analyze the frequency contents of signals whose frequencies change with time. These types of signals and methods to study them are the topics of investigation in our following sections.

5.2 Non-stationary signals

In the previous section, we saw how the Fourier cosine series representation (5.1.1)-(5.1.2) may be used to study the frequency content of periodic signals, whereas the Fourier transform is useful to study the frequency content of stationary signals as in (5.1.3) or (5.1.5).

In this section, we study signals of the form

$$f(t) = \sum_{j=1}^{N} A_j(t)\cos 2\pi\phi_j(t) + T(t), \tag{5.2.1}$$

where $A_j(t) > 0$, $\phi_j(t) \in C^2$ such that $\phi_j'(t) > 0$, and $T(t)$ is some polynomial (possibly embedded with noise). In other words, f is a superposition of the *signal components*

$$f_j(t) = A_j(t)\cos 2\pi\phi_j(t), \quad j = 1, \ldots, N. \tag{5.2.2}$$

The functions $A_j(t)$ are called *magnitude* or *amplitude functions*, generalizing the constants a_j in (5.1.3), while the functions $\phi_j(t)$ are called *phase functions*, generalizing the linear functions $\omega_j t$ in (5.1.3). The derivative

of the phase function $\phi_j'(t),\ j = 1, \ldots, N$, is therefore a natural extension of the frequency ω_j in (5.1.3), and we call each $\phi_j'(t)$ the instantaneous frequency of $f_j(t)$ (as mentioned in Chapter 1). The *trend* $T(t)$ is a generalization of the constant factor a_0 in the stationary signal model (5.1.3).

If the phase functions $\phi_j(t)$ are non-linear functions, we say that f in (5.2.1) is a non-stationary signal (as introduced in Chapter 1). If the magnitude functions $A_j(t)$ are allowed to be non-constants, f is said to be *non-linear*.

In the current signal processing literature, the signal model (5.2.1) is called the *adaptive harmonic model* (AHM) [11, 15, 20, 48, 16]. It is important to point out that when a given signal f in the AHM (5.2.1) is a blind source signal, it is definitely not feasible to determine its specific signal components $f_j(t),\ j = 1, \ldots, N$, by any decomposition scheme, without prior knowledge of these components and/or specifying appropriate restrictions on the AHM. In the literature, these restrictions are described by

$$\begin{cases} A_j \in C^1(\mathbb{R}) \cap L^\infty(\mathbb{R}); \quad \phi_j \in C^2(\mathbb{R}); \\ \inf\limits_{t\in\mathbb{R}} A_j(t) > c_1; \quad \sup\limits_{t\in\mathbb{R}} A_j(t) < c_2; \\ \inf\limits_{t\in\mathbb{R}} \phi_j'(t) > c_1; \quad \sup\limits_{t\in\mathbb{R}} \phi_j'(t) < c_2; \\ |A_j'(t)| \leq \varepsilon\phi_j'(t); \quad |\phi_j''(t)| < \varepsilon\phi_j'(t), \end{cases} \tag{5.2.3}$$

for all $t \in \mathbb{R}$, where $0 < \varepsilon \ll 1$ and $\varepsilon \ll c_1 < c_2 < \infty$. Also, this model assumes that the components are *well-separated*, in the sense that their respective phase functions $\phi_j(t)$ satisfy

$$\phi_j'(t) > \phi_{j-1}'(t); \quad \text{and} \quad |\phi_j'(t) - \phi_{j-1}'(t)| \geq d[\phi_j'(t) + \phi_{j-1}'(t)], \tag{5.2.4}$$

for some $0 < d < 1$ and all $t \in \mathbb{R}$. We will denote the class of functions f that satisfy the AHM conditions (5.2.3)-(5.2.4) by $\mathcal{A}_{\varepsilon,d}^{c_1,c_2}$.

In general, the representation of a signal component $f_j(t)$ in (5.2.2) is not unique – indeed, there exist smooth functions $\alpha(t)$ and $\beta(t)$ such that $\cos t = (1 + \alpha(t)) \cos(t + \beta(t))$. This is called the *identifiability problem* in [11]. However, it is shown in [11, Theorem 2.1] that if

$$g(t) = A(t) \cos 2\pi\phi(t) = (A(t) + \alpha(t)) \cos 2\pi(\phi(t) + \beta(t))$$

satisfies the conditions in (5.2.3), then

$$|\alpha(t)| \leq C\varepsilon \quad \text{and} \quad |\beta'(t)| \leq C\varepsilon,$$

where C is a constant depending only on c_1 and c_2. In other words, the definitions of instantaneous frequency and amplitude are rigorous in the sense that they are unique up to a negligible error when ε is small enough. (See also [15].)

We remark that the definition of the AHM in (5.2.1)-(5.2.4) may be adapted to model signals contaminated with noise (see [11, 15]), or even to model signal components in terms of general *wave shape functions* $s_j(t)$ instead of cosine functions (see [52, 15]).

5.3 Overview of time-frequency methods

Since the IF's $\phi_j'(t),\ j = 1, \ldots, N$, in (5.2.1) may be time-dependent, the Fourier transform (which provides us with a *frequency domain* representation $\hat{f}(\omega)$ of a signal $f(t)$ in the time domain) is not sufficient to study the frequency content of non-stationary signals of the form (5.2.1). This type of signal is better analyzed through methods that provide us with a signal representation in the *time-frequency plane*. These methods are commonly called *time-frequency methods* in the signal processing literature [31, 17, 23, 30, 4]. We proceed to give a brief overview of well-known time-frequency methods in the literature, namely:

- the short-time Fourier transform;
- the continuous wavelet transform;
- the Wigner distribution; and
- reassignment methods.

Short-time Fourier transform:

The *short-time Fourier transform* (STFT) or *localized Fourier transform* is one method that aims to make the traditional Fourier transform time-dependent by introducing a window function, as follows.

Definition 5.3.1 (Short-time Fourier transform) *For a window function $u \in (L^1 \cap L^2)(\mathbb{R})$ and a function $f \in L^2(\mathbb{R})$, the short-time Fourier transform $\mathcal{F}_u f$ of f with respect to u at the time-frequency point (x, ω) is defined by*

$$(\mathcal{F}_u f)(x, \omega) = \int_{-\infty}^{\infty} f(t) u(t - x) e^{-i2\pi\omega t} \mathrm{d}t, \tag{5.3.1}$$

for $x, \omega \in \mathbb{R}$.

The STFT was first considered by Dennis Gabor in his 1946 paper on the mathematical theory of communications [26], where he used the Gaussian function

$$g_\sigma(x) := \frac{1}{2\sigma\sqrt{\pi}} e^{-\left(\frac{x}{2\sigma}\right)^2},$$

with $\sigma = \frac{1}{2\sqrt{\pi}}$, as window function, leading to the Gabor transform (a special case of the STFT).

The STFT may be described as follows: the window function u in (5.3.1) is used to localize the signal f before the Fourier transform is applied, and this window is allowed to "slide" continuously along the time-axis $\mathbb{R}$. In other words, the STFT $\mathcal{F}_u f$ essentially consists of consecutive Fourier transforms, where each transform is performed on the signal f within the window u. As the window u moves along the time line, the Fourier transform is performed on the entire signal f [27].

An important feature of the STFT is that the signal f may be reconstructed from its STFT $\mathcal{F}_u f$, provided that the window function u satisfies certain conditions (see [14, Theorem 4, p.358]):

Theorem 5.3.1 (Inverse short-time Fourier transform) *Let $u \in (L^1 \cap L^2)(\mathbb{R})$ such that $\hat{u} \in (L^1 \cap L^2)(\mathbb{R})$ and $u(0) \neq 0$. If $f \in (L^1 \cap L^2)(\mathbb{R})$ with $\hat{f} \in L^1(\mathbb{R})$, then*

$$f(x) = \frac{1}{u(0)} \int_{-\infty}^{\infty} (\mathcal{F}_u f)(x, \omega) e^{i2\pi\omega x} \mathrm{d}\omega.$$

Continuous wavelet transform:

Second, the continuous wavelet transform, considered in Section 2.5 of Chapter 2, is another example of a time-frequency method. Like the STFT, the CWT makes use of a window function (the wavelet $\psi_{b,a}$) to localize the observed signal f to analyze its time and frequency content. However, where the window width of the window function u in the definition of the STFT (5.3.1) is fixed for a given window u, the window width of the wavelet $\psi_{b,a}$ is allowed to change as the scale factor a varies (as explained in Section 2.5).

Wigner distribution:

Next, the *Wigner distribution* (WD) was invented by E. Wigner in 1932 [51] in the context of quantum mechanics, and introduced in the area of signal analysis by J. Ville in 1948 [49].

Definition 5.3.2 (Wigner distribution) *For a function $f \in L^2(\mathbb{R})$, the Wigner distribution $\mathcal{W}f$ of f at the time-frequency point (x, ω) is given by*

$$(\mathcal{W}f)(x,\omega) = \int_{-\infty}^{\infty} f\left(x + \tfrac{t}{2}\right) \overline{f\left(x - \tfrac{t}{2}\right)} e^{-i2\pi\omega t} \mathrm{d}t. \tag{5.3.2}$$

Unlike the STFT and CWT, the WD does not depend on an arbitrary window function; it only depends on the signal f itself. As such, it should display the time-frequency behavior of f in a "pure, unobstructed form" [30, p.60]. However, the WD is an example of a *quadratic time-frequency method* (whereas the STFT and CWT are classified as *linear time-frequency methods*), as can be seen from its definition in (5.3.2). In other words, if we think of the WD $\mathcal{W}f$ of a signal f as $\mathcal{W}f = C(f, f)$, it follows that, for any complex numbers α and β,

$$\mathcal{W}(\alpha f + \beta h) = |\alpha|^2 \mathcal{W}f + |\beta|^2 \mathcal{W}h + \alpha\overline{\beta} C(f,h) + \overline{\alpha}\beta C(h,f).$$

Therefore, the quadratic nature of this method introduces the cross terms $C(f, h)$ and $C(h, f)$, which are difficult to analyze and interpret [30]. The cross terms may also introduce disturbing interferences in the visual representation of the WD in the time-frequency plane (see [20, 2, 24]). There are many variations on the WD which aim to reduce the effect of the cross terms, at the expense of good localization in the time-frequency plane. These include the *pseudo Wigner-Ville distribution* and the *smoothed pseudo Wigner-Ville distribution* [1].

Reassignment methods:

Lastly, *reassignment* was first introduced in the late 1970's by Kodera, Gendrin and De Villedary [41, 42], and later generalized by Flandrin and Auger (who coined the term "reassignment") [1]. The method works by creating a modified version of a time-frequency representation (like the STFT, for example) by moving its time-frequency values away from where they are computed, in order to produce a better localization of the signal components. In essence, the time-frequency values (x, ω) are moved or reassigned to the *center of gravity* or *local centroid* $(\tilde{x}, \tilde{\omega})$ of the energy contributions of the time-frequency representation [1, 2]. This improves classic time-frequency representations by providing a clearer graphical display of the oscillatory features of a signal, easing signal interpretation. It is very effective in this regard, but reconstruction of signal components is not straightforward.

More recent developments in the area of time-frequency methods include empirical mode decomposition and the synchrosqueezed wavelet transform, as introduced in Chapter 1. We will study these methods in great detail in Chapters 6 and 7, respectively.

Chapter 6

Empirical mode decomposition

The EMD algorithm, introduced by N.E. Huang and others in 1998 [36], is arguably the most popular mathematical scheme for non-stationary signal decomposition and time-frequency analysis. As briefly described in Chapter 1, the objective of EMD is to decompose a given (not necessarily stationary) signal into a number of oscillating components, called intrinsic mode functions, and a monotone or slowly oscillating remainder, which may be considered as the trend of the given signal. Each IMF is then extended to an amplitude-frequency modulated signal through the Hilbert transform in order to compute its instantaneous frequency and amplitude.

In Section 6.1, we describe the EMD algorithm in detail and provide illustrations of the method. Much research has been done to develop variations on EMD to improve the results yielded by EMD; we consider some of these variations in Section 6.2. Lastly, in Section 6.3, we describe some limitations of this method.

6.1 EMD algorithm

We start this chapter by describing the EMD algorithm.

Given a real-valued signal f on an interval $[0, T]$ for some $T > 0$, the EMD algorithm starts by setting $h_{1,0} := f$ and computing the cubic spline interpolants (as described in the beginning of Section 2.4 in Chapter 2) of the local maxima and minima of $h_{1,0}$, respectively, called the *upper* and

lower envelopes of h_{10}. Next, it computes the average $m_{1,1}$ of the upper and lower envelopes, and subtracts it from $h_{1,0}$ to obtain $h_{1,1}$. This process of finding upper and lower envelopes and subtracting their mean from the input signal is now repeated on $h_{1,1}$ to find $h_{1,2}, h_{1,3}, h_{1,4}$, and so on, until for some $\ell \geq 1$ the resulting $h_{1,\ell} = h_{1,\ell-1} - m_{1,\ell}$ satisfies the definition of an IMF:

(i) its upper and lower envelopes are (at least approximately) symmetric about the time axis; and

(ii) the difference between its number of local extrema and its number of zero crossings equals -1, 0 or 1.

In practice, $h_{1,\ell}$ is classified as an IMF when a certain stopping criterion is satisfied. In the EMD literature, various criteria have been implemented. The most common one originates from the original paper [36], namely that $h_{1,\ell}$ is defined to be an IMF when

$$\frac{\sum_{i=0}^{n} |h_{1,\ell-1}(t_i) - h_{1,\ell}(t_i)|}{\sum_{i=0}^{n} h_{1,\ell-1}^2(t_i)} < \varepsilon,$$

for all sampling points $\{t_0, \ldots, t_n\}$ in the time interval $[0, T]$. Typically, ε is set between 0.2 and 0.3 [36]. A different approach was proposed in [35, 39], called the *S-stoppage* criterion. With this approach, the sifting process stops after the number of zero crossings and the number of extrema are equal or differ by at most 1 (condition (ii) above), and these numbers stay the same for S consecutive iterations. Experimental results indicate that S should be chosen between 3 and 8 [39]. (See also [37].)

The first IMF $h_{1,\ell}$ is denoted by C_1, and this process to find an IMF is called *sifting*. To find the subsequent IMF's C_j, $j = 2, 3, \ldots$, the sifting procedure is repeated on $h_{j,0} := f - C_1 - \cdots - C_{j-1}$. The stopping criterion can be chosen by the user; usually, the algorithm stops when the remainder $R_N := f - C_1 - \cdots - C_N$ (for some $N \geq 1$) is a monotonic or slowly oscillating function [37].

The above series of sifting procedures yields a decomposition of the original signal f into the N IMF's $C_1, \ldots, C_N$, and the remainder R_N,

written as

$$f(t) = \sum_{j=1}^{N} C_j(t) + R_N(t). \tag{6.1.1}$$

This constitutes the first part of the algorithm, with the aim of extracting the intrinsic oscillating modes, at characteristic time scales, contained inside the signal f. The first IMF, C_1, constitutes the mode with the finest time scale and is extracted first. The subsequent IMF's $C_2, \ldots, C_N$ each represent modes with coarser time scales. Therefore, the IMF-expansion in (6.1.1) may be viewed as a *waveform-based decomposition.*

The second part of the algorithm is to find the instantaneous frequency and amplitude of each IMF through Hilbert spectral analysis, described in (2.6.6)-(2.6.10) in Section 2.6 in Chapter 2, so that

$$\begin{cases} f(t) = \sum_{j=1}^{N} C_j(t) + R_N(t); \\ C_j(t) = B_j(t) \cos 2\pi\theta_j(t), \quad j = 1, \ldots, N, \end{cases} \tag{6.1.2}$$

with

$$B_j(t) = |C_j^\star(t)|; \qquad \text{and} \qquad \theta_j(t) = \frac{1}{2\pi} \tan^{-1} \frac{(\mathcal{H}C_j)(t)}{C_j(t)}. \tag{6.1.3}$$

The derivative $\theta_j'(t)$ of the phase function $\theta_j(t)$ is the IF of the IMF C_j.

In Figures 6.1-6.3, we illustrate the working of the EMD-HSA approach by considering the stationary signal

$$f(t) = f_1(t) + f_2(t) + f_3(t), \tag{6.1.4}$$

with

$$f_1(t) = \cos 2\pi(8t); \quad f_2(t) = \cos 2\pi(4t); \quad f_3(t) = \cos 2\pi t. \tag{6.1.5}$$

The three components have actual frequencies 8, 4 and 1, respectively.

In Figure 6.1, we display the first part of the sifting process, with the original signal $h_{1,0} := f$ in (a), the upper envelope (in red) and lower envelope (in blue) in (b), the mean envelope $m_{1,1}$ (in purple) in (c), and

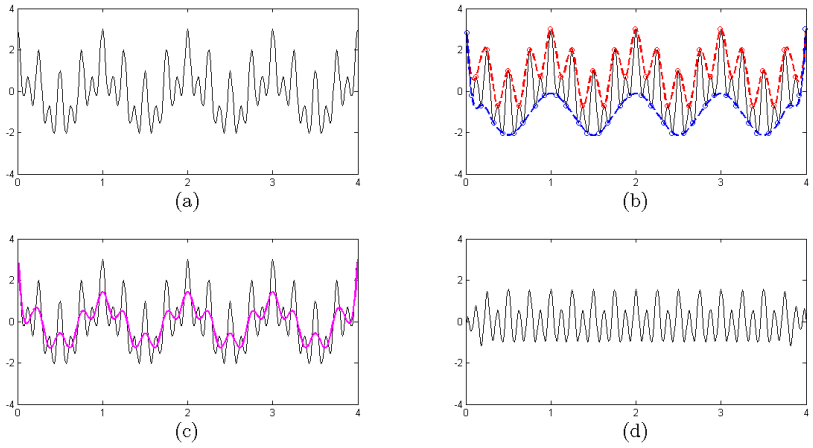

Figure 6.1 Illustration of sifting. (a) Original signal $f(t) = \cos 2\pi(8t) + \cos 2\pi(4t) + \cos 2\pi t$. (b) Construction of upper envelope (in red) and lower envelope (in blue). (c) Calculation of mean envelope (in purple). (d) Result of subtracting mean envelope from input signal.

$h_{1,1} := h_{1,0} - m_{1,1}$ in (d).

In Figure 6.2, we display the three IMF's $C_1(t)$, $C_2(t)$ and $C_3(t)$ together with the remainder $R_3(t)$, calculated by the EMD algorithm. We note that $C_i(t)$ is an approximation of $f_i(t)$ for each $i = 1, 2, 3$. For this example, the remainder is the zero function. We also note that $C_1(t)$ in (a) represents the intrinsic oscillating mode with the finest time scale (or highest frequency), while $C_3(t)$ in (c) has the coarsest time scale (or lowest frequency).

Lastly, in Figure 6.3, we display the end result of the EMD-HSA procedure. The three IMF's $C_1(t)$, $C_2(t)$ and $C_3(t)$ are displayed in (a)-(c), while the calculated IF's $\theta_1'(t)$, $\theta_2'(t)$, $\theta_3'(t)$ of the IMF's are shown in (d)-(f). The calculated IF's are estimations of the actual IF's 8, 4 and 1, respectively.

6.2 Variations on EMD

The EMD algorithm remains to be an active research field in the signal processing community, and several extensions to the original EMD formulation have been developed over the last fifteen years. In this section, we consider

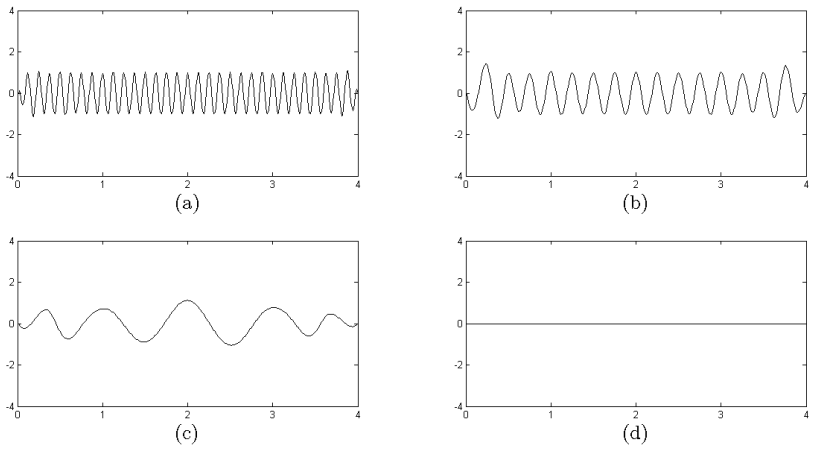

Figure 6.2 Illustration of IMF-expansion obtained through EMD. (a) $C_1(t)$ (b) $C_2(t)$ (c) $C_3(t)$ (d) $R_3(t)$

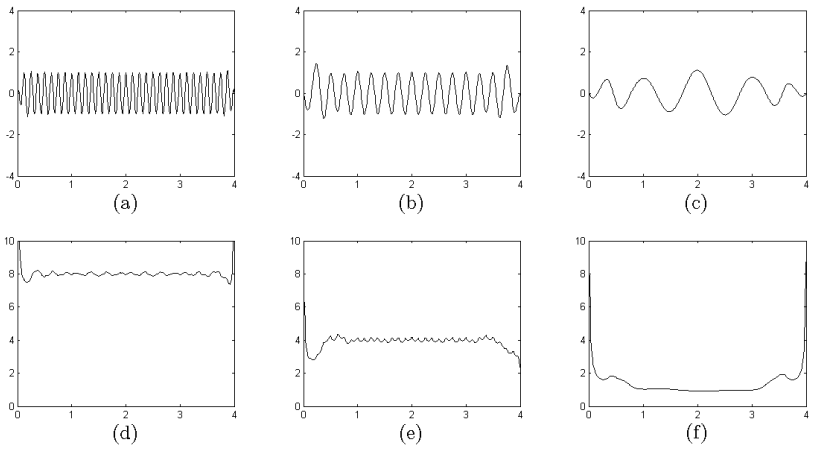

Figure 6.3 End result of EMD and HSA. (a)-(c) IMF's $C_1(t)$, $C_2(t)$, $C_3(t)$. (d)-(f) IF's $\theta_1'(t)$, $\theta_2'(t)$, $\theta_3'(t)$.

two of these.

Ensemble EMD:

The EMD algorithm works really well when it is applied to signals with "well-behaved" components – components with well-separated instantaneous frequencies, and non-intermittent components. When some of the signal components are intermittent, the end result of EMD could suffer from *mode mixing*: different oscillating modes are extracted in a single IMF, or one oscillating mode is identified in different IMF's. Of course, this restricts the physical interpretation of an IMF as representing a characteristic time scale contained in the signal [37].

In [54, 55], Z. Wu and N.E. Huang proposed an extension of EMD to overcome the mode mixing problem, called *ensemble EMD* (EEMD), a noise-assisted data analysis method. As the name suggests, EEMD can be thought of as an ensemble of EMD trials. For each trial $i = 1, \ldots, K$, for some large $K \geq 0$, the algorithm starts by adding white noise w_i with finite amplitude α to the original signal f to create the "observation"

$$f_i(t) = f(t) + \alpha w_i(t), \quad i = 1, \ldots, K$$

(mimicking an experiment with multiple observations of a data set, with measurement errors). Next, the EMD algorithm is applied to the observation f_i, yielding a set of IMF's $\{C_{i,1}, \ldots, C_{i,N}\}$, for each $i = 1, \ldots, K$. The true IMF C_j, $j = 1, \ldots, N$, of the original signal f is then defined to be the mean of the j^{th} IMF in all K trials as K approaches infinity; that is,

$$C_j(t) = \lim_{K \to \infty} \frac{1}{K} \sum_{i=1}^{K} C_{i,j}(t), \quad j = 1, \ldots, N.$$

The difference between the true IMF C_j and the result of the ensemble for K trials decreases as $\frac{1}{\sqrt{K}}$ [54, 37].

The addition of white noise to the original signal f creates a uniform reference scale distribution in f to overcome intermittency in signal components. It perturbs the signal in such a manner to encourage the method to search for all possible answers in a finite neighborhood of the true answer

[54]. Experimental results in [54, 55] indicate that EEMD is successful to overcome mode mixing problems.

According to [54], the idea of a noise-assisted data analysis method was inspired by two pioneering works. In his PhD thesis [28], R. Gledhill tested the robustness of the EMD algorithm by adding noise to an ensemble of EMD trials. Flandrin, Gonçalves and Rilling [25], on the other hand, studied the question of applying EMD to a signal that do not have enough extrema to construct upper or lower envelopes in the sifting process, like the delta function (which only has one extremum). They came up with the novel idea of adding noise with infinitesimal amplitude to make the EMD algorithm operable. However, since the method is sensitive to noise, they decided to run an ensemble of 5000 trials, with a different noise signal added every time. Both of these approaches delivered new insights into the effect of noise on the EMD algorithm.

Normalized Hilbert transform:

We have seen in Section 6.1 that, for a given signal $f(t)$, the EMD-HSA approach provides us with an IMF-expansion (6.1.1), where each IMF-component $C_j(t)$ is written as

$$C_j(t) = B_j(t)\cos 2\pi\theta_j(t), \quad j = 1, \ldots, N$$

(with $B_j(t)$ and $\theta_j(t)$ defined in (6.1.3)). Theoretically, the amplitude function $B_j(t)$ oscillates so slowly that the frequency information of $C_j(t)$ is entirely determined by $\cos 2\pi\theta_j(t)$ at any time value t inside the time interval $[0, T]$. Therefore, the IMF $C_j(t)$ should satisfy the relation

$$\mathcal{H}(B_j(t)\cos 2\pi\theta_j(t)) = B_j(t)(\mathcal{H}\cos 2\pi\theta_j)(t); \tag{6.2.1}$$

in other words, $B_j(t)\cos 2\pi\theta_j(t)$ should satisfy (2.6.3) in Bedrosian's theorem (Theorem 2.6.3). However, in practice, the assumptions in Theorem 2.6.3 are generally not satisfied by $B_j(t)$ and $\cos 2\pi\theta_j(t)$, so that (6.2.1) does not hold [37].

In [34, 38], Huang and others proposed the *normalized Hilbert transform* (NHT), a normalization algorithm to better separate a given IMF

$C_j(t),\ j = 1, \ldots, N$, into its amplitude-modulated (AM) and frequency-modulated (FM) parts, $M_j(t)$ and $F_j(t)$, respectively, so that

$$C_j(t) = M_j(t)F_j(t), \quad j = 1, \ldots, N.$$

The Hilbert transform is then only applied to the FM-part $F_j(t)$ instead of the entire IMF $C_j(t)$.

After the IMF's $C_1(t), \ldots, C_N(t)$ have been obtained through the EMD algorithm, the NHT starts by computing the local maxima of the absolute values of each IMF, $|C_j(t)|,\ j = 1, \ldots, N$. Next, for each $j = 1, \ldots, N$, it computes the envelope $e_{j,1}$ by finding the (standard) cubic spline interpolant through the local maxima of $|C_j(t)|$. With the definition

$$f_{j,1} := \frac{C_j}{e_{j,1}},$$

if $|f_{j,1}(t)| \leq 1$ for all $t \in [0, T]$, we deduce that $f_{j,1}(t) = \cos 2\pi\theta_j(t)$ (and $e_{j,1} = B_j$, with B_j obtained by applying the regular Hilbert transform method to C_j, as in (6.1.3)). In this case, the (empirical) FM-part F_j and AM-part M_j are simply $f_{j,1}$ and $e_{j,1}$, respectively.

Otherwise, we repeat this procedure on $f_{j,1}$ to obtain $f_{j,2}, \ldots, f_{j,n}$, through

$$f_{j,k} := \frac{f_{j,k-1}}{e_{j,k}}, \quad j = 1, \ldots, N;\ k = 2, \ldots, n,$$

until $|f_{j,n}(t)| \leq 1$ for all $t \in [0, T]$ for some $n \geq 2$. The (empirical) FM-part F_j and AM-part M_j are then defined by

$$F_j := f_{j,n} \quad \text{and} \quad M_j := \frac{C_j}{F_j}, \quad j = 1, \ldots, N.$$

After F_j and M_j have been found in this way, the Hilbert transform is applied to F_j (instead of C_j) to obtain the IF θ_j'.

According to [37], experimental results indicate that this method produces more accurate estimations of $\theta_j',\ j = 1, \ldots, N$, than the original EMD-HSA approach. However, studies in [33] show that, even with the NHT-extension to EMD, the Hilbert transform still produces inaccurate results, indicating that the Hilbert transform might not be the best approach

to estimating the IF's of the signal f. This brings us to the last section of this chapter, where we discuss certain limitations of the EMD algorithm.

6.3 Limitations of EMD

The EMD algorithm continues to be one of the most popular methods for non-stationary signal analysis and decomposition. It is easy to implement, and it produces good results in practice. However, there are some limitations of this method.

A major drawback of the EMD-HSA approach is that the IF's θ_j', $j = 1, \ldots, N$, produced by the Hilbert transform method, might be negative. This is a big disadvantage, since a negative IF is not physically meaningful.

When EMD was introduced in [36], the authors argued that the defining properties of an IMF (in (i) and (ii) on p.103) are necessary conditions on a function so that the Hilbert transform applied to this function produces a non-negative IF. They deduced this by considering the function

$$f(t) = \cos 2\pi ct + \alpha, \tag{6.3.1}$$

where α is a constant and $c > 0$, with Hilbert transform given by

$$(\mathcal{H}f)(t) = \sin 2\pi ct,$$

from (2.6.4)-(2.6.5) in Example 2.6.1. From (2.6.11) in Theorem 2.6.4, we know that the IF $\omega(t)$ of f, as calculated through the HSA approach, will be non-negative if and only if

$$\begin{aligned} &f(t)\left(\mathcal{H}f\right)'(t) - \left(\mathcal{H}f\right)(t)f'(t) \\ &= 2\pi c \cos 2\pi ct \left(\cos 2\pi ct + \alpha\right) + 2\pi c \sin^2 2\pi ct \\ &= 2\pi c + 2\pi c\alpha \cos 2\pi ct \geq 0, \end{aligned}$$

which will be true only if $\alpha \leq 1$ (the result obtained in [36], but with a different approach). Moreover, the IF of the signal f in (6.3.1) should (theoretically) be constant, which will only be true if $\alpha = 0$. Therefore, for the special case when f is a cosine function, a physically meaningful IF can

only be obtained when f is symmetric with respect to the zero mean level – in other words, when f is an IMF.

However, this condition is not sufficient to yield a non-negative IF. In fact, R.C. Sharpley and V. Vatchev in [46] constructed explicit counter-examples of functions that satisfy the definition of an IMF, while its IF calculated through the Hilbert transform method changes sign on intervals of positive measure (see [46, Prop. 4.1–4.4]).

A second limitation of the EMD-HSA approach stems from the fact that the Hilbert transform is defined for real-valued functions on the entire real line (see Definition 2.6.1), while real-life signals are typically defined on bounded or half-infinite intervals. Therefore, artificial extension of an IMF to the real line is necessary in order to apply the Hilbert transform, often yielding unreliable results (as also noted by [37, 33]).

Another important aspect of EMD is the construction of upper and lower envelopes through interpolation of local maxima and minima. In the original formulation of EMD in [36], the authors proposed to use standard cubic spline interpolation. Not being a local method (as described in Section 2.4 in Chapter 2), it becomes computationally expensive to obtain the interpolant when the number of extrema becomes very large. Taking care of the boundary values is also somewhat problematic. One solution mentioned in [36, 10] is to extend the data signal at the boundaries according to some user-defined rule; however, this is artificial and does not always yield accurate results.

In Chapter 9, we will describe our approach to the question of IF estimation of signal components, which will address the above limitations of the EMD-HSA approach.

Chapter 7

Synchrosqueezed wavelet transform

Described as a "mathematically sound" alternative to EMD, the synchrosqueezed wavelet transform, introduced by I. Daubechies and others [20, 21], is another approach in the literature to non-stationary signal analysis (as described briefly in Chapter 1). Instead of computing the IF's after the signal is decomposed (as is done when applying EMD), the SST approach is to first estimate the IF's of the signal components, under the assumption that the signal satisfies the properties of the AHM in (5.2.3)-(5.2.4), before recovering the signal components of the model. The details and motivation of this idea are described in Section 7.1. Limitations of the SST are discussed in Section 7.2.

7.1 SST

As the name suggests, the synchrosqueezed wavelet transform works through "squeezing" the continuous wavelet transform (which we defined in (2.5.4) in Chapter 2), where the analysis wavelet ψ of the CWT is required to be *admissible* in the sense that its Fourier transform (defined in (2.2.1) in Chapter 2) vanishes on the negative frequency axis; that is,

$$\hat{\psi}(\omega) = 0, \quad \omega < 0. \tag{7.1.1}$$

The "squeezing out" of IF's is achieved through the single *reference IF function*

$$\omega_f(b,a) := \begin{cases} \frac{\partial_b(\mathcal{W}_\psi f)(b,a)}{2\pi i(\mathcal{W}_\psi f)(b,a)}, & \text{if } (\mathcal{W}_\psi f)(b,a) \neq 0; \\ -\infty, & \text{otherwise,} \end{cases} \tag{7.1.2}$$

for any function $f \in L^2(\mathbb{R})$, where ∂_b denotes the partial derivative with respect to b. We call the function ω_f in (7.1.2) the *frequency reassignment (FRA) rule.*

The definition of the FRA rule is motivated in [20, 21] by considering the monotone signal

$$g(t) = A\cos 2\pi ct, \tag{7.1.3}$$

with frequency $c > 0$ and amplitude $A > 0$. From the definitions of the CWT in (2.5.4) and the Fourier transform in (2.2.1), we deduce that, for $b \in \mathbb{R}$ and $a > 0$,

$$\begin{aligned}
&(\mathcal{W}_\psi g)(b,a) \\
&= \frac{A}{a}\int_{-\infty}^{\infty} \cos 2\pi ct\overline{\psi\left(\frac{t-b}{a}\right)}\mathrm{d}t \\
&= \frac{A}{2a}\int_{-\infty}^{\infty} (e^{i2\pi ct} + e^{-i2\pi ct})\overline{\psi\left(\frac{t-b}{a}\right)}\mathrm{d}t \\
&= \frac{A}{2}\left(\int_{-\infty}^{\infty} e^{i2\pi cau}\overline{\psi(u)}\mathrm{d}u\right)e^{i2\pi bc} + \frac{A}{2}\left(\int_{-\infty}^{\infty} e^{-i2\pi cau}\overline{\psi(u)}\mathrm{d}u\right)e^{-i2\pi bc} \\
&= \frac{A}{2}\left(\overline{\int_{-\infty}^{\infty} e^{-i2\pi cau}\psi(u)\mathrm{d}u}\right)e^{i2\pi bc} + \frac{A}{2}\left(\overline{\int_{-\infty}^{\infty} e^{i2\pi cau}\psi(u)\mathrm{d}u}\right)e^{-i2\pi bc} \\
&= \frac{A}{2}\overline{\hat{\psi}(2\pi ac)}e^{i2\pi bc} + \frac{A}{2}\overline{\hat{\psi}(-2\pi ac)}e^{-i2\pi bc} \\
&= \frac{A}{2}\overline{\hat{\psi}(2\pi ac)}e^{i2\pi bc},
\end{aligned}$$

since ψ satisfies (7.1.1). Therefore,

$$\partial_b(\mathcal{W}_\psi g)(b,a) = i2\pi c(\mathcal{W}_\psi g)(b,a),$$

so that (7.1.2) yields

$$\omega_g(b,a) = \frac{\partial_b(\mathcal{W}_\psi g)(b,a)}{2\pi i(\mathcal{W}_\psi g)(b,a)} = \frac{i2\pi c(\mathcal{W}_\psi g)(b,a)}{2\pi i(\mathcal{W}_\psi g)(b,a)} = c.$$

In other words, the FRA rule extracts the frequency c of the monotone signal g in (7.1.3) precisely.

With these definitions, the SST may be applied to non-stationary signals of the AHM (5.2.1), satisfying the AHM conditions (5.2.3)-(5.2.4), as follows:

Definition 7.1.1 (SST) *Let $f \in \mathcal{A}_{\varepsilon,d}^{c_1,c_2}$. For a function $h \in L^1(\mathbb{R})$, let*

$$h_\alpha(t) := \frac{1}{\alpha} h\left(\frac{t}{\alpha}\right), \quad 0 < \alpha << 1, \tag{7.1.4}$$

so that $\{h_\alpha\}$ converges to the delta distribution as $\alpha \to 0$, and let ψ be an admissible wavelet that satisfies (7.1.1). Then the SST $\mathcal{S}_{\Gamma,\alpha} f$ of f at the time-frequency point (b, ξ) is defined by

$$(\mathcal{S}_{\Gamma,\alpha} f)(b,\xi) = \int_{\left\{a:|(\mathcal{W}_\psi f)(a,b)|>\Gamma\right\}} (\mathcal{W}_\psi f)(b,a) h_\alpha(|\xi - \omega_f(b,a)|) \frac{\mathrm{d}a}{a}, \tag{7.1.5}$$

where $\Gamma > 0$ is a thresholding parameter, and ω_f is defined in (7.1.2).

In other words, the SST is a special type of reassignment method (as described in Section 5.3 of Chapter 5) on the CWT which reallocates the values of the CWT from the time-scale point (b, a) to a time-frequency position (b, ξ), through the FRA rule (7.1.2).

The output of the SST may be viewed as a two-dimensional digital image representing a set of *IF curves*. An example is displayed in Figure 7.1, for the stationary signal f that we considered in (6.1.4)-(6.1.5) in Chapter 6. The original signal can be seen in (a), while (b) shows the digital image output of the SST, displaying three distinct IF curves (one for each component in f).

The set of IF curves displayed in the digital image output of the SST may now be extracted through a suitable curve fitting method (as described in [11, 48]). In practice, the curves are extracted one by one, where the image pixels that constitute a particular curve are removed from the image before the next curve is found. This process is repeated until no obvious curve remains in the digital image. The curves extracted in this way are

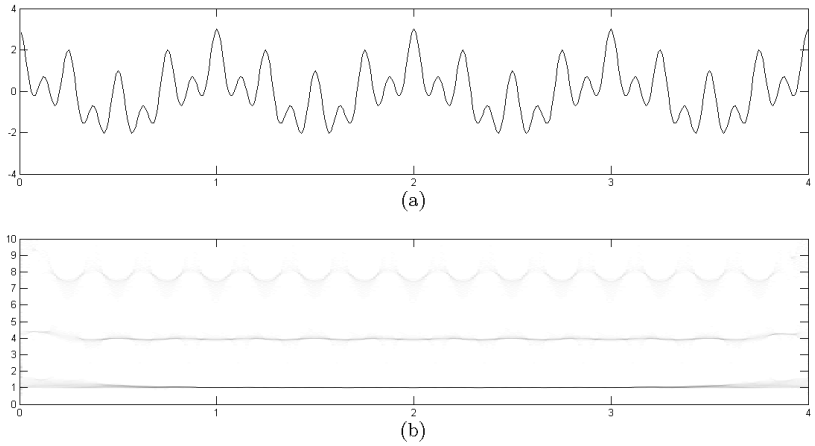

Figure 7.1 Illustration of SST. (a) Original signal $f(t) = \cos 2\pi(8t) + \cos 2\pi(4t) + \cos 2\pi t$. (b) SST output.

estimations of the IF's $\phi_j'(t)$ of the signal components $f_j(t)$ in the AHM in (5.2.2), for $j = 1, \ldots, N$. This curve extraction process requires supervision, especially if the thresholding parameter is small.

Once the N IF's $\phi_j'(t)$, $j = 1, \ldots, N$, have been determined, they may be used to estimate the signal components $f_j(t)$ in (5.2.2). For a positive constant $\Delta < \frac{d}{1+d}$ (with d defined in the AHM conditions (5.2.4)), this estimation is given by

$$f_j^{\Gamma,\Delta}(t) := \mathrm{Re}\, R_\psi^{-1} \int_{\frac{1-\Delta}{\phi_j'(t)}}^{\frac{1+\Delta}{\phi_j'(t)}} (\mathcal{W}_\psi f)(t,a) \chi_{\{a:|(\mathcal{W}_\psi f)(b,a)|>\Gamma\}}(a) \frac{\mathrm{d}a}{a}, \qquad (7.1.6)$$

where "Re" means taking the real part, and

$$R_\psi := \int_0^\infty \frac{\hat{\psi}(\zeta)}{\zeta} \mathrm{d}\zeta. \qquad (7.1.7)$$

The amplitude A_j of each f_j in (5.2.2) may be estimated through

$$A_j^{\Gamma,\Delta}(t) = |f_j^{\Gamma,\Delta}(t)|,$$

and an estimator of the phase ϕ_j of f_j in (5.2.2) may be obtained by unwrapping the phase of $\frac{f_j^{\Gamma,\Delta}(t)}{A_j^{\Gamma,\Delta}(t)}$, for each $j = 1, \ldots, N$. The interested reader is referred to [20, 11, 47] for details on these reconstruction formulas.

Lastly in this section, we provide the main result of [20], which summarizes the working of the SST and describes the robustness of the SST (see also [11, Theorem 3.1]):

Theorem 7.1.1 (SST) *Let f be a function in $\mathcal{A}_{\varepsilon,d}^{c_1,c_2}$, and set $\tilde{\varepsilon} := \varepsilon^{1/3}$. Let ψ be a wavelet in the Schwartz space (that is, the space of all functions with rapidly decreasing derivatives) such that its Fourier transform $\hat{\psi}$ is supported in $[1-\Delta, 1+\Delta]$ for $\Delta < \frac{d}{1+d}$. With the SST $\mathcal{S}_{\tilde{\varepsilon},\alpha}f$ of f defined in Definition 7.1.1, the following hold for sufficiently small ε:*

(i) $|(\mathcal{W}_\psi f)(b,a)| > \tilde{\varepsilon}$ *only when, for some* $j \in \{1, \ldots, N\}$, $(b,a) \in Z_j$, *with* $Z_j := \big\{(b,a) : |a\phi_j'(b) - 1| < \Delta\big\}$;

(ii) For each $j \in \{1, \ldots, N\}$, *and for each pair* $(b,a) \in Z_j$ *for which* $|(\mathcal{W}_\psi f)(b,a)| > \tilde{\varepsilon}$,

$$|\omega_f(b,a) - \phi_j'(b)| \leq \tilde{\varepsilon};$$

(iii) For each $j \in \{1, \ldots, N\}$, *there exists a constant C such that, for any* $b \in \mathbb{R}$,

$$\left| R_\psi^{-1} \int_{\frac{1-\Delta}{\phi_j'(b)}}^{\frac{1+\Delta}{\phi_j'(b)}} (\mathcal{W}_\psi f)(b,a) \chi_{\{a:|(\mathcal{W}_\psi f)(b,a)|>\tilde{\varepsilon}\}}(a) \frac{\mathrm{d}a}{a} - A_j(b) e^{i2\pi\phi_j(b)} \right| \leq C\tilde{\varepsilon},$$

with R_ψ defined in (7.1.7).

As explained in [20, 47], this theorem tells us that the plot of $|\mathcal{S}_{\tilde{\varepsilon},\alpha}f|$ is concentrated around the IF curves $\big\{\phi_j'(t)\big\}$, and that each $f_j(t)$ may be reconstructed as in (7.1.6)-(7.1.7). In other words, the SST provides a clearer visual representation of the IF information of a signal in the time-frequency plane, and this method provides a way to construct the signal components $f_j(t)$ once the IF's $\phi_j'(t)$ have been obtained, for $j = 1, \ldots, N$.

7.2 Limitations of SST

We have seen in the previous section that the SST provides us with a method to analyze non-stationary signals, with a rigorous mathematical foundation. In particular, since the SST is based on the AHM (5.2.1) with restrictions given in (5.2.3)-(5.2.4), the IF's $\phi_1'(t), \ldots, \phi_N'(t)$ produced by the SST are guaranteed to be non-negative. This poses a significant advantage over the EMD-HSA approach (as discussed in Section 6.3 of Chapter 6). However, there are a couple of limitations of the SST.

First, as described in Section 7.1, the output of the SST is a digital image, displaying a set of IF curves – one curve for every $\phi_j'(t),\ j = 1, \ldots, N$. These curves must then be extracted, one by one, through a suitable curve fitting scheme. This procedure could be quite complicated, particularly if the number N of IF curves is large, or when the IF curves are close together in the time-frequency plane. Therefore, the curve extraction process must be supervised.

A second obstacle of the SST approach is that the analysis wavelet of the CWT is required to be admissible, in the sense that $\hat{\psi}(\omega) = 0,\ \omega < 0$ (as given in (7.1.1)). This means the analysis wavelet cannot be compactly supported in the time domain, and is therefore not suited to real-time implementation.

In Chapter 9, we will outline our approach to estimating the instantaneous frequencies of signal components, which will address these limitations of the SST approach. In a nutshell, our idea will combine the EMD algorithm of Chapter 6 and the SST in a clever way to exploit the plus points of both methods. Before describing our approach, though, we proceed to describe the analytic vanishing moment wavelets (as introduced in Chapter 1) in the next chapter. This type of wavelet will be used as the analysis wavelet in the CWT when applied in the SST in our approach.

Chapter 8

Analytic vanishing moment wavelets

The analytic vanishing moment (VM) spline wavelets were recently introduced by C.K. Chui, Y.-T. Lin and H.-T. Wu [15] to achieve real-time implementation of the synchrosqueezed wavelet transform (described in Chapter 7). Moreover, the application of these wavelets in the SST have the added benefit that they permit an explicit formulation of the derivative of the CWT in the FRA rule $\omega_f(b,a)$ in (7.1.2), as we shall see in (8.2.2) of this chapter.

Because of these properties of the analytic VM wavelets, we will also apply these wavelets as analysis wavelet in the CWT as part of the SST in our approach (to be described in Chapter 9). Our application differs from the application in [15], though, in the sense that we construct the analytic VM spline wavelets by using a different knot sequence (to be described in (8.1.2)-(8.1.4)).

In [15], the analytic VM wavelet is defined to be the analytic signal representation (as in (2.6.6)) of a VM wavelet. In Section 8.1, we therefore start by constructing VM wavelets and discussing their derivatives, before considering their analytic representation in Section 8.2. The application of these wavelets in the CWT as part of the SST, with specific reference to applying the CWT on a bounded interval by considering analytic VM wavelets with stacked knots, is also discussed in Section 8.2.

8.1 VM wavelets

For an integer $m \geq 1$, let $\mathbf{x}$ be an arbitrary knot sequence, with $x_{j+1} \geq x_j$ and $x_{j+m} > x_j$ for all $j \in \mathbb{Z}$. Then, for an integer $n \geq 1$, the vanishing moment wavelets $\psi_{\mathbf{x},m,n,j}$, $j \in \mathbb{Z}$, are constructed in [15] in terms of the m^{th} order B-splines (as defined in (2.3.6) in Chapter 2) to have minimum support and satisfy the n vanishing moment conditions

$$\begin{cases} \displaystyle\int_{-\infty}^{\infty} x^{\ell} \psi_{\mathbf{x},m,n,j}(x) \mathrm{d}x = 0, \quad \ell = 0, 1, \ldots, n-1; \\ \displaystyle\int_{-\infty}^{\infty} x^{n} \psi_{\mathbf{x},m,n,j}(x) \mathrm{d}x \neq 0. \end{cases}$$

Under these conditions, it is shown in [15, Theorem 3.2] that the VM wavelets $\psi_{\mathbf{x},m,n,j}$ satisfy the unique formulation (up to a non-zero constant multiple)

$$\psi_{\mathbf{x},m,n,j}(x) = N^{(n)}_{\mathbf{x},m+n,j}(x), \quad j \in \mathbb{Z}. \tag{8.1.1}$$

It follows immediately that the derivative of the VM wavelet $\psi_{\mathbf{x},m,n,j}$ in (8.1.1) is given by

$$\psi'_{\mathbf{x},m,n,j}(x) = N^{(n+1)}_{\mathbf{x},m+n,j}(x) = N^{(n+1)}_{\mathbf{x},(m-1)+(n+1),j}(x) = \psi_{\mathbf{x},m-1,n+1,j}(x),$$

for any $j \in \mathbb{Z}$; in other words, the derivative of a VM wavelet is also a VM wavelet (as in [15, Corollary 3.3]).

For our application of the VM wavelets as analysis wavelet in the CWT, let us consider the knot sequence (with stacked knots)

$$\mathbf{x} : x_{-m+1} = \cdots = -L = x_0 < x_1 < \cdots < x_{m+n} = L = \cdots = x_{2m+n-1}, \tag{8.1.2}$$

with $x_0, \ldots, x_{m+n}$ uniformly spaced in the bounded interval $[-L, L]$, so that

$$x_j = -L + jh, \quad j = 0, \ldots, m+n, \tag{8.1.3}$$

with knot spacing

$$h := \frac{2L}{(m+n)}. \tag{8.1.4}$$

In this setting, we may derive an explicit representation of the *interior wavelet* $\psi_{\mathbf{x},m,n,0}$ in terms of the normalized m^{th} order B-splines, by applying

the formula (2.3.15) for the derivative of a B-spline n times to (8.1.1), starting with $N^{(n)}_{\mathbf{x},m+n,0}$; that is,

$$\begin{aligned}
&N^{(n)}_{\mathbf{x},m+n,0}(x)\\
&= \frac{m+n-1}{(m+n-1)h} N^{(n-1)}_{\mathbf{x},m+n-1,0}(x) - \frac{m+n-1}{(m+n-1)h} N^{(n-1)}_{\mathbf{x},m+n-1,1}(x)\\
&= \frac{1}{h}\left[N^{(n-1)}_{\mathbf{x},m+n-1,0}(x) - N^{(n-1)}_{\mathbf{x},m+n-1,1}(x)\right]\\
&= \frac{1}{h}\left[\frac{m+n-2}{(m+n-2)h} N^{(n-2)}_{\mathbf{x},m+n-2,0}(x) - \frac{m+n-2}{(m+n-2)h} N^{(n-2)}_{\mathbf{x},m+n-2,1}(x)\right.\\
&\qquad\left. - \frac{m+n-2}{(m+n-2)h} N^{(n-2)}_{\mathbf{x},m+n-2,1}(x) + \frac{m+n-2}{(m+n-2)h} N^{(n-2)}_{\mathbf{x},m+n-2,2}(x)\right]\\
&= \frac{1}{h^2}\left[N^{(n-2)}_{\mathbf{x},m+n-2,0}(x) - 2N^{(n-2)}_{\mathbf{x},m+n-2,1}(x) + N^{(n-2)}_{\mathbf{x},m+n-2,2}(x)\right]\\
&= \cdots\\
&= \frac{1}{h^n}\sum_{k=0}^{n}(-1)^k \binom{n}{k} N_{\mathbf{x},m,k}(x),
\end{aligned}$$

so that

$$\psi_{\mathbf{x},m,n,0}(x) = \frac{1}{h^n}\sum_{k=0}^{n}(-1)^k \binom{n}{k} N_{\mathbf{x},m,0}(x-kh).$$

We note that the support of $\psi_{\mathbf{x},m,n,0}$ spans the entire interval, so that

$$\text{supp}\psi_{\mathbf{x},m,n,0} = [-L, L].$$

The $m-1$ *boundary wavelets* $\psi_{\mathbf{x},m,n,j},\ j = -m+1,\ldots,-1$, at the left hand side endpoint $x = -L$, with supports

$$\text{supp}\psi_{\mathbf{x},m,n,j} = [-L, L+jh], \quad j = -m+1,\ldots,-1,$$

and the $m-1$ boundary wavelets $\psi_{\mathbf{x},m,n,j},\ j = 1,\ldots,m-1$, at the right hand side endpoint $x = L$, with supports

$$\text{supp}\psi_{\mathbf{x},m,n,j} = [-L+jh, L], \quad j = 1,\ldots,m-1,$$

may be obtained similarly by applying the B-spline derivative formula (2.3.15) n times to (8.1.1), starting with $N^{(n)}_{\mathbf{x},m+n,j}$, for $j = -m+1,\ldots,-1$,

$1, \ldots, m-1$, respectively (keeping in mind the stacked knots at $x = -L$ and $x = L$ in (8.1.2)).

Specifically, for $m = 4$ and $n = 1$, we have the following.

Theorem 8.1.1 (VM wavelets with m = 4, n = 1) *For the knot sequence* $\mathbf{x}$ *in (8.1.2)-(8.1.4) with* $m = 4$ *and* $n = 1$*, the cubic VM wavelets with 1 vanishing moment are given by*

$$\begin{cases} \psi_{\mathbf{x},4,1,0}(x) = \frac{1}{h}\left(N_{\mathbf{x},4,0}(x) - N_{\mathbf{x},4,0}(x-h)\right); \\ \psi_{\mathbf{x},4,1,j}(x) = \frac{4}{h}\left(\frac{1}{4+j}N_{\mathbf{x},4,j}(x) - \frac{1}{5+j}N_{\mathbf{x},4,j+1}(x)\right), \quad j = -3,-2,-1; \\ \psi_{\mathbf{x},4,1,j}(x) = \frac{4}{h}\left(\frac{1}{5-j}N_{\mathbf{x},4,j}(x) - \frac{1}{4-j}N_{\mathbf{x},4,j+1}(x)\right), \quad j = 1,2,3. \end{cases} \tag{8.1.5}$$

The derivatives of the VM wavelets $\psi_{\mathbf{x},4,1,j}, j = -3, \ldots, 3$*, are given by*

$$\psi'_{\mathbf{x},4,1,j}(x) = \psi_{\mathbf{x},3,2,j}(x), \quad j = -3, \ldots, 3.$$

The cubic VM wavelets of Theorem 8.1.1 are shown in Figures 8.1 and 8.2 (with the specific choice of $L = 5$).

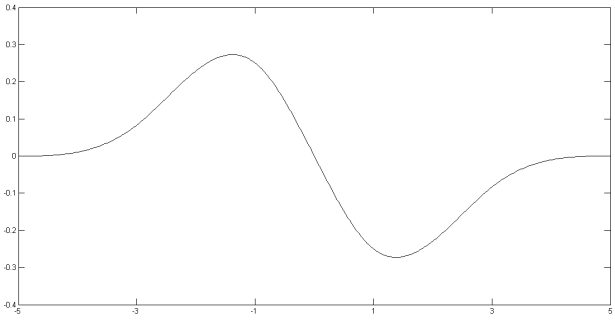

Figure 8.1 Interior wavelet $\psi_{\mathbf{x},4,1,0}$ on the interval $[-5, 5]$.

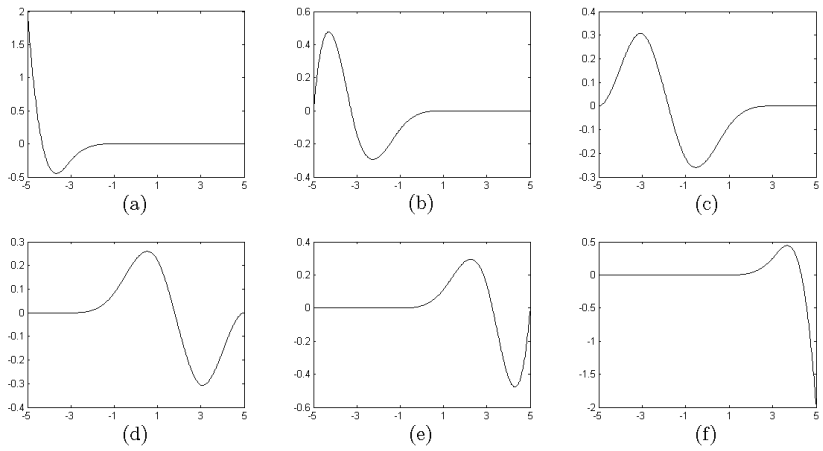

Figure 8.2 Boundary wavelets on the interval $[-5,5]$. (a)-(c) $\psi_{\mathbf{x},4,1,-3}$, $\psi_{\mathbf{x},4,1,-2}$ and $\psi_{\mathbf{x},4,1,-1}$. (d)-(f) $\psi_{\mathbf{x},4,1,1}$, $\psi_{\mathbf{x},4,1,2}$ and $\psi_{\mathbf{x},4,1,3}$.

The VM wavelets $\psi_{\mathbf{x},3,2,j},\ j=-3,\ldots,3$, can be obtained similarly to $\psi_{\mathbf{x},4,1,j},\ j=-3,\ldots,3$, in (8.1.5) by applying the B-spline derivative formula (2.3.15) twice to (8.1.1) (with $m=3$ and $n=2$). This leads to the formulations in terms of quadratic B-splines (defined in (2.3.6) with $m=3$)

$$\begin{cases} \psi_{\mathbf{x},3,2,0}(x) = \frac{1}{h^2}\left(N_{\mathbf{x},3,0}(x) - 2N_{\mathbf{x},3,0}(x-h) + N_{\mathbf{x},3,0}(x-2h)\right); \\ \psi_{\mathbf{x},3,2,-3}(x) = \frac{12}{h}\left(-\frac{3}{2}N_{\mathbf{x},3,-2}(x) + \frac{1}{4}N_{\mathbf{x},3,-1}(x)\right); \\ \psi_{\mathbf{x},3,2,j}(x) = \frac{12}{h}\left(\frac{1}{(4+j)(3+j)}N_{\mathbf{x},3,j}(x) - \left[\frac{1}{(4+j)^2} + \frac{1}{(5+j)(4+j)}\right]N_{\mathbf{x},3,j+1}(x)\right. \\ \qquad\qquad \left. + \frac{1}{3(5+j)}N_{\mathbf{x},3,j+2}(x)\right), \quad j=-2,-1; \\ \psi_{\mathbf{x},3,2,j}(x) = \frac{12}{h}\left(\frac{1}{3(5-j)}N_{\mathbf{x},3,j}(x) - \left[\frac{1}{(4+j)^2} + \frac{1}{(5+j)(4+j)}\right]N_{\mathbf{x},3,j+1}(x)\right. \\ \qquad\qquad \left. + \frac{1}{(4-j)(3-j)}N_{\mathbf{x},3,j+2}(x)\right), \quad j=1,2; \\ \psi_{\mathbf{x},3,2,3}(x) = \frac{12}{h}\left(\frac{1}{4}N_{\mathbf{x},3,3}(x) - \frac{3}{2}N_{\mathbf{x},3,4}(x)\right). \end{cases} \tag{8.1.6}$$

8.2 Analytic VM wavelets

We now turn our attention to applying the VM wavelets $\psi_{\mathbf{x},4,1,j}$, $j = -3,\ldots,3$, developed in Section 8.1, to the CWT (defined in (2.5.4)), employed as part of the SST in Definition 7.1.1.

To this end, our first task is to pick an analysis wavelet ψ that is admissible according to the definition of the SST; that is, it satisfies (7.1.1). With the definition

$$\psi_j(x) := \psi_{\mathbf{x},4,1,j}(x), \quad j = -3,\ldots,3,$$

we will consider the analytic representation of ψ_j as in (2.6.6) in Chapter 2; that is,

$$\psi_j^\star(x) = \psi_j(x) + i(\mathcal{H}\psi_j)(x), \quad j = -3,\ldots,3, \tag{8.2.1}$$

with the Hilbert transform given in Definition 2.6.1 of Chapter 2. The wavelet $\psi_j^\star$ in (8.2.1) is called an analytic VM wavelet. We note that $\psi_j^\star$ is admissible, since, by recalling (2.6.2) in Theorem 2.6.2,

$$\begin{aligned}\hat{\psi}_j^\star(\omega) = \hat{\psi}_j(\omega) + i\widehat{(\mathcal{H}\psi_j)}(\omega) &= \hat{\psi}_j(\omega) + i(-i\,\mathrm{sgn}\,\omega)\hat{\psi}_j(\omega) \\ &= \begin{cases} 2\hat{\psi}_j(\omega), & \text{if } \omega \geq 0; \\ 0, & \text{if } \omega < 0. \end{cases}\end{aligned}$$

We therefore use $\psi_0^\star$ as the "center" interior analysis wavelet in the CWT, while $\psi_j^\star$, $j = -3,\ldots,-1,1,\ldots,3$, are used to take care of the boundaries at $x = -L$ and $x = L$, respectively. The scaling and translation operations on the analysis wavelet when applied in the CWT, as indicated in (2.5.3), are applied as follows.

When scaling by $0 < a < 1$, we note that $\psi_0(\frac{x}{a})$ is a VM wavelet on the uniformly spaced knot sequence

$$\mathbf{x}_a : -L < -L + ah < -L + 2ah < \cdots < L - 2ah < L - ah < L,$$

with knot spacing ah, where $h := \frac{2L}{5}$, according to (8.1.4), and with the support of $\psi_0(\frac{x}{a})$ given by

$$\mathrm{supp}\psi_0(\tfrac{x}{a}) = [-aL, aL].$$

$\psi_0(\frac{x}{a})$ is also translated by $\frac{b}{a}$, where $-L(1-a) \leq b \leq L(1-a)$, to ensure that $\psi_0(\frac{x-b}{a})$ stays inside the bounded interval $[-L, L]$.

For the boundary wavelets, we apply a similar scaling operation, with $0 < a < 1$. For the boundary wavelets at the left hand side endpoint, let $b = -L(1-a)$, so that the supports of $\psi_j(\frac{x-b}{a}),\ j = -3, -2, -1$, are given by

$$\text{supp}\psi_j(\tfrac{x-b}{a}) = [-L, -L(1-2a) + jah], \quad j = -3, -2, -1.$$

On the other hand, for the boundary wavelets at the right hand side endpoint, we set $b = L(1-a)$, so that the supports of $\psi_j(\frac{x-b}{a}),\ j = 1, 2, 3$, are given by

$$\text{supp}\psi_j(\tfrac{x-b}{a}) = [L(1-2a) + jah, L], \quad j = 1, 2, 3.$$

As mentioned at the beginning of this chapter, the derivative property in Theorem 8.1.1 is one of the key reasons for employing the VM wavelets in the SST. The first step in the execution of the SST is to calculate the FRA rule in (7.1.2), and this involves the calculation of the derivative of the CWT. From Theorem 8.1.1, we have an explicit formulation for this derivative – therefore, the FRA rule in (7.1.2) applied to a function f becomes

$$(\omega_f)(b,a) = \frac{\partial_b(\mathcal{W}_{\psi_j^\star} f)(b,a)}{2\pi i(\mathcal{W}_{\psi_j^\star} f)(b,a)} = \frac{\langle f(x), \partial_b \psi_j^\star(\frac{x-b}{a})\rangle}{2\pi i \langle f(x), \psi_j^\star(\frac{x-b}{a})\rangle} = \frac{-\frac{1}{a}\langle f(x), \psi_{\mathbf{x},3,2,j}^\star(\frac{x-b}{a})\rangle}{2\pi i \langle f(x), \psi_{\mathbf{x},4,1,j}^\star(\frac{x-b}{a})\rangle}, \tag{8.2.2}$$

for $j = -3, \ldots, 3$ (unless $(\mathcal{W}_{\psi_{\mathbf{x},4,1,j}^\star} f)(b,a) = 0$), with $\psi_{\mathbf{x},3,2,j}$ and $\psi_{\mathbf{x},4,1,j}$ given in (8.1.6) and (8.1.5), respectively. Therefore, there is no need to carry out inaccurate estimation of the derivative of the CWT in the FRA rule (7.1.2) when using the analytic VM wavelets as analysis wavelet; these wavelets permit an explicit formulation of the FRA rule, as shown in (8.2.2).

Lastly in this section, we describe the computation of $\mathcal{H}\psi_j$ in the construction of the analytic VM wavelets in (8.2.1). Since each $\psi_j = \psi_{\mathbf{x},4,1,j}$ is a linear combination of the B-splines $N_{\mathbf{x},4,-3}, \ldots, N_{\mathbf{x},4,4}$ (according to (8.1.5)), and since the Hilbert transform is translation invariant (as shown in Theorem 2.6.1), the computation of $\mathcal{H}\psi_j$ consists in finding $\mathcal{H}N_{\mathbf{x},4,-3}, \ldots, \mathcal{H}N_{\mathbf{x},4,4}$. It has been shown by Chen and others [10] that the recursive formulation

for the computation of B-splines in (2.3.11) in Theorem 2.3.2 is preserved by the Hilbert transform, so that, for $\ell = 2, 3, 4$,

$$(\mathcal{H}N_{\mathbf{x},\ell,k})(x) = \frac{x - x_k}{x_{\ell+k-1} - x_k}(\mathcal{H}N_{\mathbf{x},\ell-1,k})(x) + \frac{x_{\ell+k} - x}{x_{\ell+k} - x_{k+1}}(\mathcal{H}N_{\mathbf{x},\ell-1,k+1})(x),$$

with initial function

$$(\mathcal{H}N_{\mathbf{x},1,k})(x) = \frac{1}{\pi} \ln \left| \frac{x - x_k}{x - x_{k+1}} \right|.$$

This recurrence formulation may therefore be used to construct the analytic VM wavelets $\psi_j^\star = \psi_{\mathbf{x},4,1,j}^\star$, $j = -3, \ldots, 3$, in (8.2.1). The same procedure may be applied to obtain $\psi_{\mathbf{x},3,2,j}^\star$, required in (8.2.2).

Chapter 9

Hybrid EMD-SST scheme

With the empirical mode decomposition and the synchrosqueezed wavelet transform defined in Chapters 6 and 7, respectively, we are now ready to describe our approach to the question of instantaneous frequency estimation of signal components. Our idea is to develop a hybrid EMD-SST computational scheme by combining the "best" parts of EMD and SST: we propose to use the EMD algorithm to separate a given signal into IMF components, after which we will apply the SST, instead of Hilbert spectral analysis (as in the original EMD approach), to each IMF to compute its instantaneous frequency.

This approach has a number of advantages. First, the SST assures non-negative instantaneous frequencies of the IMF's, since it is built on the AHM in (5.2.1)-(5.2.4), thereby addressing one of the main obstacles of the original EMD-HSA approach (as discussed in Section 6.3 of Chapter 6). Second, with our EMD-SST approach, the reliance upon the Hilbert transform to compute the instantaneous frequency of each IMF is eliminated, solving many computational issues (described in Section 6.3 as well). Third, since the SST is only applied to one IMF component at a time (instead of to the mixed signal as in the original SST approach), there is no need to extract multiple IF curves (one by one) from the SST digital image output anymore, solving a major obstacle of the original SST approach (as discussed in Section 7.2 of Chapter 7). This simplifies and streamlines the method significantly, and also produces clearer results (as we shall see in Section 9.2).

Besides combining EMD and SST in this novel way, we also propose to modify the EMD algorithm by applying our real-time spline interpolation scheme for a bounded interval (described in Chapters 3 and 4) in the sifting process of EMD. As discussed at the start of Chapter 4, this scheme has a local formulation and is designed to include shape-preserving conditions at the boundary values, which yield more accurate results near the boundaries than the standard cubic spline interpolation used in the original formulation of EMD (as we shall see in Section 9.2).

Furthermore, we modify the SST to process signals on bounded or half-infinite time intervals by applying analytic VM wavelets with stacked knots (as described in Chapter 8) as analysis wavelets in the CWT (as part of the SST). These wavelets facilitate an exact formulation of the time derivative of the CWT in the FRA rule in (7.1.2), as shown in (8.2.2) in Chapter 8, and permit a real-time implementation of the SST.

Lastly, we apply a smoothing spline curve fitting scheme, with automatic optimal smoothing through generalized cross-validation (GCV), to the digital image output of the SST, instead of the least-squares curve fitting scheme described in [11, 47].

In what follows, we provide more detail on our approach described above, we test our approach using different types of test signals, and we compare our approach with the original EMD-HSA method. In Section 9.1, we provide details of the implementation of our hybrid EMD-SST method and of the curve fitting scheme based on GCV. Examples, visual results and comparison of errors are discussed in Section 9.2.

9.1 Implementation

Our proposed method of instantaneous frequency estimation of signal components can be summarized as follows:

1. Given a signal composed of a number of (not necessarily stationary) oscillating components, we apply EMD, equipped with our real-time spline interpolation scheme (described in Chapters 3 and 4), to separate the signal into its IMF components. Specifically, for easy imple-

mentation, we apply the blending cubic spline interpolation operator $\mathcal{P}_4^E$ in (4.3.1).

2. We apply the SST, with the analytic VM wavelet in (8.2.1) as analysis wavelet in the CWT, to each IMF separately to estimate its IF.

3. Lastly, we apply a smoothing spline curve fitting scheme, with automatic optimal smoothing parameter selection through GCV, to the digital image produced by the SST to obtain the IF curve of a given IMF.

In practice, to apply this curve fitting scheme to the SST grayscale image, we proceed as follows.

Let S be the $\mu \times \nu$ output matrix of the SST, and let the entries in S be denoted by $p_{i,j}$ for $i = 1, \ldots, \mu$, and $j = 1, \ldots, \nu$. The entries $p_{i,j}$ may be interpreted as grayscale image pixel intensities, with the definition that an entry value of 0 represents a white pixel, and increasingly higher values represent increasingly darker pixels. (Note that pixels with a low intensity usually represent dark pixels in practice, while high intensity pixels usually represent light pixels. This setup is inverted in the above definition for application to the SST output matrix S.)

For each $j = 1, \ldots, \lfloor \frac{\nu}{n} \rfloor$, if

$$p_{nj}^* := \max \{p_{1,nj}, \ldots, p_{\mu,nj}\} > M,$$

where $M > 0$ (a thresholding parameter) and $n > 0$ (typically between 10 and 20) are chosen by the user, we record the row index of p_{nj}^* and denote this value by r_{nj} (so that $1 \leq r_{nj} \leq \mu$). Otherwise, we record the mean of the row indices of the pixel intensities higher than the 99^{th} percentile of $\{p_{1,nj}, \ldots, p_{\mu,nj}\}$ and set this equal to r_{nj}.

Applying this process for each $j = 1, \ldots, \lfloor \frac{\nu}{n} \rfloor$, we obtain a sequence of ordered pairs $\left\{(n, r_n), \ldots, (n\lfloor \frac{\nu}{n} \rfloor, r_{n\lfloor \nu/n \rfloor})\right\}$, to which we fit a smoothing spline curve $s_\lambda(t)$ with smoothing parameter $\lambda \geq 0$. More precisely, following the approach described in [8], an estimator of $s_\lambda(nj)$, $j = 1, \ldots, \lfloor \frac{\nu}{n} \rfloor$, is

given by

$$\tilde{s}_\lambda(nj) = \arg \min_{s_\lambda \in C^2[n, n\lfloor \nu/n \rfloor]} \left(\sum_{j=1}^{\lfloor \nu/n \rfloor} (r_{nj} - s_\lambda(nj))^2 + \lambda \int_n^{n\lfloor \nu/n \rfloor} (s''_\lambda(x))^2 \mathrm{d}x \right), \tag{9.1.1}$$

where the amount of smoothing is controlled by λ. The unique solution of (9.1.1) is a natural cubic spline. The optimal smoothing parameter λ is determined through generalized cross-validation: the GCV estimate λ is defined to be the minimzer of the *GCV score*

$$G(\lambda) = \frac{1}{\lfloor \nu/n \rfloor} \cdot \frac{\sum_{j=1}^{\lfloor \nu/n \rfloor} \left(r_{nj} - \tilde{s}_\lambda(nj) \right)^2}{\left(1 - \lfloor \nu/n \rfloor^{-1} \mathrm{tr} A(\lambda) \right)^2},$$

where $A(\lambda)$ is the *hat matrix* for a given λ; that is, $A(\lambda)$ is the $\lfloor \nu/n \rfloor \times \lfloor \nu/n \rfloor$ matrix satisfying $\left(\tilde{s}_\lambda(n), \ldots, \tilde{s}_\lambda(n\lfloor \nu/n \rfloor) \right)^T = A(\lambda) \left(r_n, \ldots, r_{n\lfloor \nu/n \rfloor} \right)^T$. More details are given in [50, 18, 29, 8].

We remark that the choice of using the 99^{th} percentile of $p_{1,nj}, \ldots, p_{\mu,nj}$, $j = 1, \ldots, \lfloor \nu/n \rfloor$, as a thresholding parameter produces good results in practice, but it may be adjusted by the user.

9.2 Numerical experiments

We proceed to test our method on three representative signal types.

Example 1:

Our first test signal is a stationary signal with three components with integer frequencies, given by

$$f(t) = f_1(t) + f_2(t) + f_3(t), \tag{9.2.1}$$

where

$$f_1(t) = \tfrac{1}{2} \cos 2\pi(16t); \quad f_2(t) = 2 \cos 2\pi(4t); \quad f_3(t) = 8 \cos 2\pi t. \tag{9.2.2}$$

The signal f and its three components are displayed in Figure 9.1.

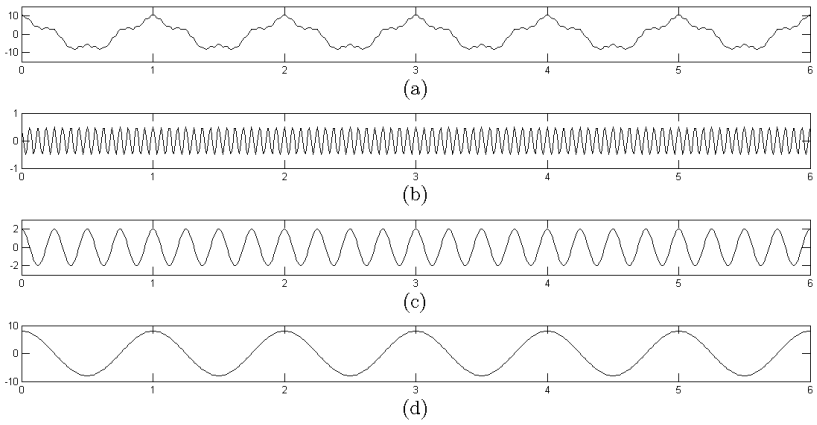

Figure 9.1 Ex. 1: graphs of originals. (a) Original signal $f(t)$. (b)-(d) Components $f_1(t)$, $f_2(t)$, $f_3(t)$.

Figure 9.2 displays the three IMF's $C_1,\ C_2$ and C_3, approximating the components $f_1,\ f_2$ and f_3, respectively, constructed through applying EMD with our real-time cubic spline interpolation scheme of Chapters 3 and 4 (specifically, we apply the blending operator $\mathcal{P}_4^E$ in (4.3.1)).

In Figure 9.3, we illustrate the results of applying our modified SST (with the analytic VM wavelet of Chapter 8) to each IMF $C_1,\ C_2$ and C_3 obtained from the modified EMD. The SST digital image output is shown in grayscale in each case. The pixels selected for curve fitting are circled in red, and the resulting smoothing spline curve is shown as a red dashed line in each case. With the true IF's given by $\phi_2'(t) = 4$ and $\phi_3'(t) = 1$, the estimated IF's ϕ_2' and ϕ_3', in (b) and (c) in Figure 9.3, respectively, are very accurate. For the higher frequency component, the SST digital image in Figure 9.3(a) displays a more noisy result, causing a lower estimated IF than the true value of 16, although it still reveals a constant frequency. We remark that greater noise reduction may be achieved by choosing an analytic VM wavelet with a higher number of vanishing moments (at the expense of computation time). The result here was obtained with an analytic VM wavelet with 5 vanishing moments (in terms of cubic B-splines so that $m = 4$).

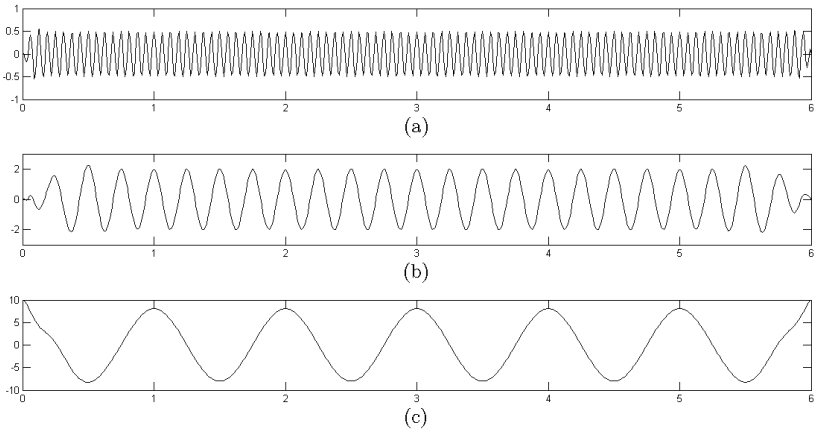

Figure 9.2 Ex. 1: IMF's constructed through EMD with our real-time cubic spline interpolation scheme. (a)-(c) $C_1(t)$, $C_2(t)$, $C_3(t)$.

Next, we proceed to compare the results of our hybrid EMD-SST approach with the original EMD-HSA approach. In Figure 9.4, we compare the construction of IMF's through the original EMD (with standard cubic spline interpolation) and the modified EMD (with our real-time spline interpolation). The true components f_1, f_2 and f_3 are shown in the left hand side column. The middle column displays the IMF's C_1^O, C_2^O and C_3^O constructed through the original EMD algorithm using standard cubic spline interpolation in the sifting process, while the right hand side column shows the IMF's C_1^S, C_2^S and C_3^S obtained by applying the modified EMD using our real-time cubic spline interpolation scheme in the sifting process. The results are comparable for the first two components; however, our real-time interpolation scheme produces a closer approximation of the third component, especially close to the boundaries. This is supported by the comparison of maximum errors, mean errors and standard deviation of errors, displayed in Tables 9.1, 9.2 and 9.3, respectively.

A comparison of the estimated IF's is given in Figure 9.5. The column on the left displays the true IF's $\phi_1'(t) = 16$, $\phi_2'(t) = 4$ and $\phi_3'(t) = 1$. The middle column displays the estimated IF's $\phi_1'^O$, $\phi_2'^O$ and $\phi_3'^O$, obtained by

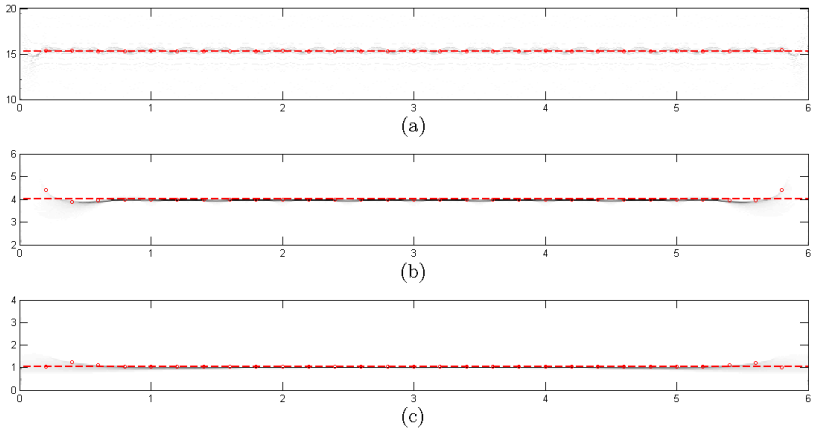

Figure 9.3 Ex. 1: digital image output of SST (in grayscale) with IF's estimated through curve fitting (in red). (a)-(c) $\phi_1'(t)$, $\phi_2'(t)$, $\phi_3'(t)$.

applying Hilbert spectral analysis to each IMF C_j^O, $j = 1, 2, 3$. On the right we show our estimated IF's $\phi_1'^S$, $\phi_2'^S$ and $\phi_3'^S$, constructed through smoothing spline curve fitting (with generalized cross-validation) to our modified SST applied to each C_j^S, $j = 1, 2, 3$, separately. Especially close to the endpoints, our hybrid EMD-SST method yield better results than the original EMD-HSA approach. This is also evident from the error analysis in Table 9.1, where the relatively high maximum errors in the estimation of ϕ_1', ϕ_2' and ϕ_3' by the EMD-HSA approach occur at the endpoints of the time interval. Although our estimation $\phi_1'^S$ shows a constant frequency, it is a bit lower than the true value of 16. As explained previously, this could be improved upon by implementing an analysis wavelet with a higher number of vanishing moments.

Example 2:

Second, we test our method on another stationary signal with three components, two of which have irrational frequency values, given by

$$g(t) = g_1(t) + g_2(t) + g_3(t), \tag{9.2.3}$$

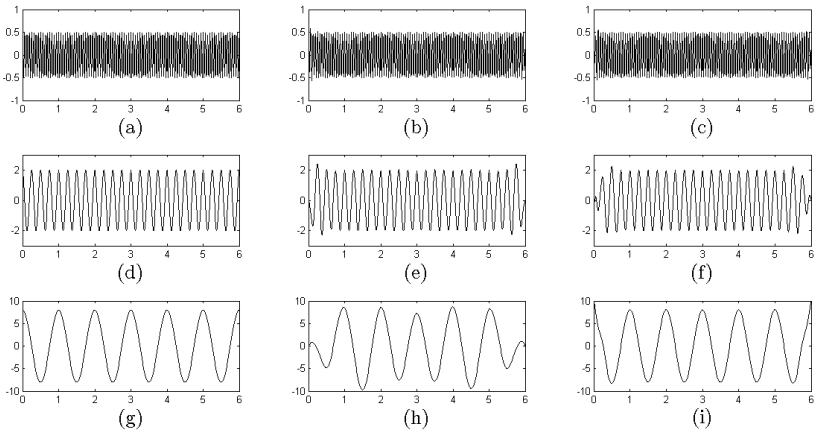

Figure 9.4 Ex. 1: comparison of IMF's. (a),(d),(g) True components $f_1(t)$, $f_2(t)$, $f_3(t)$. (b),(e),(h) IMF's $C_1^O(t)$, $C_2^O(t)$, $C_3^O(t)$, obtained from the original EMD with standard cubic spline interpolation. (c),(f),(i) IMF's $C_1^S(t)$, $C_2^S(t)$, $C_3^S(t)$, obtained through applying EMD with our real-time cubic spline interpolation scheme.

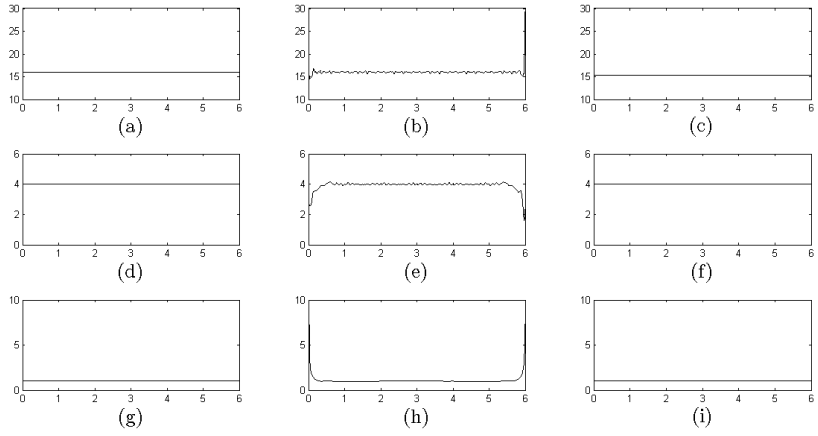

Figure 9.5 Ex. 1: comparison of IF estimation. (a),(d),(g) True IF's $\phi_1'(t)$, $\phi_2'(t)$, $\phi_3'(t)$. (b),(e),(h) Estimated IF's $\phi_1'^O(t)$, $\phi_2'^O(t)$, $\phi_3'^O(t)$, obtained by applying HSA to the original EMD. (c),(f),(i) Estimated IF's $\phi_1'^S(t)$, $\phi_2'^S(t)$, $\phi_3'^S(t)$, obtained through smoothing spline curve fitting of our modified SST applied to each IMF C_j^S, $j = 1, 2, 3$ separately.

	EMD-HSA	EMD-SST
$f_1(t)$	0.5	0.5
$f_2(t)$	2.0186	2
$f_3(t)$	8	2.5
$\phi_1'(t)$	13.2339	0.6724
$\phi_2'(t)$	2.3882	0.0145
$\phi_3'(t)$	8.9178	0.0564

Table 9.1 Ex. 1: comparison of maximum errors produced by EMD-HSA and EMD-SST approaches.

	EMD-HSA	EMD-SST
$f_1(t)$	0.0124	0.0156
$f_2(t)$	0.0972	0.1240
$f_3(t)$	1.4110	0.1210
$\phi_1'(t)$	0.1898	0.6724
$\phi_2'(t)$	0.1147	0.0145
$\phi_3'(t)$	0.1450	0.0564

Table 9.2 Ex. 1: comparison of mean errors produced by EMD-HSA and EMD-SST approaches.

	EMD-HSA	EMD-SST
$f_1(t)$	0.0291	0.0340
$f_2(t)$	0.2485	0.2841
$f_3(t)$	1.4427	0.2888
$\phi_1'(t)$	0.8111	0
$\phi_2'(t)$	0.2910	0
$\phi_3'(t)$	0.6925	0

Table 9.3 Ex. 1: comparison of standard deviation of errors produced by EMD-HSA and EMD-SST approaches.

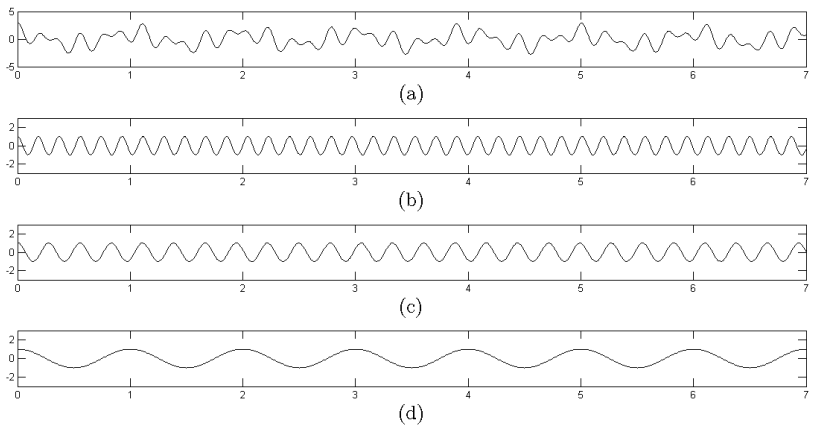

Figure 9.6 Ex. 2: graphs of originals. (a) Original signal $g(t)$. (b)-(d) Components $g_1(t)$, $g_2(t)$, $g_3(t)$.

where

$$g_1(t) = \cos 2\pi(\sqrt{29}t); \quad g_2(t) = \cos 2\pi(\sqrt{13}t); \quad g_3(t) = \cos 2\pi t. \quad (9.2.4)$$

The signal g and its three components are displayed in Figure 9.6.

Figure 9.7 displays the three IMF's C_1, C_2 and C_3, approximating the components g_1, g_2 and g_3, respectively, while Figure 9.8 illustrates the results of applying our modified SST to each IMF C_1, C_2 and C_3, with the SST digital image output in grayscale, the pixels selected for curve fitting circled in red, and the resulting smoothing spline curve shown as a red dashed line in each case. The estimated IF's obtained through curve fitting applied to the SST digital image are remarkably accurate in each case.

Next, we compare the results of our hybrid EMD-SST method with the original EMD-HSA approach. In Figure 9.9, we compare the construction of IMF's using the original EMD (with standard cubic spline interpolation) and EMD with our real-time cubic spline interpolation scheme. The true components g_1, g_2 and g_3 are shown in the left hand side column. The middle column displays the IMF's C_1^O, C_2^O and C_3^O constructed through the original EMD algorithm using standard cubic spline interpolation, while

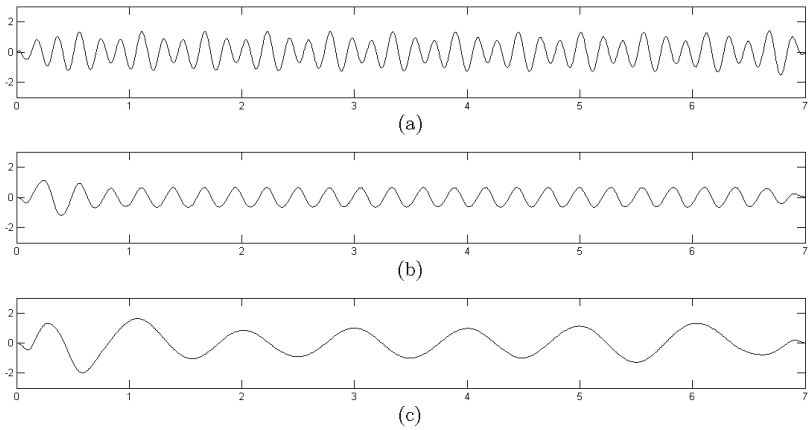

Figure 9.7 Ex. 2: IMF's constructed through EMD with our real-time cubic spline interpolation scheme. (a)-(c) $C_1(t)$, $C_2(t)$, $C_3(t)$.

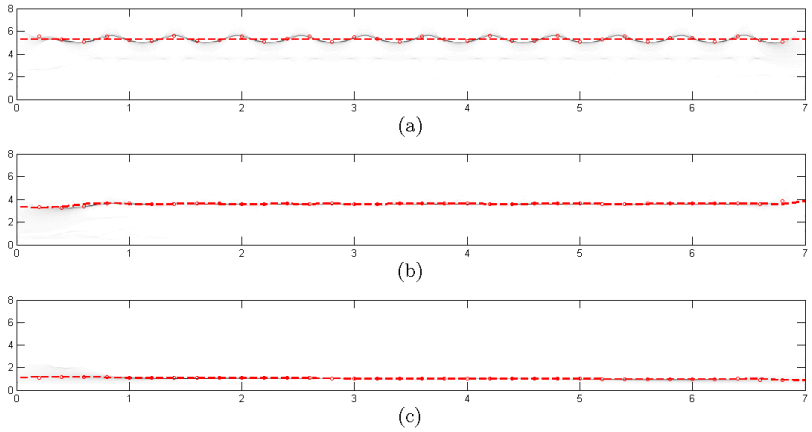

Figure 9.8 Ex. 2: digital image output of SST (in grayscale) with IF's estimated through curve fitting (in red). (a)-(c) $\phi_1'(t)$, $\phi_2'(t)$, $\phi_3'(t)$.

	EMD-HSA	EMD-SST
$g_1(t)$	0.9433	0.9433
$g_2(t)$	1.1180	1.3256
$g_3(t)$	1.3108	1.6277
$\phi_1'(t)$	11.5341	0.0754
$\phi_2'(t)$	7.9199	0.3342
$\phi_3'(t)$	8.8720	0.1716

Table 9.4 Ex. 2: comparison of maximum errors produced by EMD-HSA and EMD-SST approaches.

the right hand side column shows the IMF's C_1^S, C_2^S and C_3^S obtained by applying the modified EMD using our real-time cubic spline interpolation scheme. Our method provides a better approximation of especially the first and second components (rows 1 and 2). This is also supported by the comparison of mean errors and standard deviation of errors, provided in Tables 9.5 and 9.6, respectively. The comparison of maximum errors is displayed in Table 9.4.

A comparison of the estimated IF's is given in Figure 9.10. The column on the left displays the true IF's $\phi_1'(t) = \sqrt{29} \approx 5.385$, $\phi_2'(t) = \sqrt{13} \approx 3.606$ and $\phi_3'(t) = 1$. The middle column displays the estimated IF's $\phi_1'^O$, $\phi_2'^O$ and $\phi_3'^O$, obtained by applying Hilbert spectral analysis to each IMF C_j^O, $j = 1, 2, 3$. On the right we show our estimated IF's $\phi_1'^S$, $\phi_2'^S$ and $\phi_3'^S$, constructed through smoothing spline curve fitting (with generalized cross-validation) and our modified SST applied to each C_j^S, $j = 1, 2, 3$, separately. Our hybrid EMD-SST scheme yield much better estimations of all three IF's ϕ_1', ϕ_2' and ϕ_3' than the original EMD-HSA approach, as is also evident from the comparison of errors in Tables 9.4-9.6. Again, the relatively high maximum errors in the estimation of ϕ_1', ϕ_2' and ϕ_3' by the EMD-HSA approach (in Table 9.4) are produced at the endpoints of the time interval, illustrating one of our main motivations for replacing HSA with the SST (as discussed in Section 6.3 in Chapter 6).

Example 3:

Lastly, we implement our method for a non-linear, non-stationary signal

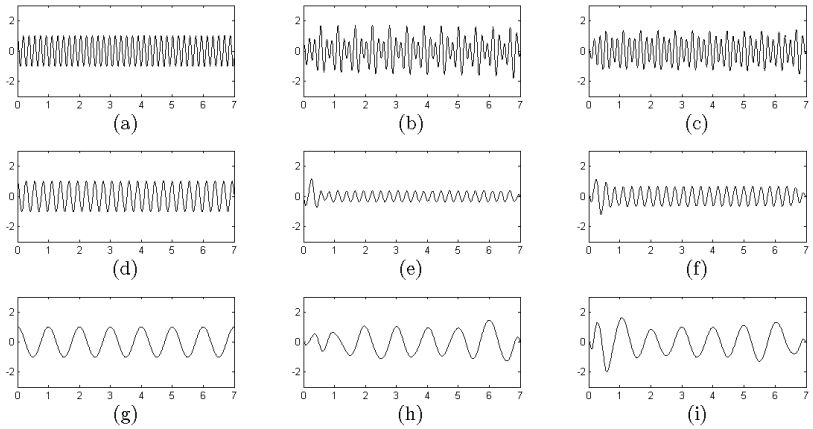

Figure 9.9 Ex. 2: comparison of IMF's. (a),(d),(g) True components $g_1(t)$, $g_2(t)$, $g_3(t)$. (b),(e),(h) IMF's $C_1^O(t)$, $C_2^O(t)$, $C_3^O(t)$, obtained from the original EMD with standard cubic spline interpolation. (c),(f),(i) IMF's $C_1^S(t)$, $C_2^S(t)$, $C_3^S(t)$, obtained through applying EMD with our real-time cubic spline interpolation scheme.

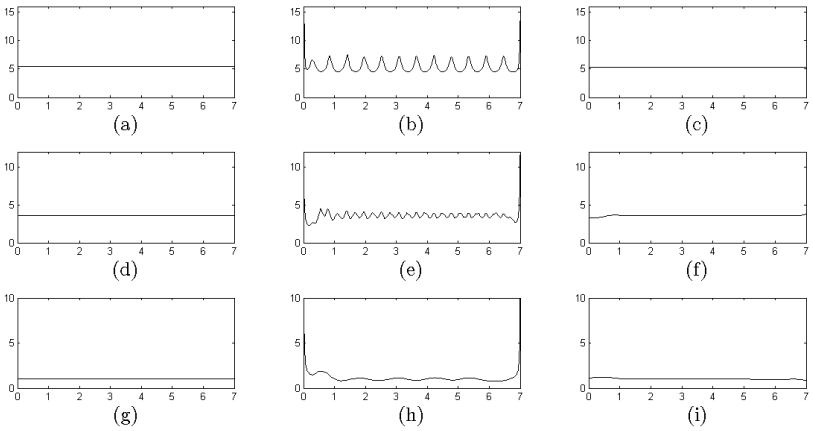

Figure 9.10 Ex. 2: comparison of IF estimation. (a),(d),(g) True IF's $\phi_1'(t)$, $\phi_2'(t)$, $\phi_3'(t)$. (b),(e),(h) Estimated IF's $\phi_1'^O(t)$, $\phi_2'^O(t)$, $\phi_3'^O(t)$, obtained by applying HSA to the original EMD. (c),(f),(i) Estimated IF's $\phi_1'^S(t)$, $\phi_2'^S(t)$, $\phi_3'^S(t)$, obtained through smoothing spline curve fitting of our modified SST applied to each IMF C_j^S, $j = 1, 2, 3$ separately.

	EMD-HSA	EMD-SST
$g_1(t)$	0.4103	0.2431
$g_2(t)$	0.4228	0.2604
$g_3(t)$	0.2262	0.2845
$\phi_1'(t)$	0.8188	0.0754
$\phi_2'(t)$	0.3275	0.0531
$\phi_3'(t)$	0.2546	0.0557

Table 9.5 Ex. 2: comparison of mean errors produced by EMD-HSA and EMD-SST approaches.

	EMD-HSA	EMD-SST
$g_1(t)$	0.2097	0.1403
$g_2(t)$	0.2214	0.1821
$g_3(t)$	0.2582	0.3450
$\phi_1'(t)$	0.8489	0
$\phi_2'(t)$	0.5168	0.0817
$\phi_3'(t)$	0.6685	0.0481

Table 9.6 Ex. 2: comparison of standard deviation of errors produced by EMD-HSA and EMD-SST approaches.

with two components, given by

$$h(t) = h_1(t) + h_2(t), \tag{9.2.5}$$

where

$$\begin{cases} h_1(t) = 0.1(t^4 - 12t^3 + 44t^2 - 48t)\cos 2\pi(3t + 0.2t^2); \\ h_2(t) = e^{(-0.15t)}\cos 2\pi(2t + 0.2\cos t), \end{cases} \tag{9.2.6}$$

so that

$$\phi_1'(t) = 3 + 0.4t; \quad \phi_2'(t) = 2 - 0.2\sin t.$$

The signal h and its two components are shown in Figure 9.11.

Figure 9.12 displays the two IMF's C_1 and C_2, approximating the components h_1 and h_2, respectively, while Figure 9.13 illustrates the results of

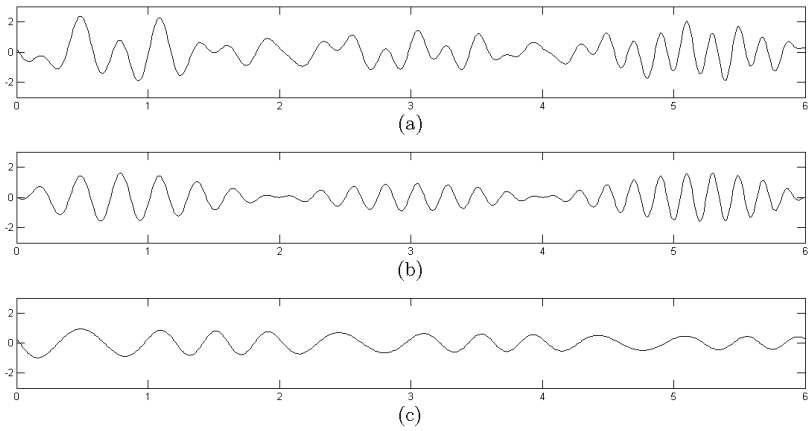

Figure 9.11 Ex. 3: graphs of originals. (a) Original signal $h(t)$. (b)-(c) Components $h_1(t)$, $h_2(t)$.

applying our modified SST to each IMF C_1 and C_2, with the SST digital image output in grayscale, the pixels selected for curve fitting circled in red, and the resulting smoothing spline curve shown as a red dashed line in each case.

In Figure 9.14, we compare the construction of IMF's through the original EMD (with standard cubic spline interpolation) and EMD with our real-time cubic spline interpolation. The true components h_1 and h_2 are shown in the left hand side column. The middle column displays the IMF's C_1^O and C_2^O constructed through the original EMD algorithm using standard cubic spline interpolation in the sifting process, while the right hand side column shows the IMF's C_1^S and C_2^S obtained by applying the modified EMD using our real-time cubic spline interpolation scheme in the sifting process. The maximum errors, mean errors and standard deviation of errors are provided in Tables 9.7, 9.8 and 9.9, respectively. With respect to the estimation of signal components, the results of the two methods are comparable.

Lastly, a comparison of the estimated IF's, constructed through the original EMD-HSA approach and our hybrid EMD-SST scheme, is given in

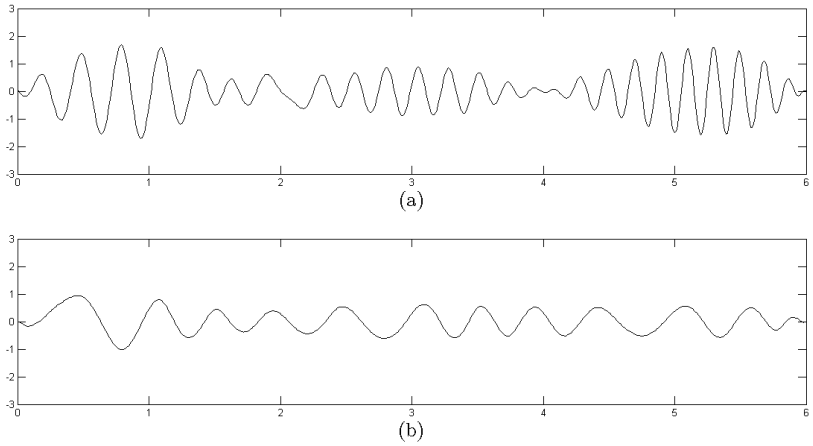

Figure 9.12 Ex. 3: IMF's constructed through EMD with our real-time cubic spline interpolation scheme. (a)-(b) $C_1(t)$, $C_2(t)$.

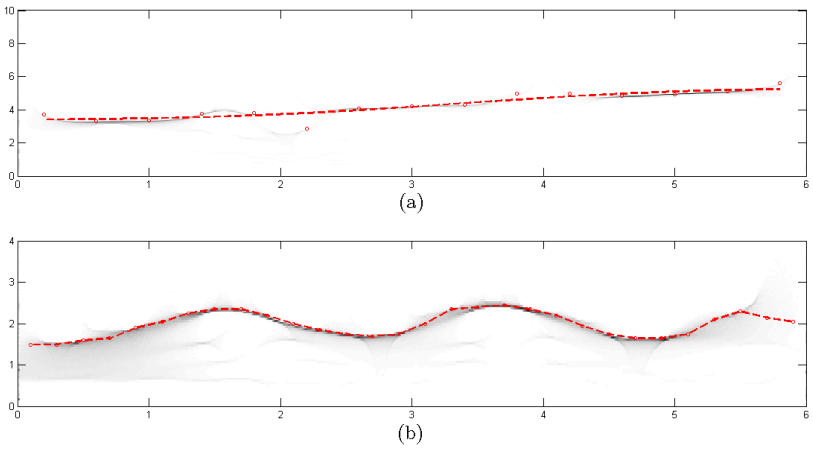

Figure 9.13 Ex. 3: digital image output of SST (in grayscale) with IF's estimated through curve fitting (in red). (a)-(b) $\phi_1'(t)$, $\phi_2'(t)$.

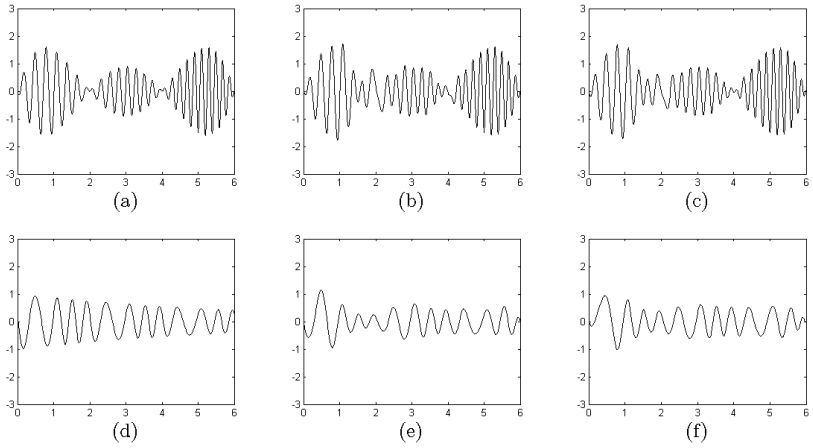

Figure 9.14 Ex. 3: comparison of IMF's. (a),(d) True components $h_1(t)$, $h_2(t)$. (b),(e) IMF's $C_1^O(t)$, $C_2^O(t)$, obtained from the original EMD with standard cubic spline interpolation. (c),(f) IMF's $C_1^S(t)$, $C_2^S(t)$, obtained through applying EMD with our real-time cubic spline interpolation scheme.

	EMD-HSA	EMD-SST
$h_1(t)$	0.6567	0.4766
$h_2(t)$	0.5536	1.0273
$\phi_1'(t)$	6.5744	0.3421
$\phi_2'(t)$	7.4990	0.5039

Table 9.7 Ex. 3: comparison of maximum errors produced by EMD-HSA and EMD-SST approaches.

Figure 9.15. The column on the left displays the true IF's $\phi_1'(t) = 3 + 0.4t$ and $\phi_2'(t) = 2 - 0.2\sin t$. The middle column displays the estimated IF's $\phi_1'^O$ and $\phi_2'^O$, obtained by applying Hilbert spectral analysis to each IMF C_j^O, $j = 1, 2$. On the right we show our estimated IF's $\phi_1'^S$ and $\phi_2'^S$, constructed through smoothing spline curve fitting (with generalized cross-validation) and our modified SST applied to each C_j^S, $j = 1, 2$, separately. Our hybrid EMD-SST provide much better estimations of the IF's of both signal components. This is also supported by the error analysis in Tables 9.7-9.9.

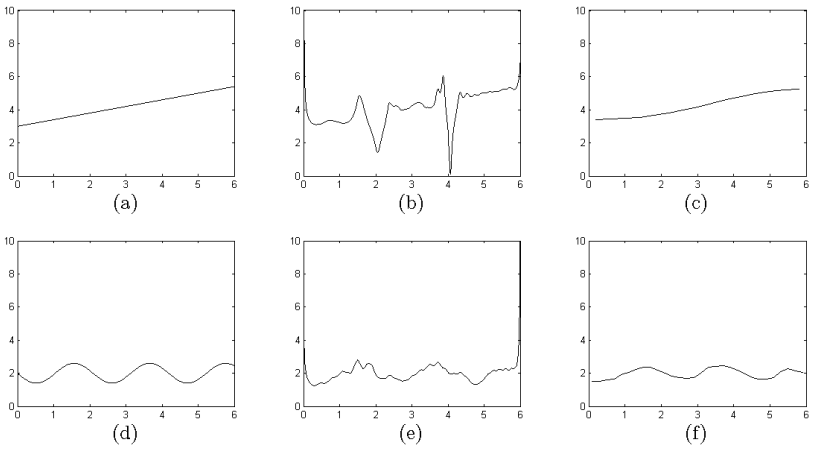

Figure 9.15 Ex. 3: comparison of IF estimation. (a),(d) True IF's $\phi_1'(t)$, $\phi_2'(t)$. (b),(e) Estimated IF's $\phi_1'^O(t)$, $\phi_2'^O(t)$, obtained by applying HSA to the original EMD. (c),(f) Estimated IF's $\phi_1'^S(t)$, $\phi_2'^S(t)$, obtained through smoothing spline curve fitting of our modified SST applied to each IMF C_j^S, $j = 1, 2$ separately.

	EMD-HSA	EMD-SST
$h_1(t)$	0.1143	0.0818
$h_2(t)$	0.1474	0.1537
$\phi_1'(t)$	0.4460	0.0970
$\phi_2'(t)$	0.1920	0.1683

Table 9.8 Ex. 3: comparison of mean errors produced by EMD-HSA and EMD-SST approaches.

	EMD-HSA	EMD-SST
$h_1(t)$	0.1402	0.1081
$h_2(t)$	0.1329	0.1847
$\phi_1'(t)$	0.7896	0.0827
$\phi_2'(t)$	0.4852	0.1193

Table 9.9 Ex. 3: comparison of standard deviation of errors produced by EMD-HSA and EMD-SST approaches.

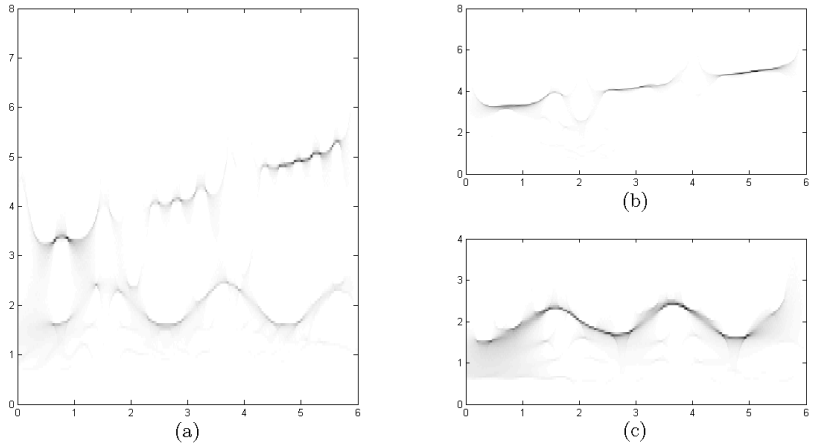

Figure 9.16 Ex. 3: comparison of our hybrid EMD-SST scheme and original SST approach. (a) The output from the (improved) SST (with our analytic VM wavelet and boundary considerations) applied to the mixed input signal. (b)-(c) The output from the hybrid EMD-SST approach.

To illustrate the advantage of first decomposing a given signal using the EMD algorithm before estimating each component's IF using the modified SST, we also display, in Figure 9.16, the result of the original SST approach applied to the mixed signal h in (9.2.5)-(9.2.6) (where we used our analytic VM wavelet in the CWT with boundary considerations), as well as the result of our hybrid EMD-SST approach. We note that, as a result of first applying EMD to separate the input signal into IMF components, the shapes of the IF curves displayed in the digital SST images from our hybrid EMD-SST approach are much clearer than in the original SST output.

Chapter 10

Final remarks

The contributions of this dissertation can be grouped into two categories.

First, we formulate a new spline interpolation scheme for a bounded interval in terms of the m^{th} order B-splines, by combining a quasi-interpolation spline operator with a local spline interpolation operator. The end result is a blending operator with a local formulation that preserves polynomials of degree $\leq m-1$ and satisfies certain Hermite interpolation conditions at a given sequence of discrete data points. A corresponding approximation order analysis is also derived rigorously for both quasi-interpolation and blending interpolation operators.

The local formulation and boundary considerations of the method make this spline interpolation scheme particularly useful, since it facilitates real-time implementation for fast computation (without extending the signal in any way). It may be applied in applications such as the empirical mode decomposition algorithm, where an interpolation scheme is required in its sifting procedure.

Second, we introduce a novel approach to instantaneous frequency estimation of (non-stationary) signal components. This approach consists of combining the "best" parts of the empirical mode decomposition and the synchrosqueezed wavelet transform into a hybrid EMD-SST scheme. In a nutshell, we apply a modified SST to each IMF produced by a modified EMD. While our modified SST assures non-negative instantaneous frequencies of the IMF's, the EMD eliminates the guessing work of the number of

signal components from the digital image of the original SST approach. More specifically, we modify the SST to process signals on bounded or half-infinite time intervals by applying VM wavelets with stacked knots, whereas we replace the standard cubic spline interpolation in the sifting process of EMD with our real-time spline interpolation scheme for bounded intervals. In addition, we replace the Hilbert transform of the original EMD approach by our modified SST to avoid artificial extension of the IMF's to the real line, solving many computational issues.

We apply this scheme to different test signals to obtain visual results and error comparisons. According to these results, our approach provides a significantly more accurate instantaneous frequency estimation of signal components than the original EMD-HSA approach. The construction of IMF's through EMD is also improved by our real-time spline interpolation scheme.

In this dissertation, we have implemented the original formulation of the EMD algorithm, only replacing the standard cubic spline interpolation scheme by our real-time spline interpolation method. Further work must be done to improve this algorithm by implementing some of the many extensions to EMD in the literature. One example of such an extension is the ensemble EMD, which aims to make EMD more accurate and robust to noise.

In addition, it is our goal to replace the SST in our hybrid EMD-SST approach by the direct method for instantaneous frequency estimation, introduced recently in [16]. This method can be realized in near real-time, and it can be extended directly to the multivariate setting.

Bibliography

[1] F. Auger and P. Flandrin. Improving the readability of time-frequency and time-scale representations by the reassignment method. *Signal Processing, IEEE Transactions on*, 43(5):1068–1089, 1995.

[2] F. Auger, P. Flandrin, Y.-T. Lin, S. McLaughlin, S. Meignen, T. Oberlin, and H.-T. Wu. Time-frequency reassignment and synchrosqueezing: An overview. *Signal Processing Magazine, IEEE*, 30(6):32–41, 2013.

[3] E. Bedrosian. A Product Theorem for Hilbert transforms. *Proc. IEEE*, 51:868–869, 1963.

[4] B. Boashash. *Time frequency analysis*. Gulf Professional Publishing, 2003.

[5] C. de Boor. On calculating with B-splines. *Journal of Approximation Theory*, 6(1):50–62, 1972.

[6] C. de Boor. *A Practical Guide to Splines*, volume 27 of *Applied Mathematical Sciences*. Springer, 2001.

[7] C. de Boor and G. Fix. Spline approximation by quasi-interpolants. *Journal of Approximation Theory*, 8:96–110, 1973.

[8] J. Carew, G. Wahba, X. Xie, E. V. Nordheim, and M. Meyerand. Optimal spline smoothing of fmri time series by generalized cross-validation. *NeuroImage*, 18(4):950–961, 2003.

[9] G. Chen, C. K. Chui, and M. J. Lai. Construction of real-time spline quasi-interpolation schemes. *Approx. Theory and its Appl.*, 4(4):61–75, 1988.

[10] Q. Chen, N. Huang, S. Riemenschneider, and Y. Xu. A B-spline approach for empirical mode decompositions. *Advances in Computational Mathematics*, 24(1-4):171–195, 2006.

[11] Y.-C. Chen, M.-Y. Cheng, and H.-T. Wu. Non-parametric and adaptive modelling of dynamic periodicity and trend with heteroscedastic and dependent errors. *Journal of the Royal Statistical Society: Series B (Statistical Methodology)*, 76(3):651–682, 2014.

[12] C. K. Chui. *Wavelets: A Mathematical Tool for Signal Analysis*. Society for Industrial and Applied Mathematics, 1997.

[13] C. K. Chui and H. Diamond. A general framework for local interpolation. *Numerische Mathematik*, 58(1):569–581, 1990.

[14] C. K. Chui and Q. Jiang. *Applied Mathematics: Data Compression, Spectral Methods, Fourier Analysis, Wavelets, and Applications*. Atlantis Press, 2013.

[15] C. K. Chui, Y.-T. Lin, and H.-T. Wu. Real-time dynamics acquisition from irregular samples – with application to anesthesia evaluation. *Analysis and Applications*, 2015.

[16] C. K. Chui and H. Mhaskar. Signal decomposition and analysis via extraction of frequencies. *Appl. and Comput. Harmon. Anal.*, 2015. http://dx.doi.org/10.1016/j.acha.2015.01.003.

[17] L. Cohen. *Time-frequency analysis*, volume 778. Prentice Hall PTR Englewood Cliffs, NJ:, 1995.

[18] P. Craven and G. Wahba. Smoothing noisy data with spline functions. *Numerische Mathematik*, 31(4):377–403, 1978.

[19] H. Curry and I. Schoenberg. On Pólya frequency functions IV. The fundamental spline functions and their limits. *Journal d'Analyse Mathématique*, 17(1):71–107, 1966.

[20] I. Daubechies, J. Lu, and H.-T. Wu. Synchrosqueezed wavelet transforms: An empirical mode decomposition-like tool. *Appl. Comput. Harmon. Anal.*, 30:243–261, 2011.

[21] I. Daubechies and S. Maes. A nonlinear squeezing of the continuous wavelet transform based on auditory nerve models. In A. Aldroubi and M. Unser, editors, *Wavelets in Medicine and Biology*, pages 527–546. CRC Press, 1996.

[22] J. de Villiers. *Mathematics of Approximation.* Atlantis Press, Paris, 2012.

[23] P. Flandrin. *Time-Frequency/Time-Scale Analysis.* Wavelet Analysis and Its Applications. Elsevier Science, 1998.

[24] P. Flandrin, F. Auger, and E. Chassande-Mottin. Time-frequency reassignment: from principles to algorithms. In A. Papandreou-Suppappola, editor, *Applications in Time-Frequency Signal Processing*, pages 179–203. CRC Press, 2003.

[25] P. Flandrin, P. Gonçalves, and G. Rilling. Emd equivalent filter banks, from interpretation to applications. *Hilbert-Huang transform and its applications*, pages 57–74, 2005.

[26] D. Gabor. Theory of communication. *J. Inst. Elec. Engineers, Part III: Radio and Communication Engineering*, 93(26):429–441, 1946.

[27] R. Gao and R. Yan. *Wavelets: Theory and Applications for Manufacturing.* SpringerLink : Bücher. Springer, 2010.

[28] R. J. Gledhill. *Methods for investigating conformational change in biomolecular simulations.* PhD thesis, University of Southampton, 2003.

[29] G. H. Golub, M. Heath, and G. Wahba. Generalized cross-validation as a method for choosing a good ridge parameter. *Technometrics*, 21(2):215–223, 1979.

[30] K. Gröchenig. *Foundations of time-frequency analysis.* Springer, 2001.

[31] F. Hlawatsch and G. Boudreaux-Bartels. Linear and quadratic time-frequency signal representations. *IEEE Signal Processing Magazine*, 9(2):21–67, 1992.

[32] R. Horn and C. Johnson. Topics in matrix analysis. *Cambridge University Presss, Cambridge*, 37:39, 1991.

[33] N. Huang. Computing instantaneous frequency by normalizing hilbert transform, 2005. US Patent 6,901,353.

[34] N. Huang. Empirical mode decomposition for analyzing acoustical signals, 2005. US Patent 6,862,558.

[35] N. Huang, Z. Shen, and S. Long. A new view of nonlinear water waves: The hilbert spectrum 1. *Annual review of fluid mechanics*, 31(1):417–457, 1999.

[36] N. Huang, Z. Shen, S. Long, M. Wu, H. Shih, Q. Zheng, N.-C. Yen, C. Tung, and H. Liu. The empirical mode decomposition and the Hilbert spectrum for nonlinear and non-stationary time series analysis. *Proceedings of the Royal Society of London. Series A: Mathematical, Physical and Engineering Sciences*, 454(1971):903–995, 1998.

[37] N. Huang and Z. Wu. A review on Hilbert-Huang transform: Method and its applications to geophysical studies. *Reviews of Geophysics*, 46(2), 2008.

[38] N. Huang, Z. Wu, S. R. Long, K. C. Arnold, X. Chen, and K. Blank. On instantaneous frequency. *Advances in Adaptive Data Analysis*, 1(02):177–229, 2009.

[39] N. E. Huang, M.-L. C. Wu, S. R. Long, S. S. P. Shen, W. Qu, P. Gloersen, and K. L. Fan. A confidence limit for the empirical mode decomposition and hilbert spectral analysis. *Proceedings of the Royal Society of London. Series A: Mathematical, Physical and Engineering Sciences*, 459(2037):2317–2345, 2003.

[40] F. King. *Hilbert Transforms*, volume 1. Cambridge University Press, Cambridge, UK, 2009.

[41] K. Kodera, C. de Villedary, and R. Gendrin. A new method for the numerical analysis of non-stationary signals. *Physics of the Earth and Planetary Interiors*, 12(2):142–150, 1976.

[42] K. Kodera, R. Gendrin, and C. de Villedary. Analysis of time-varying signals with small bt values. *Acoustics, Speech and Signal Processing, IEEE Transactions on*, 26(1):64–76, 1978.

[43] V. G. Papanicolaou. Some results on ordinary differential operators with periodic coefficients. *arXiv preprint arXiv:1412.5423*, 2014.

[44] I. Schoenberg and A. Whitney. On Pólya frequency functions III. The positivity of translation determinants with an application to the interpolation problem by spline curves. *Transactions of the American Mathematical Society*, 74(2):246–259, 1953.

[45] L. Schumaker. *Spline Functions: Basic Theory*. Cambridge University Press, Cambridge, UK, 1981.

[46] R. C. Sharpley and V. Vatchev. Analysis of the intrinsic mode functions. *Constructive Approximation*, 24(1):17–47, 2006.

[47] G. Thakur, E. Brevdo, N. Fučkar, and H.-T. Wu. The synchrosqueezing algorithm for time-varying spectral analysis: Robustness properties and new paleoclimate applications. *Signal Processing*, 93(5):1079 – 1094, 2013.

[48] G. Thakur and H.-T. Wu. Synchrosqueezing-based recovery of instantaneous frequency from nonuniform samples. *SIAM J. Mathematical Analysis*, 43(5):2078–2095, 2011.

[49] J. Ville. Théorie et applications de la notion de signal analytique. *Cables et transmission*, 2A:61–74, 1948.

[50] G. Wahba. Smoothing noisy data with spline functions. *Numerische Mathematik*, 24(5):383–393, 1975.

[51] E. Wigner. On the quantum correction for thermodynamic equilibrium. *Physical Review*, 40(5):749, 1932.

[52] H.-T. Wu. Instantaneous frequency and wave shape functions (i). *Appl. and Comput. Harmon. Anal.*, 35(2):181 – 199, 2013.

[53] Z. Wu and N. Huang. A study of the characteristics of white noise using the empirical mode decomposition method. *Proceedings of the Royal Society of London. Series A: Mathematical, Physical and Engineering Sciences*, 460(2046):1597–1611, 2004.

[54] Z. Wu and N. Huang. Ensemble empirical mode decomposition: a noise-assisted data analysis method. Technical Report COLA Tech. Rep. 193, Cent. for Ocean-Land-Atmos. Stud., Calverton, Md., 2005.

[55] Z. Wu and N. Huang. Ensemble empirical mode decomposition: a noise-assisted data analysis method. *Advances in adaptive data analysis*, 1(01):1–41, 2009.